9-2020

Development of a Semi-Quantitative Methodology for Evaluation of Whole-Body Chemical, Biological, Radiological, and Nuclear Decontamination Using an Ultraviolet Fluorescent Aerosol

Emily M. Titus

DEVELOPMENT OF A SEMI-QUANTITATIVE METHODOLOGY FOR EVALUATION OF WHOLE-BODY CHEMICAL, BIOLOGICAL, RADIOLOGICAL, AND NUCLEAR DECONTAMINATION USING AN ULTRAVIOLET FLUORESCENT AEROSOL

THESIS

Emily M. Titus, Contractor

AFIT-ENV-MS-20-S-081

DEPARTMENT OF THE AIR FORCE
AIR UNIVERSITY

AIR FORCE INSTITUTE OF TECHNOLOGY

Wright-Patterson Air Force Base, Ohio

AFIT-ENV-MS-20-S-081

DEVELOPMENT OF A SEMI-QUANTITATIVE METHODOLOGY FOR EVALUATION OF WHOLE-BODY CHEMICAL, BIOLOGICAL, RADIOLOGICAL, AND NUCLEAR DECONTAMINATION USING AN ULTRAVIOLET FLUORESCENT AEROSOL

THESIS

Presented to the Faculty

Department of Systems Engineering and Management

Graduate School of Engineering and Management

Air Force Institute of Technology

Air University

Air Education and Training Command

In Partial Fulfillment of the Requirements for the

Degree of Master of Science in Industrial Hygiene

Emily M. Titus, BS

Contractor

August 2020

AFIT-ENV-MS-20-S-081

DEVELOPMENT OF A SEMI-QUANTITATIVE METHODOLOGY FOR EVALUATION OF WHOLE-BODY CHEMICAL, BIOLOGICAL, RADIOLOGICAL, AND NUCLEAR DECONTAMINATION USING AN ULTRAVIOLET FLUORESCENT AEROSOL

Emily M. Titus, BS

Contractor

Committee Membership:

Dr. Jeremy Slagley
Chair

Col Robert Eninger, PhD
Member

Lt Col Casey Cooper, PhD
Member

Abstract

The following work describes an extensive literature review which was conducted on publicly available literature in the field of chemical, biological, radiological, and nuclear (CBRN) decontamination to gain an understanding of the body of knowledge and gaps in this body of knowledge. Several gaps were identified, including the assumption that disrobing after a CBRN incident will remove 90% of contamination. Also included is a description of the design and characterization of an aerosol test chamber which was constructed for use in this and future research. Finally, the bulk of this work describes the development of a semi-quantitative methodology by which contamination and decontamination can be visualized. This methodology utilizes an ultraviolet fluorescent tracer delivered as an aerosol to simulate contamination, such as by a chemical warfare agent, and leverages image analysis to determine the difference in contamination from one step to another. The use of this method showed that it was highly repeatable, with deposition area variability being less than 40 in^2 (total area 230 in^2). This method development was aimed towards performing experiments which would evaluate the claim of 90% contamination removal by disrobing. Several iterations of experiments were conducted with different clothing which allowed the conclusion that disrobing can remove up to 95% (mean 93.9%, with 95% confidence intervals of 91.0-96.8%) of contamination in certain situations, such as when Tyvek suits are well-sealed. In other situations, however, it was shown that disrobing may only remove 70% of contamination present (mean 69.2%, with 95% confidence intervals of 64.9-73.6%), such as when

Tyvek suits are worn with cuffs open. Thus, while disrobing may not always remove the stated 90% of contamination, it was demonstrated to remove at least 65% of contamination.

Acknowledgments

I would like to thank Dr. Slagley for his enthusiasm and guidance, as well as willingness to explore different options for completing the work even with current events making things difficult. I would like to thank Colonel Eninger for his support and advice on literature reviews and data organization. Thanks also to Lieutenant Colonel Cooper for his advice regarding aerosols and the use of the JSLIST suit. In addition I would like to thank Centauri for allowing me the opportunity to attend AFIT in this program. Finally, I'd like to thank my fiancé for all his support and allowing me to turn the garage and backyard into my lab these last few months.

Emily M. Titus

Table of Contents

Page

List of Figures

Page

List of Tables

Page

List of Equations

Page

DEVELOPMENT OF A SEMI-QUANTITATIVE METHODOLOGY FOR EVALUATION OF WHOLE-BODY CHEMICAL, BIOLOGICAL, RADIOLOGICAL, AND NUCLEAR DECONTAMINATION USING AN ULTRAVIOLET FLUORESCENT AEROSOL

I. Introduction

1.1 General Issue

Decontamination is extremely important after a hazardous materials (HAZMAT) or weapons of mass destruction (WMD) incident to aid victims involved as well as protect first responders from secondary effects. Decontamination is done to remove the material from a person's skin to avoid adverse health outcomes which can arise from dermal absorption, accidental ingestion from the skin, or inhalation due to vaporization of the contaminant. Many different actions can be considered decontamination. Disrobing is often considered the first step to decontamination, as it removes contaminated clothing from contact with the skin. After disrobing, further decontamination can be done by either dry or wet methods, depending on the situation.

1.2 Problem Statement

This work attempts to validate the claim that 70-90% of contamination can be removed by disrobing [1]–[5]. This statistic is a central tenet of disaster planning guidelines used by both the Department of Defense, as well as civilian disaster planning agencies [6]–[8]. The assumption of 70-90% decontamination by disrobing is applied broadly across many populations, from fully prepared military populations wearing protective gear such as the Joint Service Lightweight Integrated Suit Technology

(JSLIST) suit, to civilian populations who would not have access to such gear. It is intuitive that in certain situations that clothing would cover up to 90% of the body surface area and thus that disrobing may remove that much contamination. However, there is little open source literature which backs this assumption, nor reason to believe that it would apply in all situations.

This text describes the development of a method which can be used to visualize the extent of contamination and decontamination by using an ultraviolet (UV) fluorescent dye delivered as an aerosol. This delivery was meant to imitate delivery of a chemical warfare agent (CWA) or other hazardous aerosol contaminant. After visualization and image capture, image analysis is used to semi-quantify the contamination and reduction in contamination due to disrobing or other decontamination methods.

1.3 Research Objectives/Questions/Hypotheses

Three research objectives are addressed in this document. The first aim was to conduct an extensive literature review and gap analysis of the field of CBRN (chemical, biological, radiological, nuclear) patient decontamination to understand the research needs of the field.

Second, was to characterize the aerosol test chamber which was to be used during experiments. There were two components to this characterization, the first being to describe the air velocity profiles within the chamber and the second being to understand the spatial variability of particles within the chamber using gravimetric or other methods.

The third research objective was to investigate the credibility of the assumption of 70-90% decontamination due to disrobing by creating a methodology using a UV fluorescent tracer. There were several parts to this objective, with the first being to create a reproducible methodology which could consistently deliver an aerosolized UV dye (used to mimic aerosol CWA exposure) to a mannequin, visualize the extent of contamination, and finally analyze the differences in contamination after disrobing. In addition to disrobing, a simulated patient decontamination protocol was developed following procedures found in guidance documents and evaluated.

1.4 Thesis Outline

This thesis is organized into five chapters which describe the work conducted. Chapter I describes the issue, background, problem statement and research objectives. Chapter II includes an extensive literature review and gap analysis of the field of CBRN decontamination and patient decontamination. Chapter III details the work involved in building and characterizing an aerosol test chamber. Chapter IV describes the development of a reproducible method to deliver and visualize contamination from a UV fluorescent aerosol as well as disrobing and decontamination procedures. Chapter V contains a discussion of the conclusions and limitations of the work overall, as well as recommendations for future work.

II. CBRN Patient Decontamination Gap Analysis

Chapter Overview

The purpose of this chapter is to summarize the findings of an extensive literature review and gap analysis conducted in the area of CBRN decontamination research. The search was focused on chemical and biological agents and their decontamination as it is widely accepted that decontamination of radiological and nuclear contaminants is well understood. In addition, radioactive materials are easily detected by direct reading instruments which can aid in decontamination. This gap analysis was used to guide the author to a research question which would benefit from further study.

Publication Details

The article contained in this chapter was accepted and published by the American Journal of Disaster Medicine in September 2019. The citation is shown below [9].

[6] E. Titus, G. Lemmer, J. Slagley, and R. Eninger, "A review of CBRN topics related to military and civilian patient exposure and decontamination," Am. J. Disaster Med., vol. 14, no. 2, pp. 137–149, 2019.

Abstract

Chemical and biological (CB) warfare have long been practiced, and although these types of warfare are not acceptable in modern times, this does not prevent them from occurring. This makes it important for societies to be able to appropriately respond to these events, including the best way to decontaminate victims to keep them and emergency responders safe. Decontamination methods such as chemical, physical, wet,

and dry methods are discussed, as well as their downsides. Secondary contamination, which played a significant role in the Tokyo sarin attacks, has long been noted by anecdotal evidence, though it has been little studied. Biological agents cause more problems after infection has taken place, and thus preventing the spread of infection is the largest concern. There are many differences between military and civilian populations, and the response to mass casualty attacks differs accordingly. There are several emerging technologies which can make this process easier on all parties, such as bioscavengers, antitoxins, and color changing bleach for visualization. A reliable way to quantify decontamination is also needed, which would allow for better care of victims both in normal hospital situations, as well as during aeromedical transport. In addition, several gaps were identified, such as the lack of scientific basis for 90 percent reduction during decontamination, a way to quantify decontamination, and the lack of studies on toxic industrial chemicals and secondary contamination.

III. Characterization of the Multi-Use Research for Particulate Hazards and Environmental Exposures (MURPHEE) Aerosol Test Chamber

Chapter Overview

This chapter describes work undertaken to characterize a newly built aerosol exposure test chamber. The chamber was designed to have a 3’ by 3’ cross-section and is 21’ long, and air can be moved through the chamber by use of a centrifugal fan. The fan allows air speeds to reach up to 1 m/s. This work was submitted in May for publication to

the journal Aerosol Science and Technology and is currently undergoing revision. The originally submitted draft is found in Appendix A.

Abstract

Aerosol test chambers are used to contain aerosols during experiments to protect researchers and provide a stable research environment. This work describes the design and characterization of a novel test chamber, the Multi-Use Research for Particulate Hazards and Environmental Exposures (MURPHEE) Chamber. Design was made modular to accommodate current and future research needs, although it was not possible to ensure laminar airflow. Characterization methods consisted of air velocity mapping as well as spatial variability of ultrafine particulate aerosols. Air speeds within the chamber varied but were homogenous enough for confidence in data collection. Particulate size distributions were similar, but there was high variability in the counts, leading experiments to require large sample sizes. In addition, a computational fluid dynamics model was created and validated using the data to guide future work and allow planning and pilot tests to be conducted more swiftly and with less cost.

IV. Semi-Quantitative Decontamination of a Mannequin Using UV Fluorescence and Image Analysis

Chapter Overview

This chapter details work done towards developing a methodology for semi-quantitative evaluation of decontamination using a UV fluorescent tracer delivered as a

liquid aerosol and image analysis. A literature search was conducted to determine whether a basis for this method could be established as well as understand challenges inherent in the method. Review showed that significant challenges are associated with image analysis of UV fluorescence which had to be addressed and overcome during the course of this work. This chapter will address the evolution of the process as challenges were encountered and the solutions necessary to overcome them.

In addition, this work was intended to be completed using the aerosol test chamber described in Chapter III. Due to shutdowns associated with the COVID-19 pandemic, access to the laboratory where the chamber is located (referred to as "at UES" or "in the MURPHEE chamber") was severely restricted until late in the data collection process. For this reason, other options were explored to allow work to be completed in a timely manner, although the experimental set-up was not what was anticipated (referred to as "experiments done at home" due to being set-up in the author's garage and yard).

Introduction

Previous decontamination research depends on contamination of small swatches of skin or material to test. Research on skin decontamination efficacy often uses flow-through diffusion cells, which allow a small surface area of skin to be contaminated and samples to be taken periodically from the upper and lower chambers to determine the penetration rate of the contaminant [4], [10], [11]. These skin samples are then wiped, and the wipes are analyzed for contamination left on the skin surface, as well as dissolved to determine the amount left in the dermal reservoir. However, the difficulties associated

with performing these kinds of experiments and analyses on the significantly larger surface areas of a mannequin mean that relatively few studies have been performed to quantify contamination or decontamination of a mannequin [12], [13]. In order to evaluate the claims of 90% decontamination due to disrobing however, a full-scale mannequin experiment was required.

As mentioned, skin wipes are often used as a method for analysis of contamination. These wipes, or the rinsate from skin, or the skin itself are then analyzed by high-performance liquid chromatography (HPLC) or gas chromatography-mass spectrometry (GC-MS) [14]–[22]. When experiments are performed on the scale of skin and material swatches, this is a feasible method for analysis. Due to the surface area involved in experiments with a full-body mannequin, this methodology seemed impractical and other methods were considered.

First, a colored or fluorescent powder or dye could be used as a simulated contaminant. Images could be taken before and after contamination and decontamination and image analysis software leveraged to determine the percentage of the body contaminated. This approach has been used with varying degrees of success. It has been used in hospital infectious disease training programs to show trainees how easily biological contamination can be spread. One research group created a highly realistic mannequin called VIOLET (Visualizing Infection with Optimized Light for Education and Training) which simulated many types of bodily fluids common to viral hemorrhagic fevers and respiratory illnesses [23]. Vomit, diarrhea, sweat, and coughing were simulated, each with a differently colored fluorophore incorporated. After trainees

interacted with the mannequin and performed several patient care tasks, they were imaged under UV-A light, instructed to doff their PPE, then imaged again. This gave personnel qualitative feedback about both their interactions with the patient and the importance of care during PPE doffing to ensure that cross contamination does not occur. A similar technique was used in another nursing training program to demonstrate the spread of biological aerosols and areas of contamination within patient care facilities [24]. Issues common to fluorescence imaging were elucidated, including that it can be unreliable and subject to interference from differences in skin tone as well as naturally occurring materials. For instance, the paper towels used to dry hands contained micro fibers which appeared very similar to the fluorescent powder used in the study [24]. In addition, large amounts of fluorescent material may be needed in order for them to image correctly, or transfer from one surface to another during training.

A fluorescent contaminant was utilized by one research group during a full-scale decontamination exercise which was aimed at understanding the difficulties involved in directing mass casualty decontamination, particularly with so-called “at-risk” patients (those that cannot hear or don’t understand the language, those that have disabilities, or children and the elderly) [14]. Curcumin in methyl salicylate was used as a fluorescent tracer. Methyl salicylate is also a common simulant for lipophilic medium-volatility chemical warfare agents like sulfur mustard and soman so protocols are in place for chemical analysis of methyl salicylate [14]. Volunteers were dosed using a spray bottle of the curcumin-methyl salicylate mixture in several places on their body. They then participated in a mass casualty decontamination situation including disrobing, dry

decontamination, and the ladder-pipe system. After completing decontamination volunteers were imaged under UV light to examine decontamination efficacy and understand cross contamination, as well as having the dosing sites swabbed for chemical analyses [14].

Fluorescence was also utilized in a study to understand the possible cross contamination of agricultural workers during pesticide application [19], [25]. This research group created a quantitative video imaging technique which would correlate fluorescence to deposition of pesticide on the worker's skin and clothing.

As this literature review showed, there is a precedent for using fluorescence as a measure of contamination, even by aerosol deposition. However, due to the many challenges involved, other methods were also considered which might be appropriate to quantify contamination and decontamination. These included swipe sampling or measurement of off-gassing or radioactivity. Swipe sampling would be difficult to perform at this scale as the number of wipes which would be needed to cover the entire surface area of the mannequin would be quite high. In addition, it would not be possible to measure the amount of contamination after exposure in the same experiments that decontamination was also measured due to sampling removing contamination. Off-gassing could be used as a surrogate for contamination but provides its own challenges for measurement due to the difficulties involved in applying a volatile contaminant, and the differing absorbency and subsequent vaporization rates of various materials. Radioactive particles could be used as a contaminant as they are fairly easily measured by real-time detection instruments. However, radioactive materials have their own hazards

which would need to be considered if they were used. For these reasons, fluorescence and image analysis was chosen as the method for simulating and measuring contamination.

Methods and Supplies

This research was in part a method development which will be described below. An overview of the final experimental process is as follows and materials used will be described in order of the steps that they are used in (Figure 1). First an unclothed mannequin was imaged under UV light, which gives a background reading for any surface "skin" fluorescence. Next the mannequin was dressed in clothing. Then the clothed mannequin was imaged under UV light, which gives a background reading for any inherent fluorescence of the clothing. After imaging, the mannequin was moved to the exposure booth where the mannequin was exposed to a UV fluorescent aerosol. After contamination the mannequin was again imaged under UV light, which shows the extent of contamination on clothing. The mannequin was then disrobed. Next the unclothed mannequin was imaged again under UV light to show the extent of contamination on the skin. Then the mannequin was decontaminated using soap and water in a wet decontamination protocol developed based on current guidance. Finally, the decontaminated mannequin was imaged again under UV light to establish the effectiveness of decon and show residual contamination. After data was collected, image analysis was conducted to quantify the extent of contamination present in each step.

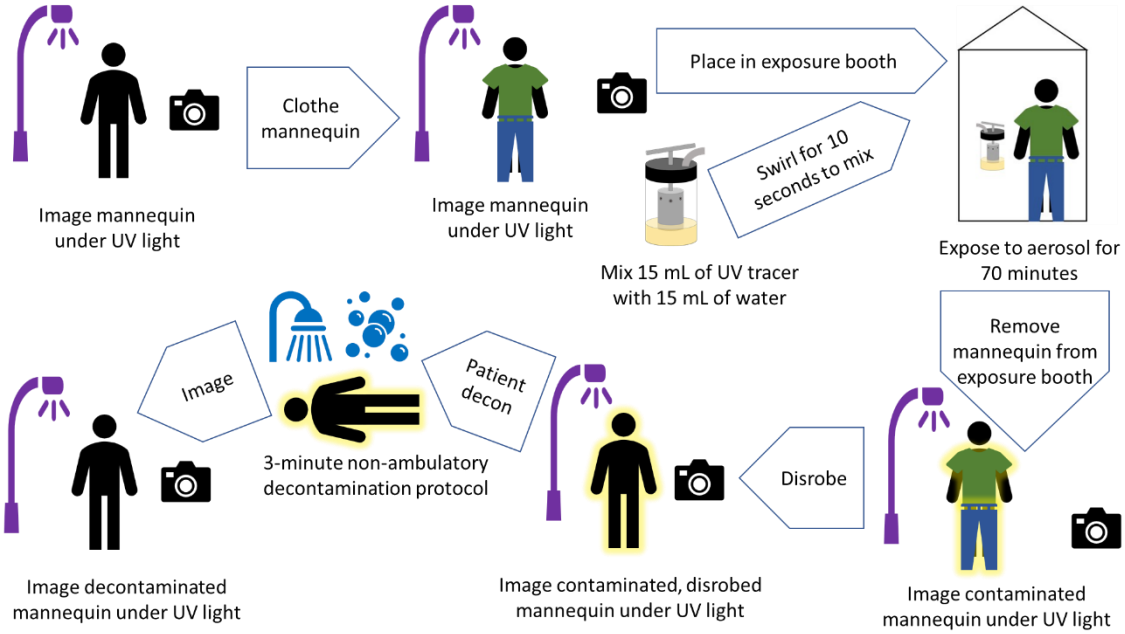

Figure 1. Overview of the experimental process

Imaging Set-Up

Imaging was done in a darkened room under illumination of ultraviolet light. During experiments conducted at home, the garage was used as the imaging area, with blackout curtains sealing light from the window and the black surface of the curtain used to provide a uniform background for images (Figure 2A). Experiments which took place in the UES lab were done in a darkened office room. Blackout curtains were hung from a PVC frame to block light from the door as well as provide the same uniform background (Figure 2B). The UV fluorescent lights used were mounted in an appropriate shop light fixture (1233 Linear 4-ft Shop Light, Lithonia Lighting, Atlanta, GA) which was attached to a photography light stand (AmazonBasics Aluminum Light Photography Tripod Stand, Amazon, Seattle, WA) using duct tape. UV fluorescent lights were purchased from Lowe's (GE 40-Watt 48-in T12 Black Fluorescent Lightbulb, GE Lighting, East

Cleveland, OH). The stands were placed slightly off-center, approximately 4 feet (3.5 feet at UES) from the mannequin's location and angled towards the mannequin. The camera was located on a tripod situated between and slightly behind the lights, approximately 6 feet (4 feet at UES) from the mannequin. The manufacturer was contacted regarding the wavelength of light emitted but did not provide the requested information. The optimal wavelength of light for exciting the UV dye used was stated to be 365 nm, though excitation would occur at 395 nm. Precautions were taken to not place the researcher in front of the lights while they were on, and UV-filtering safety glasses (99%) were worn during the entire imaging process [26].

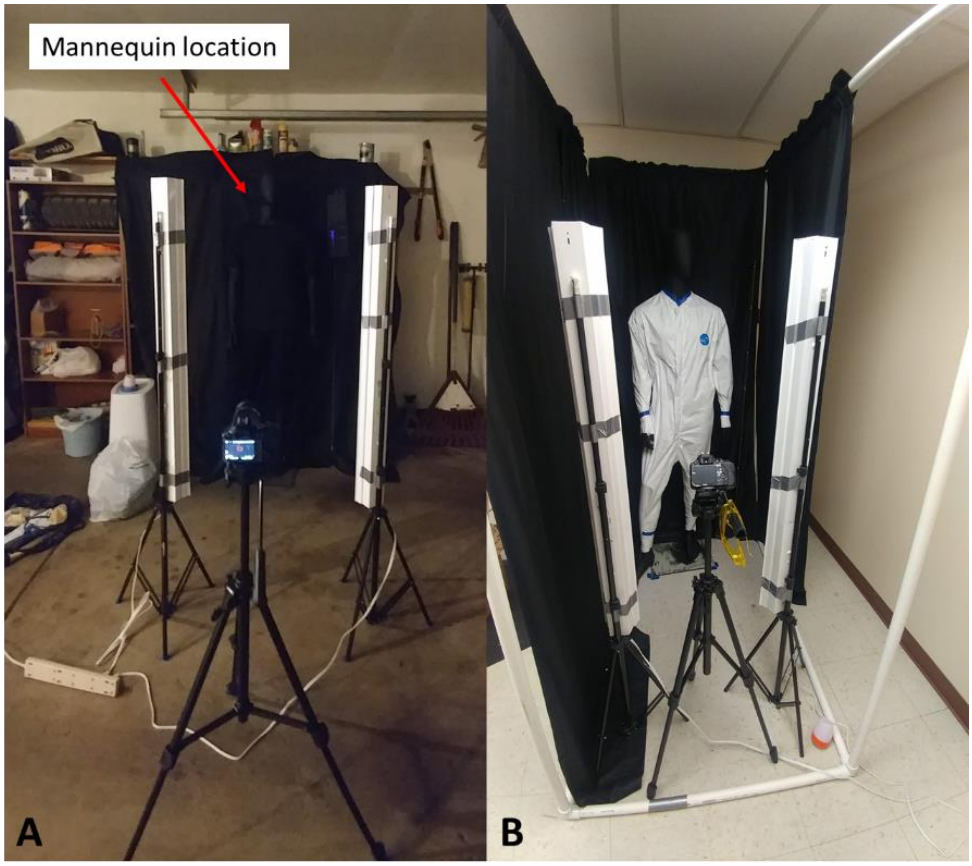

Figure 2. Imaging set-up. A) At the authors home. B) At UES.

Two standards were placed in the frame of each image captured for calibration of images during processing. The first standard was a Stouffer 21-Step Sensitivity Guide and the second was a serial dilution of the UV dye used. These will be described further in the Image Processing and Analysis section.

Images were taken using a Nikon D3500 DSLR camera (Nikon Inc. USA, Melville, NY) mounted on a tripod (Sony VCT-R640, Sony Electronics Inc, San Diego, CA). Settings are shown in Table 1. Shutter speed describes the length of time taken to capture the image. ISO describes the sensitivity of the image sensor. Larger ISO numbers indicate better sensitivity for low-light applications. Aperture describes the opening in the camera lens through which light can pass. It is described by f-numbers which are related to the diameter of the opening (the ratio of focal length to aperture diameter). One image was taken at each shutter speed starting from 1 second, then this was repeated twice for a total of 3 replicates. In addition, images were taken and saved in both JPEG format and a proprietary raw format called NEF.

Table 1. Image Capture Settings

Shutter Speed (seconds)	ISO	Aperture (f/ stop)
1	3200	4.5
1/2	3200	4.5
1/2.5	3200	4.5

Images were taken in several sections due to the field of view of the camera. Images were taken of the front of the mannequin, then the back, and of each body region

sequentially (Figure 3). In order to avoid moving either the mannequin or the camera excessively images were taken from the feet to the head, then back down the other side of the mannequin. Then the mannequin was clothed and imaged up the back and down the front.

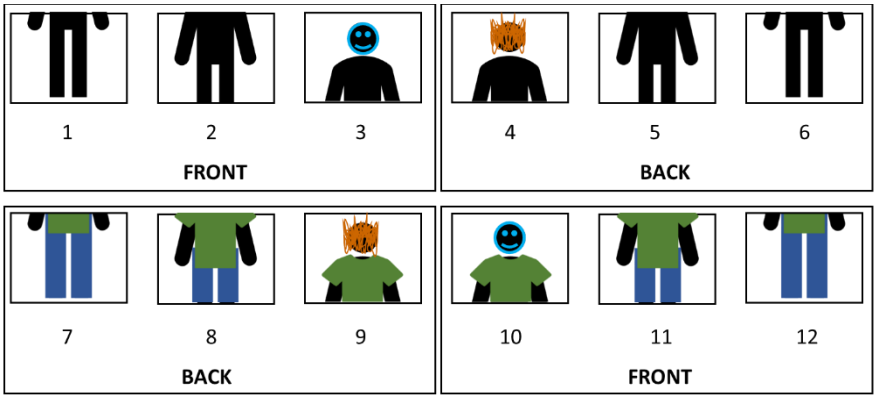

Figure 3. Image Capture Order Prior to Experiments

Mannequin and Clothing Used

Experiments were conducted using a standard retail mannequin (Abstract Fiberglass Male Mannequin, Style B, TSI Store Supplies, Simi Valley, CA). The mannequin came in a glossy black finish. This finish caused reflections during imaging which interfered with analysis, so the mannequin was refinished using a matte black chalkboard spray paint (Specialty Chalkboard Spray Paint, Black, Rust-Oleum, Vernon Hills, IL). This finish was reapplied as needed throughout the data collection period. For all images as well as during exposure the mannequin was placed on the provided stand, which inserted into the back of the left calf.

Several different types of clothing were used during the course of experiments (Figure 4). Initial literature review indicated that contrast of fluorescence would be greatest on black clothing (Figure 4A). To that end black cotton t-shirts were purchased

in bulk (Gildan Adult Softstyle T-shirt, 100% Cotton, Gildan, Montreal, Quebec, Canada). Suitable options for pants were not found in bulk so pants were sourced from the local thrift store. Prior to trials, clothing was washed using Woolite DARKS Liquid Laundry Detergent which contains no fluorescent whitening agents (Parsippany, NJ). These clothes were intended to be representative of a civilian population due to type and style of clothing. Visualization issues were encountered which prompted further trials to be conducted using different clothing materials.

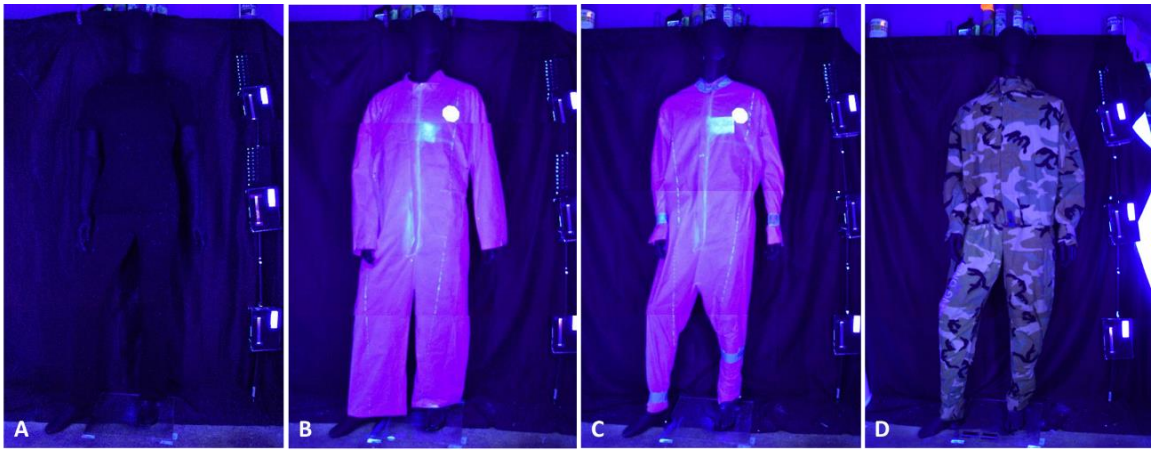

Figure 4. Clothing types used during experiments. A) Black cotton. B) Tyvek suit, cuffs and neck open. C) Tyvek suit, cuffs and neck taped. D) JSLIST suit

Subsequent trials were performed by dressing the mannequin in Tyvek suits (Tyvek 400 coveralls TY120SWH, Dupont Tyvek, Wilmington, DE). Despite the fact that the coveralls appear white under normal lighting conditions, they image faintly purple under UV light, and bright white once contaminated so there was suitable contrast for imaging purposes.

Due to the author's personal skepticism towards the ability to visualize fluorescence on the Tyvek a limited number of suits were purchased initially. This led to a question of whether the suits could be washed and re-used for data collection due to issues ordering further suits after their suitability was established. During these tests the mannequin was dressed in the suits as normal, but suits were removed without cutting for ease of reuse. In addition, during these tests the cuffs at wrists, ankle, and neckline were left open rather than being secured during the exposure period (Figure 4B). In this pilot study to determine the possibility of re-using suits, 2 trials were run with new suits, and 3 with re-used suits.

A third set of data was collected using new Tyvek suits with all cuffs and the neckline left open as above (Figure 4B). Fifteen trials were included in this data set. These trials were intended to simulate an unprepared military population which would be wearing clothing covering the full legs and arms but not necessarily protective gear. A fourth set was collected by using new Tyvek suits, but instead securing the cuffs and neckline using tape (Figure 4C). Cuffs of pant legs and wrists were secured by pulling the clothing tightly and wrapping excess around the ankle or wrist, then securing the ends with either masking tape or duct tape. The neckline was also taped closed using masking tape. Again, fifteen trials were included in this data set. These trials were intended to simulate a prepared military population dressed in fully protective JSLIST suit.

In addition to the simulated JSLIST scenario assumed by using Tyvek suits with all openings secured, a single JSLIST suit was obtained for experimental use (Figure 4D). All drawstrings and Velcro straps were tightened to the fullest extent possible. The hood

was left down and secured around the neck rather than over the top of the head to better correlate with the Tyvek suits. No tape was used to supplement the closure of any points on the uniform. Only one run was able to be performed using the JSLIST suit.

Finally, access to the MURPHEE aerosol chamber was able to be obtained in order to run 3 trials. These were run using new Tyvek suits which were taped at cuffs and neck (Figure 4C).

Chemical Warfare Agent Simulant and Dispersal

A commercial water-soluble UV fluorescent tracer dye was used as a chemical warfare agent simulant (IFWB-C01PT, Risk Reactor Inc., Santa Ana, CA). A summary of its characteristics is found in Table 2. This dye was chosen for its invisibility under normal lighting conditions but bright fluorescence under UV light. It was also chosen for its ability to be cleaned from the mannequin, clothing, and exposure test chamber surfaces, reasonable similarity to chemical warfare agents of interest, and price point. While it is not a perfect match for any chemical warfare agent, it is of similar density and solubility to sarin (Table 3). In the form used in this study, it is likely also of similar viscosity to sarin. The dye was mixed 1:1 with water, which has a viscosity of 1.0 centipoise (cP) and the resulting solution had similar viscosity to water.

Table 2. Summary of Water-based UV Fluorescent Dye Characteristics

Ingredients	Triethanolamine (10-15%) Urea (10-15%) Other ingredients unspecified
Color	Yellow
Physical Form	Liquid
Odor	Ammonia-like
Flash Point	>200°F
Specific Gravity	1.1
VOC by Weight	~2% by EPA method 24/24a
pH	10-11
Toxicology Results	Oral LD_{50}: 14,530 mg/kg (rat) Dermal LD_{50}: >2000 mg/kg (rabbit)

Table 3. Summary of Chemical Properties of CWAs and Surrogate

	UV-Fluorescent Surrogate[a]	VX[b]	GB (Sarin)[b]	HD (Mustard)[b]
Density (g/cm^3)	1.1 (specific gravity)	1.008[c]	1.089[c]	1.27[d]
Vapor Pressure (mm Hg)		0.0007[c]	2.9[c]	610[d]
Volatility (mg/m^3)	2% (by weight)	10.5[c]	22000[c]	610[d]
Solubility in water	Miscible	Slightly	Miscible	<1%
Viscosity (cP)		10.041[c, e]	1.397[c, e]	3.951[c, e]

[a]From the manufacturer SDS. [27]
[b]From Buide for the Selection of Chemical, Biological, Radiological, and Nuclear Decontamination Equipment for Emergency First Responders. [28]
[c]At 77°F
[d]At 68°F
[e]From Potential Military Chemical/Biological Agents and Compounds. [29]
[f]From PubChem. [30]

An oil-based dye from the same manufacturer was also considered as a possible CWA simulant. However, pilot tests on polycarbonate (the material used for the walls of the MURPHEE aerosol chamber) showed that after a 30-minute application of the neat

dye, a fluorescent residue was left on the polycarbonate which was unable to be removed by any cleaner attempted (Figure 5). Figure 5A and B show droplets of the neat oil-based dye at the start of the experiment. Figure 5 C-E show the location of the same droplets 30 minutes after the start of the experiment. Figure 5C and E show the residue remaining after removing the dye using both a damp paper towel and Clorox wipe, while D and F show the appearance of the neat dye under those conditions. Though fluorescence was much less after clean-up than for the neat dye (Figure 5C vs D), there was a significant fluorescent residue. Although an oil-based tracer would likely be a more accurate simulant for most CWAs, the water-based tracer was ultimately used to ensure that shared lab equipment would remain in good condition for future work.

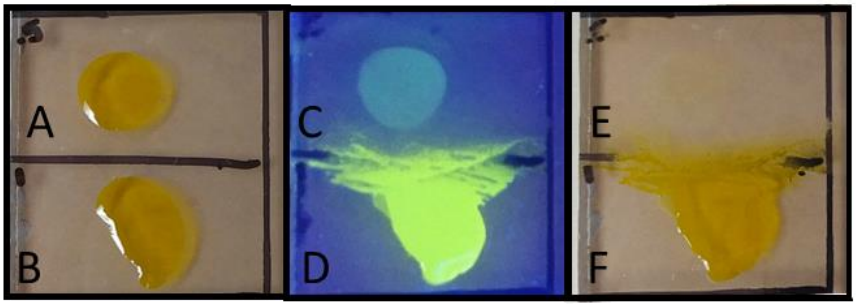

Figure 5. Material compatibility test between polycarbonate and neat droplets of the oil-based dye. A) and B) Start of the experiment, normal light. C) and D) 30 minutes after start, UV light. E) and F) 30 minutes after start, normal light.

A 6-jet Collison nebulizer (CH Technologies, Westwood, NJ) was used to deliver the CWA simulant to the mannequin. Compressed air was delivered to the nebulizer at a pressure of 20 psi, giving an aerosol dispersal rate of 12 LPM [31]. The UV fluorescent dye was mixed 1:1 with water in the nebulizer jar and swirled for 10 seconds to mix

thoroughly. To determine the volume to be aerosolized, it was initially decided to target a deposition of 10 g/m^2 from the specifications for the Joint Service Lightweight Integrated Suit Technology (JSLIST) [32]. Using the average body surface area of an adult human, 1.9 m^2 (average value from the Environmental Protection Agency's Exposure Factors Handbook) and the deposition mass of 10 g/m^2, then 19 g of the fluorescent contaminant would need to be deposited onto the mannequin [33] (Equation 1). The specific gravity of the fluorescent dye was given to be 1.1, which would give a mixture of equal parts water and the dye a density of 1.05 g/mL [27] (Equation 2). Given the density of the solution and the requirement for 19 g of the contaminant, then 18.10 mL of the contaminant solution would need to be aerosolized to approximately deposit the required amount onto the mannequin (Equation 3). This is a rough approximation as not all of the aerosolized material would deposit onto the mannequin, but it was considered the best approximation available.

$$SA_{Human} = 1.9\ m^2$$

$$Deposition = 10\frac{g}{m^2}$$

$$Mass\ aerosolized = 10\frac{g}{m^2} * 1.9\ m^2 = 19\ g$$

Equation 1

Where:

SA_{Human} = Body surface area of an average adult human [33]
Deposition = Target deposition rate for testing JSLIST suits [32]
Mass aerosolized = Mass needed to be aerosolized to achieve the deposition

$$\rho = \frac{m}{V} \rightarrow V = \frac{m}{\rho} \rightarrow m = \rho V$$

$$\rho_{mix} = \frac{m_{mix}}{V_{mix}} = \frac{m_1 + m_2}{V_1 + V_2} = \frac{\rho_1 V_1 + \rho_2 V_2}{V_1 + V_2}$$

If $V_1 = V_2 = V$

$$\rho_{mix} = \frac{\rho_1 V + \rho_2 V}{V + V} = \frac{\rho_1 V + \rho_2 V}{2V} = \frac{V(\rho_1 + \rho_2)}{V(2)} = \frac{\rho_1 + \rho_2}{2}$$

$$\rho_{mix} = \frac{1.00\left(\frac{g}{mL}\right) + 1.10\left(\frac{g}{mL}\right)}{2} = \frac{2.10\left(\frac{g}{mL}\right)}{2} = 1.05\frac{g}{mL}$$

Equation 2

Where:

ρ = density (g/mL)
m = mass (g)
V = volume (mL)
ρ_{mix} = density of the dye-water solution
m_{mix} = mass of the dye-water solution
V_{mix} = volume of the dye-water solution
m_1 = mass of water
m_2 = mass of dye
ρ_1 = density of water
ρ_2 = density of dye
V_1 = volume of water
V_2 = volume of dye

$$V_{aerosolized} = \frac{19\ g}{1.05\left(\frac{g}{mL}\right)} = 18.10\ mL$$

Equation 3

Where:

$V_{aerosolized}$ = Minimum volume of dye solution to be aerosolized in order to achieve the target deposition

The prior calculations and assumptions were used throughout experimental data collection. However, near the end of the data collection period the U.S Army Test and Evaluation Command Test Operations Procedure for Chemical Vapor and Aerosol System-Level Testing of Chemical/Biological Protective Suits was found [34]. This source explained a method for testing aerosols and vapors specifically, requiring aerosol generation to be at an average of 167 mg/m^3 throughout a 30 minute period [34]. Based on the volume of the exposure booth (approximately 48" x 48" x 86" or 3.2469 m^3) and this aerosol generation rate, then 542.23 mg would need to be aerosolized, or 18.07 mg/min, to achieve the required aerosol (Equation 4). Given the density of the contaminant and approximately 20 mL of a 1:1 dilution aerosolized, then 10 mL of the contaminant are aerosolized during the 70-minute exposure period. This gives 11000 mg of contaminant aerosolized, and a rate of 157.1 mg/min achieved. This means that the mass of aerosol used during these exposures is 8.7 times more than the mass required by the testing protocol. Though the protocol does not state whether this is a low- or high-end estimate of possible contamination, it is reasonable to assume that it is likely a conservative estimate, which means that the results presented below would be even more protective.

$$V_{booth} = 48\ in * 48\ in * 86\ in = 198144\ in^3 * \frac{ft^3}{12^3 in^3} * \frac{0.3048^3 m^3}{ft^3} = 3.2469\ m^3$$

$$m_{aerosol} = \frac{167\ mg}{m^3} * 3.2469\ m^3 = 542.3\ mg$$

$$rate_{aerosol} = \frac{542.3\ mg}{30\ minutes} = 18.07 \frac{mg}{min}$$

$$m_{actual} = \frac{1.1\ g}{mL} * \frac{1000\ mg}{g} * 10\ mL = 11000\ mg$$

$$rate_{actual} = \frac{11000\ mg}{70\ minutes} = 157.1 \frac{mg}{min}$$

Equation 4

Where:

V_{booth} = Volume of aerosol exposure booth
$m_{aerosol}$ = Mass of aerosol required in the given volume to meet the target concentration of 167 mg/m^3 over 30 minutes
$rate_{aerosol}$ = Rate of aerosol generation required in the given volume to meet the target concentration of 167 mg/m^3 over 30 minutes
m_{actual} = Mass of aerosol actually generated from the volume aerosolized
$rate_{actual}$ = Rate of aerosol generation actually achieved over the exposure time

In addition to calculations to determine the appropriate volume of contaminant to be delivered and the time it would take to do that, measurements were taken to determine the particle size characteristics. A NanoScan Scanning Mobility Particle Sizer (SMPS) Spectrometer (TSI Inc., Shoreview, MN) was used to sample the aerosol. Sampling was done in the aerosol test chamber described in Chapter III. Sampling was isokinetic to the direction of airflow and the end of the probe was placed 4.5 feet downstream of the nebulizer. Due to equipment scheduling issues, only two individual runs were able to be completed. Samples were taken every minute for the duration of each run (60 and 65 minutes), as well as for short periods before and after to determine background levels of

particles and ensure that levels of particles were reduced to background before the chamber was opened. Results of these two runs showed that the total number of particles generated varied greatly, both within and between runs (ranges of 641 – 14747, and 6409 – 59161 for runs 1 and 2 respectively). Particle size distributions based on the average count per bin in each run are shown in Figure 6. A summary of the size characteristics is shown in Table 4. The count mean diameter was 84.4 nm and the mass mean diameter was 197.0 nm. These are small particles, which represent aerosols defined as fumes, smogs, smokes, fogs, and mists [35]. Aerosols in this size range can be generated by combustion (oil, tobacco, diesel smoke). In addition, many bioaerosols are in this size range [35]. The characterization of this aerosol as an ultrafine aerosol means that the particles would behave similarly to gas molecules, further justifying the use of this aerosol as a sarin simulant. The characteristics of aerosols generated during experiments at-home were assumed to be similar to those generated in these tests. The nebulizer was run by using compressed air at a pressure of 20 psi, set by use of an in-line pressure regulator. Tests conducted at UES used the building compressed air line, while tests conducted at home utilized a small personal air compressor. The SMPS was chosen based on a study which examined the influence of nebulizer flow rates on particle size distributions, as well as a second study which reported that the peak of the distribution of their particles was just under 1 μm [36], [37]. Additionally, while Collison nebulizers can generate particles greater than 400 nm in size, equipment scheduling issues also prevented the measurement of particles by any other instrument to determine the

distribution at other sizes. One study reported that only 1% of particle generated are larger than 10 µm so it was presumed that smaller sizes would be of more interest [38].

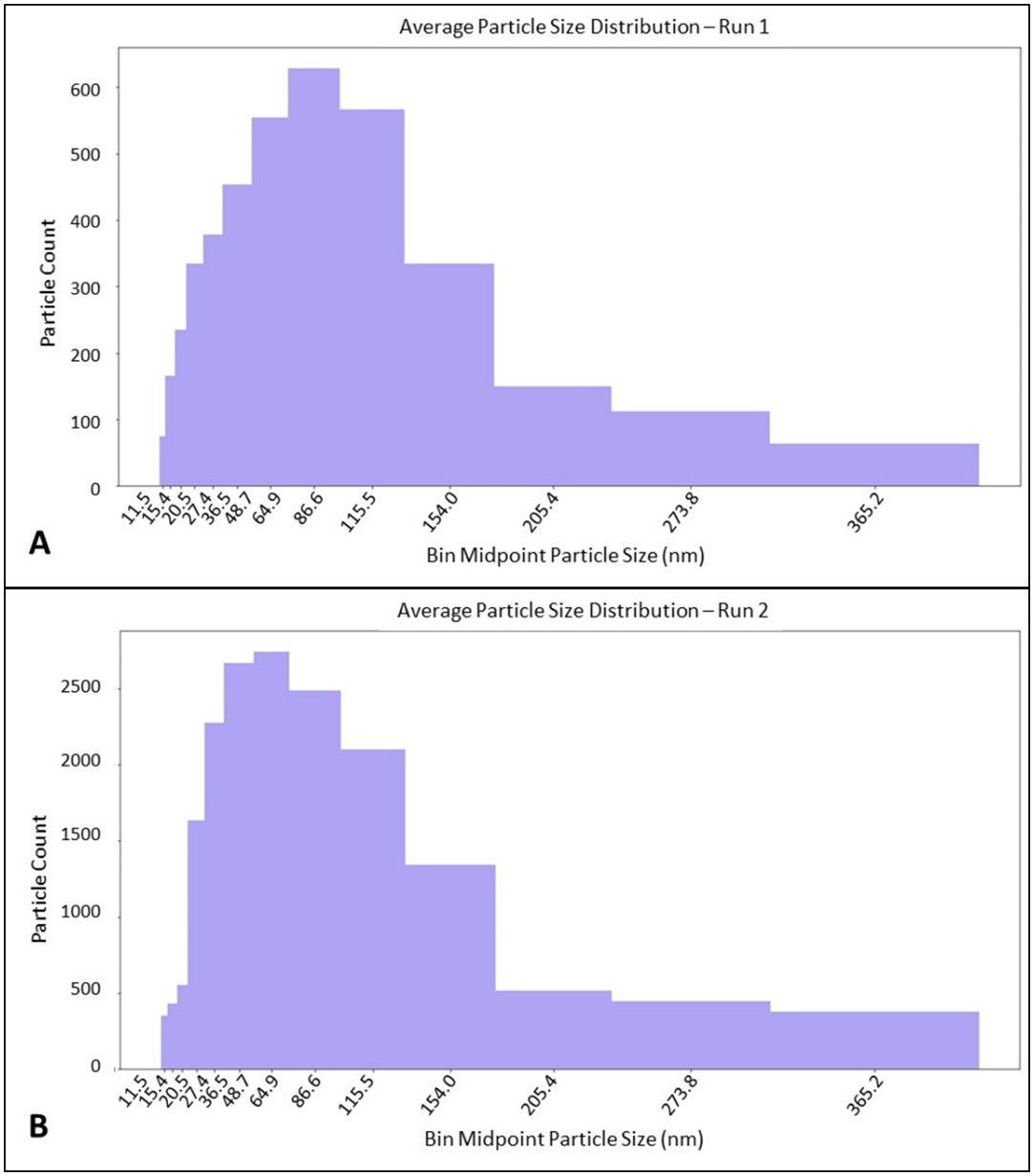

Figure 6. Particle Size Distribution. A) First Run. B) Second Run.

Table 4. Particle Size Characteristics Summary

Count Mean Diameter	84.4 nm
Count Median Diameter	64.8 nm
Mass Mean Diameter	197.0 nm
Mass Median Diameter	188.2 nm

Aging of Chemical Warfare Agent Simulant Dye

Before any experiments were undertaken, a single pilot experiment was conducted to ensure that there was no significant loss of fluorescence of the dye due to exposure to the UV light over the course of imaging. To achieve this, a dilution series was created of the water-based dye in water from 1:1 to 1:24, as well as 10-fold dilutions from 1:10 through 1:10000 and a concentrated drop of dye. This was set up in the imaging booth in front of the camera on the video setting. A video was started recording, then the UV lights were turned on. Five seconds of the video were analyzed frame by frame (60 frames per second) for brightness of fluorescence. These five seconds captured one second prior to the light being turned on as well as four seconds after the light was turned on. Immediately after the lights were turned on it took a few frames for brightness to peak, but once peak brightness was achieved, intensity was constant throughout the analyzed period.

Exposure Booth and Set-Up

Exposures for most of the data sets collected were carried out at the author's home. To create an enclosed space to contain the aerosol during the exposure period, a

commercial camping shower tent was used (Ozark Trail, Walmart Inc., Bentonville, AR). It has dimensions of 48” long by 48” wide by 86” tall. Mesh openings at the bottom and top were sealed by duct taping plastic over the openings. The tent had a small slit which was used to feed the air hose for the nebulizer into the tent. During trials the nebulizer was placed into a cardboard stand in one corner of the tent, at waist height of the mannequin. The aerosol outlet was pointed away from the mannequin to prevent immediate impact onto the mannequin’s side. The mannequin was positioned in the opposite corner of the tent to provide as much space for aerosol to flow around the mannequin while still being separated from the nebulizer (Figure 7).

Figure 7. Exposure booth showing mannequin and nebulizer placement.

For experiments carried out in the MURPHEE aerosol chamber, set-up was somewhat different. The nebulizer was clamped to a ring stand with the aerosol outlet perpendicular to the airflow. The aerosol outlet was located 1.5 feet from the walls and floor and 2 feet upstream of the mannequin's head. For these tests, it was attempted to suspend the mannequin using wall hooks attached to the upper corners of the chamber and fishing line strung between the two with the mannequin's neck and ankles resting in each fishing line loop (Figure 8). This was to allow air to pass around all sides of the mannequin and facilitate contamination of the back of the mannequin as well as the front. However, during the first trial the fishing line was not secured properly so the mannequin fell to the bottom of the chamber where it remained for the remaining 65 minutes of the exposure period. A better method to secure the line was derived for the second and third runs to ensure that the mannequin remained suspended. During these trials, the fan was turned on to 0.2 m/s (16 Hz) and allowed to run for 1 minute to stabilize airflows prior to the start of aerosol generation. The fan continued to run for 10 minutes after the end of aerosol generation to allow any remaining aerosol to disperse before chamber entry.

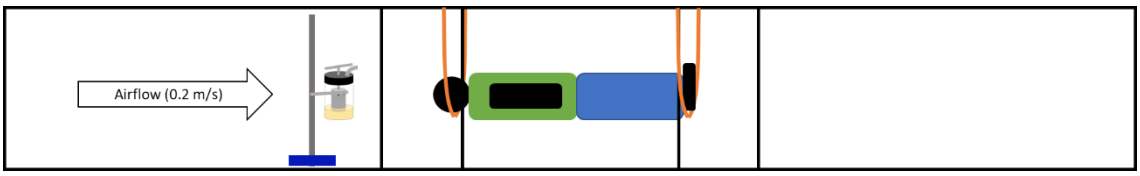

Figure 8. Mannequin and nebulizer placement within the MURPHEE aerosol chamber.

Disrobing after Experiments

Disrobing of the mannequin after exposure was done by simulating a non-ambulatory patient scenario. This was done by cutting clothing off using bandage scissors (Walgreens Bandage Scissors, Walgreen Co., Deerfield, IL) down the chest of the

mannequin from neck to waist, then down each sleeve from the neckline to the wrist [39], [40]. Pants were cut by starting at the waist and cutting down each leg [39], [40]. The cut clothing was then pulled from underneath the mannequin.

Development of a Wet Decontamination Protocol

Decontamination was also conducted by simulating a non-ambulatory patient. A 3-minute decontamination protocol was developed based on two disaster planning guidance documents and AFTTP 4-42.32 which provided vague guidance which was clarified by communication with the In-Place Patient Decontamination (IPPD) team from the 88th Medical Group at Wright-Patterson Air Force Base. The National Planning Guidance for Communities (NPGC), developed by the Department of Homeland Security and the Department of Health and Human Services recommends using a high volume but low pressure (50-60 psi) stream of tepid water to wash casualties [8]. They also recommend limiting the wet decontamination process to 3 minutes or less in order to avoid the possibility of the wash-in effect [8]. The wash-in effect is when dermal absorption of a chemical is enhanced due to the presence of water [41]. The Primary Response Incident Scene Management (PRISM) guidance for chemical incidents recommends a protocol which takes ~4 minutes for a non-ambulatory patient [7]. This protocol suggests taking 90 seconds to perform a rinse-wipe-rinse of the front of the patient's body. Then the patient is carefully rolled to the side and another 90 second interval is used to perform the rinse-wipe-rinse of the patient's back, as well as the spinal board used to move the patient through the technical decontamination line. The patient is returned to their back and a final 10 seconds are taken to do a final rinse of the patient. In

addition to these timings, it is recommended that the water be warm (95-104°F), a detergent should be used if available (0.1-0.5% v/v) along with a washing aid (such as a sponge), and that washing should be done from head to toe to avoid cross contamination of the face [7]. Finally, AFTTP 3-42.32 provides vague guidelines, including that patients should be disrobed, followed by decontamination using soap (dishwashing liquid, such as Dawn) and water, but no specifics on the protocols to be used for decontamination [6]. The IPPD group at WPAFB shared their training information to clarify some information and recommended washing the patient from head-to-toe and from the midline to the side. Their protocol recommends washing the patient's front using a sponge and water containing detergent (10 oz per gallon of water), rolling the patient to one side and washing the back as well as the litter, rolling the patient to the other side and washing the back and litter then rinsing using plain water [39]. The patient is then returned to their back and the front is rinsed using plain water [39]. In addition, the water nozzles have a mist-like dispersal pattern.

These documents and discussions resulted in the creation of a decontamination protocol which was used in all trials. Timing of steps is shown in Table 5. In total the decontamination protocol took 3 minutes. The water source was a common house outside faucet with attached hose splitter to allow both soapy and plain water to be used during the experiments. Soap (Dawn Dishwashing Detergent, Procter and Gamble, Cincinnati, OH) was delivered by placing neat detergent into a hose end sprayer (ORTHO Dial n' Spray, Scotts Miracle-Gro Company, Marysville, OH). The sprayer was set on a shower setting and the dilution rate was set to 8 oz per gallon which was the highest setting. This

sprayer was used for the wash steps of the decontamination protocol, while the rinse steps utilized an adjustable spray pattern hose nozzle, also set to the shower setting (Black & Decker, Jackson, TN). While a mist-like spray was desired, it was not possible to set the soap sprayer to this type of spray, so both water sprays were kept consistent with the shower spray pattern. The flow rates for each sprayer were measured to be 2.002 gallons per minute (GPM) for the soap dispenser sprayer and 0.739 GPM for the plain water sprayer.

Table 5. Decontamination Protocol Timings

Time after start (seconds)	Step of Protocol
0-15	Wash front and down sides with soapy water and sponge
15-30	
30-45	
45-60	Roll onto side, wash back, exposed side, and litter with soapy water and sponge
60-75	
75-90	
90-105	Roll to other side, wash back, exposed side, and litter with soapy water and sponge
105-120	
120-135	Rinse back, exposed side, and litter with plain water
135-150	
150-165	Roll onto back, rinse front with plain water
165-180	

Photobleaching of Chemical Warfare Agent Simulant Dye

Due to the location used for the decontamination procedure (outside in the author's yard, in the full shade provided by a mature tree) photobleaching during the decontamination experiments was a concern. This potential issue was identified partway through data collection (after all cotton T-shirt trials and the trials comparing new and reused Tyvek suits) and thus not accounted for during initial testing but was tracked

throughout the rest of the experiments. This was done by spray painting small cardboard coupons with the same matte chalkboard paint used to finish the mannequin. Two coupons were placed at the feet of the mannequin during exposure and imaging. During the decontamination procedure, one coupon was taken and placed near the decontamination location while the other one was left on a darkened shelf during that time. A pilot was also done where one coupon was placed in direct sunlight for 20 minutes while the other was kept in the dark.

Table 6 contains a summary of the number of replicates and other details about all of the experiments run.

Table 6. Summary of Experiments Run

Location	Description/Purpose	Decon Conducted?	Number of Replicates
Home, tests performed using an enclosed exposure booth	Cotton clothing (black t-shirt and pants)	No	6
	Tyvek (ankles, wrists, neck open) Done to test whether suits can be re-used reliably	Yes	5 (2 new suits, 3 re-used suits)
	Tyvek (ankles, wrists, neck open) New suits used for every replicate, photobleaching control in use	Yes	15
	Tyvek (ankles, wrists, neck taped) New suits used for every replicate, masking tape or duct tape used to secure cuffs and neckline, photobleaching control in use	Yes	15
	JSLIST suit, all ties tied as tightly as possible, photobleaching control in use	Yes	1
UES, tests performed in the MURPHEE aerosol chamber	Tyvek (ankles, wrists, neck taped) New suits used for every replicate, masking tape used to secure cuffs and neckline	No	3

Image Processing and Analysis

After experiments were completed, the images were processed to aid further analysis. Processing included separating the JPEG and NEF file types into different folders to allow them to be used for separate purposes. Due to compression algorithms used to reduce the file size of JPEGs, they are not suitable for quantitation but are helpful for other purposes. NEF is a proprietary raw file type which means that no compression algorithms are used making this the suitable file type for analysis.

After separating the images by file type, the images were relabeled to allow them to be organized by body region. A four-letter naming scheme, along with two sets of numbers, was used to identify images. In addition, the original file name was maintained for data integrity and to allow easier cross-referencing between the two file types. This resulted in file names of the format: ABCD_#_# DSC_####, which is elaborated upon in Table 7.

After images were renamed, the NEF files were converted to TIF format using a proprietary, but freely available, software, CAPTURE NX-D (Nikon Inc. USA, Melville, NY). NEF images were taken at the highest bit depth possible, 12-bit. However, the TIF format only supports 8- or 16-bit images. To avoid creating artefacts by converting to a larger number of bits, the images were converted to 8-bit TIF files using the software.

Table 7. Description of Naming Conventions Used

ABCD				#	#	DSC_####
Description of body region, side of body, whether clothing was present, and whether exposure had occurred or not				Shutter speed used	Replicate number	Original file name assigned by camera during capture
A	B	C	D			
Body Region	Side of Body	Clothing Presence	Exposure Status			
F = feet	F = front	N = no clothing	B = before exposure	1 = 1 second exposure	1	
M = middle/ Torso	B = back	C = clothed	P = post exposure	2.0 = 1/2 second exposure	2	
H = head			N = after patient decon	2.5 = 1/2.5 second exposure	3	
FFNP_2.0_2 DSC_0229	This file name indicates that the image is of the feet and legs region of the mannequin's front, that the image was captured after exposure took place and that the mannequin is unclothed (meaning that disrobing has already occurred).					

The open source software ImageJ (FIJI) was used to analyze images for area of contamination and differences in contamination before and after exposure [42]. First, all images of a given body region, regardless of time point were opened in FIJI. Then they were sorted into a stack based on the exposure and clothing status (this combines all replicates at that state into one file). After stacking, the images were converted to 8-bit grayscale, then the stack was Z-projected by average and a new file was created. This function looks at the value of a given pixel at the same location in each image of the stack and averages these values to create a new file with a pixel in that same location with the average value. Although the camera tripod was marked to improve the accuracy of taking images of the same area of the body every time, occasionally there were issues with alignment that needed to be corrected by cropping the averaged images. Once images were cropped so they aligned correctly, the Image Calculator function of ImageJ was

employed. This function performs operations (basic math functions, minimum/maximum, difference, etc.) on two images to create a third image. For this analysis the difference function was chosen (Equation 5).

$$\boldsymbol{Difference = |img_1 - img_2|} \qquad \textbf{Equation 5}$$

Where:

Difference = Pixel value at the given location in the resulting image
img_1 = Pixel value at the given location in image 1
img_2 = Pixel value at the given location in image 2

The difference was chosen rather than a straight subtraction because it would account for potential cross contamination or "movement" of contamination during steps of the process. In addition, the subtraction function skews results towards exclusion when there are alignment issues, while the difference function skews results towards inclusion when there are alignment issues. This results in subtraction providing an underestimation of area while difference provides an overestimation of area. The Image Calculator operations that were performed are shown in Table 8.

Table 8. Image Calculator Calculations

Operation	Image 1	Image 2	Reason	Result
Difference	Post Exposure Clothed	Before Exposure Clothed	Background subtraction to remove any inherent fluorescence on clothing	Image showing only contamination due to exposure
Difference	Post Exposure Unclothed	Before Exposure Unclothed	Background subtraction to remove any inherent/residual fluorescence on skin	Image showing only contamination due to exposure
Difference	Post Decon Unclothed	Before Exposure Unclothed	Background subtraction to remove any inherent/residual fluorescence on skin	Image showing contamination left after or "moved" due to decontamination process

After the image calculations were complete, regions of interest (ROIs) for each body region were created (feet, middle, head, and front and back of each). These ROIs were applied to all images during analysis and only modified if necessary due to slight differences in position from experiment to experiment. Applying the ROI to each image limited analysis to only pixels contained within the ROI. This simplified the analysis and allowed analysis to be done only on the mannequin body without including the entire field of view (Figure 9).

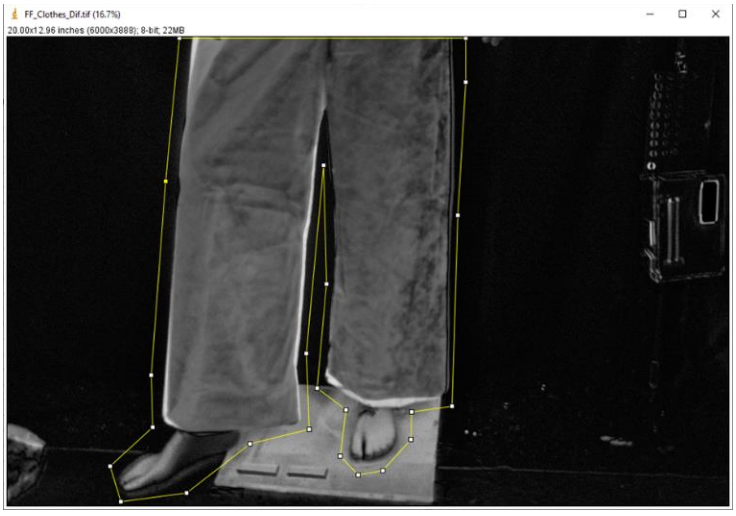

Figure 9. Clothed difference result with ROI for analysis shown in yellow.

Pixels in these images can have values ranging from 0-255 due to the 8-bit file type used in the analysis. Each value corresponds to a shade of gray (with 0 being black and 255 being white), which allows the appearance of different colors, but also the measurement of these colors in a numerical form. Early images were examined, and it was determined that shades of gray corresponding to pixel gray values of 26-255 could be considered contamination (Figure 12). This was done by trial and error which was necessitated by the difficulties in distinguishing the steps on the step-wedge, as well as a lack of sensitivity of the dilutions made to create an internal standard. The Stouffer step-wedge is a strip of film with sections of differing transmissivity (Stouffer Graphic Arts, Mishawaka, IN). This was planned to be used to correlate image gray values to optical density during the analysis process. However, due to the size of the strip compared to the field of view of the camera and resolution of images, it was impossible to distinguish between sections. The second standard was created by making a serial dilution of the UV dye (Figure 10). While brightness of fluorescence differed between droplets of the standard (i.e. between 1:10 and 1:10000), differences were not significant enough to be able to correlate brightness of fluorescence with amount of UV dye present. As a result, neither method was able to be used to calibrate images during analysis and gray values were assumed to be equivalent across all images captured.

1:10	1:100	1:1000	1:10000
1:20	1:200	1:2000	
1:30	1:300	1:3000	
1:40	1:400	1:4000	
1:50	1:500	1:5000	
1:60	1:600	1:6000	
1:70	1:700	1:7000	
1:80	1:800	1:8000	
1:90	1:900	1:9000	
1:1			

Figure 10. Dilution of each drop on the internal fluorescence standard

Figure 11A shows the appearance of the mannequin before exposure, B shows the appearance of the mannequin after exposure, and C shows the extent of contamination, represented by the difference between B and A. Figure 11C shows the image that is ultimately used to measure contamination.

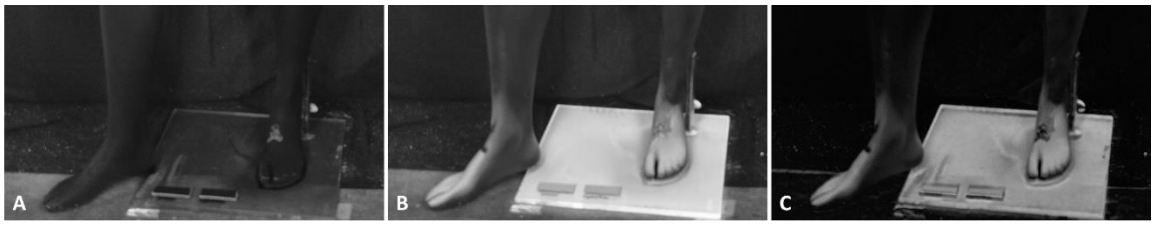

Figure 11. A) Before exposure. B) After exposure. C) Difference between before and after exposure.

Contaminated pixels are represented by larger gray values, meaning that they appear lighter in color. Figure 11C is shown again in Figure 12 along with both the background threshold (gray values 0-25, Figure 12A) and the contamination threshold (gray values 26-255, Figure 12B) applied.

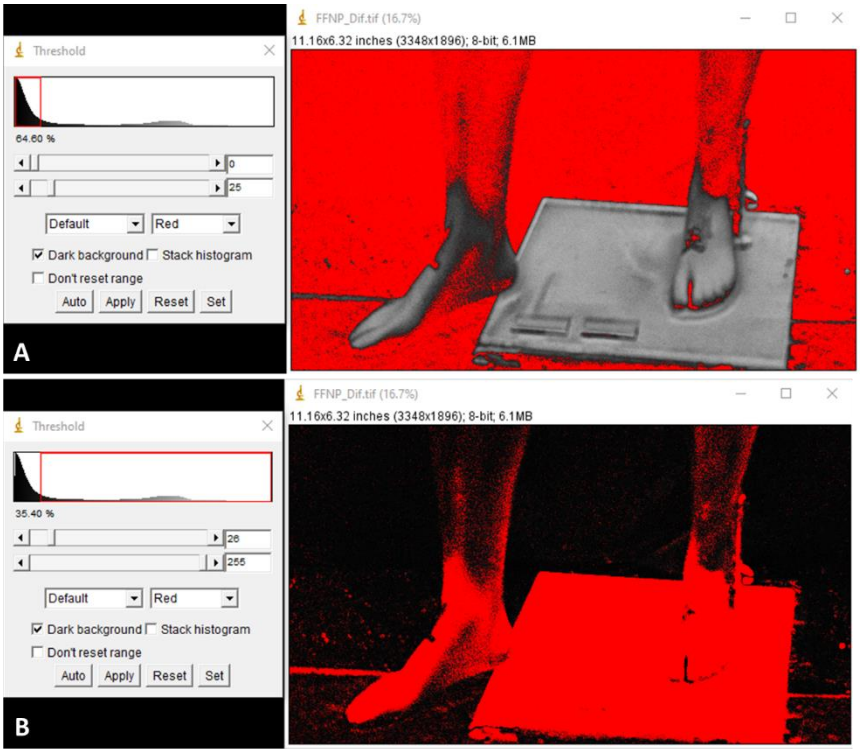

Figure 12. Measurement of contamination. A) Background threshold, 0-25 gray value. B) Contamination threshold, 26-255 gray value.

After the ROI was applied to each image, measurements were taken at three different gray value thresholds. The first two are shown above, the background and contamination thresholds (0-25 and 26-255 gray values respectively). The third threshold measured was 0-255 gray value and was used as a measure of total body area. Figure 13 shows both the contamination area and the total body area (A and B respectively). Once the threshold was applied, ImageJ automatically measured various characteristics such as the area contained at a given threshold, and mean, maximum, and minimum gray value for pixels measured and the results were exported to Excel.

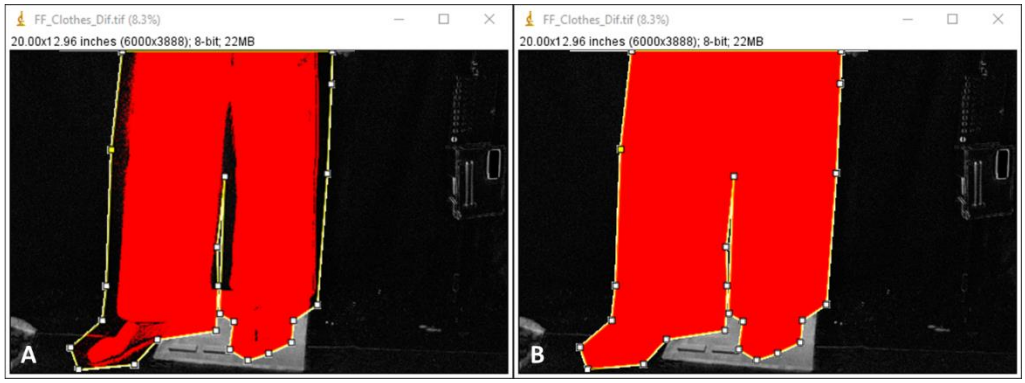

Figure 13. Representative image for measurement of contamination. A) Contamination threshold of 26-255 applied to body region. B) Total area threshold of 0-255 applied to body region.

After ImageJ measurement of the area of contamination, Excel was used to finish the analysis. First, the total body area was determined by summing the results of Figure 13B for each side of the mannequin (front and back). Then the total area of contamination was determined by summing the results of Figure 13A for each side of the mannequin. Due to the overlap between areas imaged, this total area was corrected by the amount of overlap. For instance, if the 3 images were placed side by side, the total height of the images was 9 inches. However, when they were overlapped to align correctly the height of the images might only be 6.8 inches. This height was determined for the first set of trials with black cotton clothing and the new vs re-used Tyvek trials and the average was used for all subsequent trials. This gave an average reduction in height of 21.03% so the summed areas were multiplied by 0.7897 to get the adjusted area. This is only an approximation of the true correction that would be needed, however issues with being able to align the images correctly in ImageJ necessitated this approximation. In future, it

would be ideal to be able to measure a full-body ROI area and see how that compares to the sum of individual body region ROIs.

Once the total area was corrected, the fractional area was determined for each step of the experiment (i.e. fraction of contaminated area for the front clothed, front unclothed, and front after decon) by dividing the area of contamination (gray values of 26-255) by the total area (gray values of 0-255). Next the difference in contaminated area resulting from each step (disrobing, decontamination, and aggregate difference) was calculated (Equation 6).

$$Difference_{Disrobing} = A_{Clothing} - A_{Skin,after\ exposure}$$

$$Difference_{Decon} = A_{Skin,after\ exposure} - A_{Skin,after\ decon}$$

$$Difference_{Aggregate} = A_{Clothing} - A_{Skin,after\ decon} \quad \textbf{Equation 6}$$

After the difference in contamination for each treatment was calculated the fractional reduction was calculated by dividing the calculated difference by the total area of contamination for that difference which normalized the reduction in contamination to the area actually contaminated, rather than the body area (Equation 7).

$$\%Reduction_{Disrobing} = \frac{A_{Clothing} - A_{Skin,after\ exposure}}{A_{Clothing}} * 100\%$$

$$\%Reduction_{Decon} = \frac{A_{Skin,after\ exposure} - A_{Skin,after\ decon}}{A_{Skin,after\ exposure}} * 100\%$$

$$\%Reduction_{Aggregate} = \frac{A_{Clothing} - A_{Skin,after\ decon}}{A_{Clothing}} * 100\%$$

Equation 7

In addition to these calculations, statistical tests were conducted. First, boxplots were created to show the spread of the data, a Grubbs test was used to identify outliers, and mean, standard deviation, and 95% confidence intervals were calculated. Normality was tested using the Shapiro-Wilks test which is suitable for small sample sizes. Levene's test was used to determine equal variance which can be used when data is not normally distributed. In the case of the new and re-used Tyvek suits, the Variance Ratios Rule of Thumb was also considered to determine equal variance. This rule of thumb considers variances to be equal if the ratio of the larger variance to the smaller variance has a value between 1 and 3. If the ratio is larger than 3, the variances are assumed to be unequal. Finally, a t-test was used to determine whether the means of two groups were statistically different. Welch's t-test was used if equal variance could not be assumed, while a standard Student's t-test was used if equal variance could be assumed.

Results

As a starting point for analysis and a thought experiment towards understanding whether 90% reduction in contamination is a reasonable assumption, a basic model was

created based on values from the U.S. Environmental Protection Agency's Exposure Factors Handbook [33]. Recommended average values for total body surface area and the surface area for each body part are shown in Table 9. Percent of the whole body was calculated from these values.

Table 9. Average Body Surface Area Values from the EPA Exposure Factors Handbook – Adult Male

	Surface Area (m^2)	Percent of Whole Body (%)
Whole Body	2.065714	100
Head	0.136	6.58
Trunk	0.827	40.03
Arms	0.314	15.20
Hands	0.107	5.18
Legs	0.682	33.02
Feet	0.137	6.63

These values were then used in consideration of three separate scenarios. In all three scenarios, it was assumed that deposition of the contaminant was uniform across the entire body and that there was no penetration of contaminant through clothing. The first scenario was considered to be the most protective and envisioned a military population, or civilian population during cold weather, in which long sleeves and pants would be worn, along with full-coverage shoes or boots. This would leave only the head and hands uncovered and result in 88.24% of contamination being removed by disrobing (Table 10).

The second scenario considered a civilian population in a spring or fall weather scenario, or a military population without the jacket, in which short sleeved shirt, long pants, and full-coverage shoes would be worn. This would leave approximately three-quarters of the arms uncovered, along with the head and hands, resulting in 76.84% of contamination being removed by disrobing (Table 10). The final scenario considered a civilian population in summer months and assumed that clothing would consist of short sleeved shirt, knee-length shorts, and full-coverage shoes. This leaves three-quarters of the arms, half of the legs, and all of the head and hands uncovered, which would allow just 60.33% of contamination to be removed by disrobing.

While this is a very rough approximation due to the assumptions of uniform distribution and no penetration, as well as neglecting the possible protective ability of hair, it was an interesting thought experiment. It shows that even if penetration through clothing were not a concern, that the maximum amount of contamination that would be removed by disrobing was 88%. In a less protective or less clothed situation, 60% or less of contamination would be removed by disrobing. These results were a rough approximation, but they were performed to give an indication of removal that could be expected during experiments.

Table 10. Models of Three Different Clothing Scenarios

Scenario 1 – Full Military Uniform, Civilian Winter			
Body Part	Percent Uncovered	Percent of Whole Body Uncovered	Percent of Contamination Removed
Head	100%	6.58%	88.24%
Trunk	0%	0%	
Arms	0%	0%	
Hands	100%	5.18%	
Legs	0%	0%	
Feet	0%	0%	
Scenario 2 – Partial Military Uniform, Civilian Spring/Fall			
Body Part	Percent Uncovered	Percent of Whole Body Uncovered	Percent of Contamination Removed
Head	100%	6.58%	76.84%
Trunk	0%	0%	
Arms	75%	11.40%	
Hands	100%	5.18%	
Legs	0%	0%	
Feet	0%	0%	
Scenario 3 – Civilian Summer			
Body Part	Percent Uncovered	Percent of Whole Body Uncovered	Percent of Contamination Removed
Head	100%	6.58%	60.33%
Trunk	0%	0%	
Arms	75%	11.40%	
Hands	100%	5.18%	
Legs	50%	16.51%	
Feet	0%	0%	

Photobleaching results

The pilot photobleaching trial placed the coupon in direct sunlight for 20 minutes, while the control coupon was left on a dark shelf. At the end of this time, there was a significant loss of fluorescence, indicating that photobleaching may be a source of error if the mannequin is left in direct sunlight for a period of time (Figure 14).

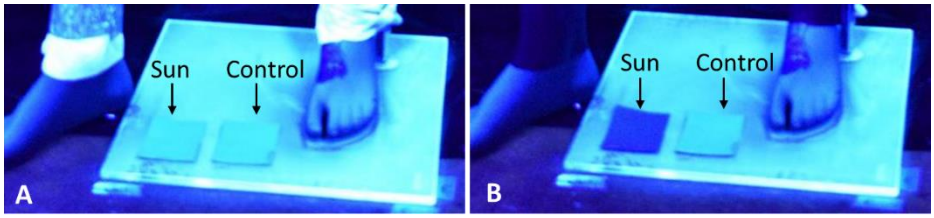

Figure 14. Initial Photobleaching Trial. A) Appearance of coupons prior to sun exposure. B) Appearance of coupons after sun exposure.

During all subsequent experiments, care was taken to ensure that the mannequin was exposed to sunlight for the minimum amount of time possible, as well as making sure that a coupon stayed with the mannequin under similar conditions when exposure to sunlight was unavoidable. Visual inspection of the coupons showed that minimal photobleaching occurred in the shade over the amounts of time exposed (Figure 15, Figure 16).

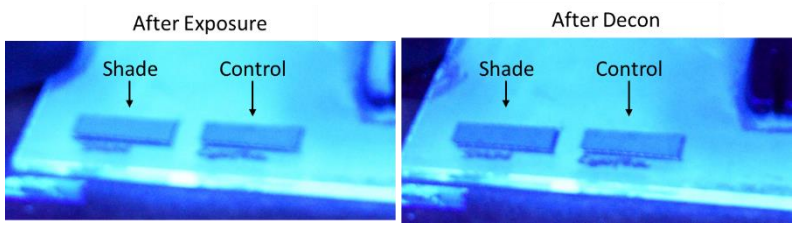

Figure 15. Photobleaching effect during a trial. A) Appearance of coupons prior to shade exposure but after contamination. B) Appearance of coupons after shade exposure during the decontamination protocol.

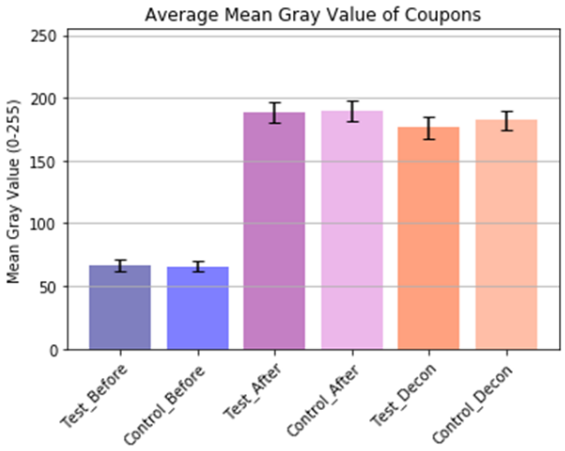

Figure 16. Average Gray Value of Coupons before exposure, after exposure, and after decontamination.

Mean gray values for both coupons before and after exposure differed little, by a value of 1.5 or less (Table 11). The mean gray values for the two coupons after decontamination differed by slightly more, a value of 5.5, but the values were within 1 standard deviation of each other. However, testing for equal means using a Mann-Whitney U-test showed that there was a significant difference in the means of the control and test coupons. This indicates that experiments may be subject to error due to photobleaching. While not ideal, these conditions are representative of the environments where mass decontamination would take place so it should not be considered a detriment to the work. This error would slightly overestimate the efficacy of decontamination, though since the difference in mean gray values is small it is expected that it would not be a significant overestimation. Maximum amount of time outside was approximately 10 minutes, with a total of 2 minutes or less exposure to sunlight during movement from the garage to the shaded area and back.

Table 11. Average Mean Gray Value of Coupons and p-values of Statistical Tests

	Mean Gray Value (95% CI)	Shapiro-Wilks (Normality)	Levene's (Equal Variance)	Mann-Whitney (Equal Means)
Test Coupon, Before Exposure	66.9 (57.4, 76.3)	0.372	0.663	0.335
Control Coupon, Before Exposure	65.9 (57.2, 74.5)	0.0423*		
Test Coupon, After Exposure	188.4 (171.5, 205.4)	0.0136*	0.728	0.641
Control Coupon, After Exposure	189.7 (173.9, 205.5)	0.734		
Test Coupon, After Decon	176.6 (159.5, 193.7)	0.0547	0.776	0.0205*
Control Coupon, After Decon	182.1 (166.3, 197.9)	0.108		
		*Not normally distributed	*Not equal variance	*Not equal means

Black Cotton Clothing Trials

Black cotton clothing was used for the initial tests but was quickly abandoned due to visualization issues (Figure 17). In these trials, only disrobing was done, no decontamination was conducted. Shown in Figure 17 are representative results from a trial which was run where the mannequin was clothed in black cotton clothing. Figure17A and B show the mannequin prior to exposure while Figure17C and D show the mannequin after exposure. Contamination, or the presence of the fluorescent dye, is demonstrated by light blue areas on the mannequin and clothing surfaces. As seen in Figure17 B and C, the mannequin's forearms are distinctly different colors before and after exposure. However, contamination on clothing is only evident in a few small spots, such as the upper right thigh, or left torso (Figure 18). This difficulty in visualization of contamination on clothing, in combination with the high amount of contamination

evident on the bare skin of the mannequin (Figure 17D), resulted in calculation of negative decontamination due to disrobing (i.e. that disrobing *caused* contamination of the skin, rather than removing it). This error is shown in Figure 19.

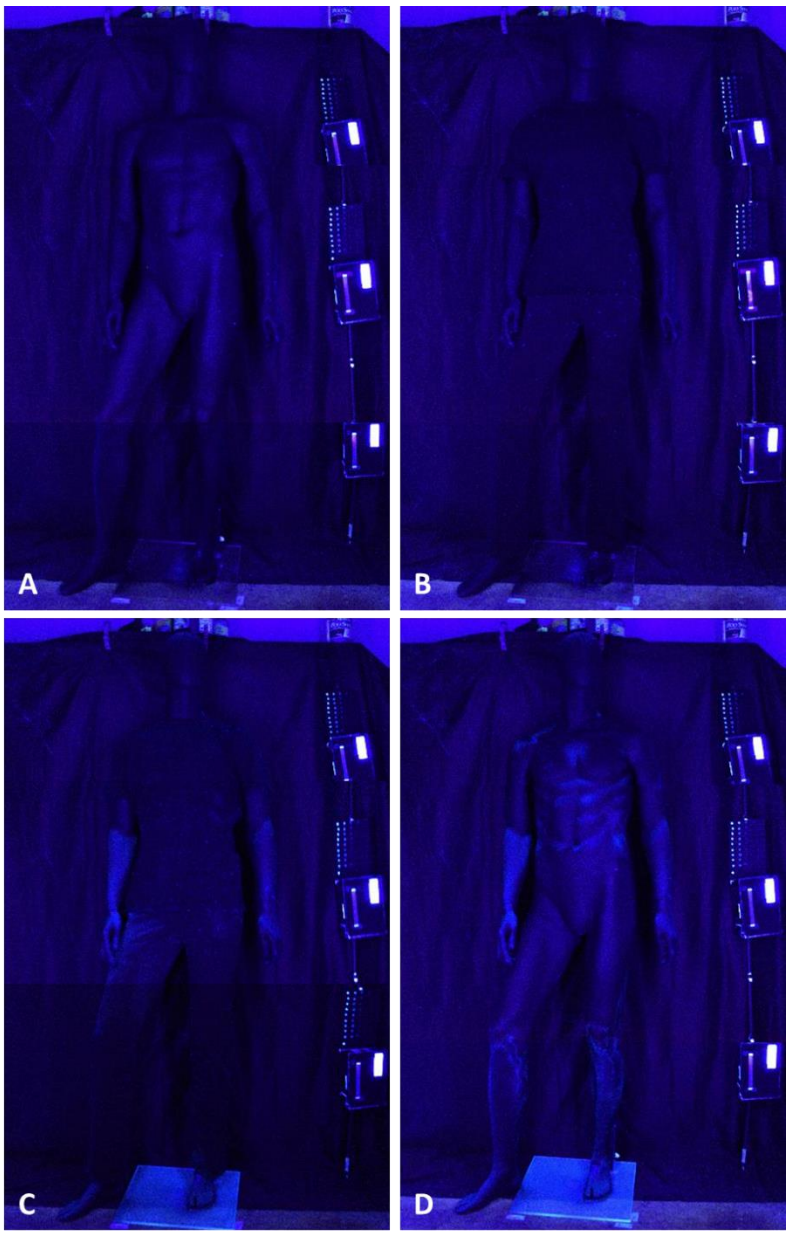

Figure 17. Representative images from a black cotton trial. A) Mannequin, no clothing, prior to exposure. B) Mannequin, clothed, prior to exposure. C) Mannequin, clothed, after exposure. D) Mannequin, no clothing, after exposure.

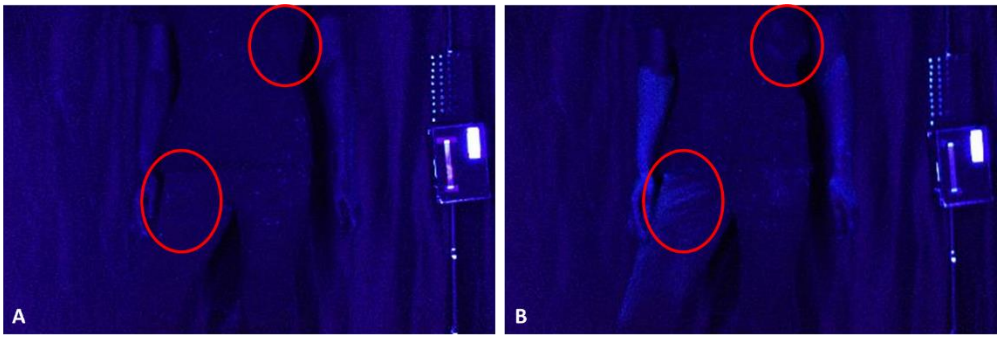

Figure 18. Comparison of clothed torso before and after exposure. Circled areas are the same location on both images. A) Before exposure. B) After exposure.

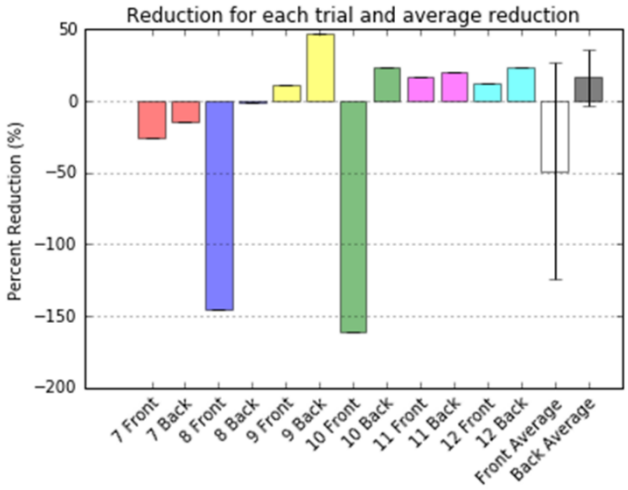

Figure 19. Percent reduction in contamination due to disrobing in each trial.

Each trial is shown in a separate color, with both front and back values shown side by side. The white bar shows the average percent reduction for the mannequin front with error bars. The black bar shows the average percent reduction for the mannequin back. Visual images for Trial 8 are shown in Figures 17 and 18. Trial 8 in particular shows significant negative reduction in contamination due to disrobing, with a -145.8% reduction in contamination (or an apparent increase in contamination of 145.8% due to

disrobing). In addition, due to visualization difficulties, the variability and error was very high within this data set (range of 178.3 and 61.5 and standard deviations of 75.5 and 19.8 for front and back respectively).

Re-Used Tyvek Suit Trials

Due to supply chain issues once the decision was made to move away from black cotton clothing it was proposed that perhaps the Tyvek suits could be re-used for some trials until new supplies were acquired. Towards that end a pilot experiment consisting of five total data points was conducted. Two trials were done using brand new suits which were then washed with soap and water and dried after each trial, while 3 trials were conducted using suits which had been re-used. Representative images from two trials are shown in Figure 20.

Visual analysis of the images shows that there is significant residual fluorescence on the re-used suit, even after washing with soap and water (Figure 20 B and G). In addition, either residual dye on the inside of the suit or a loss of suit integrity due to the washing process resulted in much higher fluorescence on the mannequin surface after exposure and disrobing. There was little difference between the new and re-used suits as far as extent of contamination on the clothing or extent of residual contamination after decontamination (Figure 20 C and H and Figure 20 E and J).

Figure 20. Representative images from 1) Trial with new suit and 2) Trial with re-used suit. From left to right images show the mannequin before exposure (A, B, F, G), the mannequin after exposure (C, D, H, I) and the mannequin after decontamination (E, J).

Figure 21 shows a summary of the results of this experiment. Disrobing data (shown in oranges and blues) indicates that a higher percentage of contamination is removed by disrobing when a new suit is used (dark orange and dark blue bars), while a much lower percent is removed when a re-used suit was used (light orange and light blue bars). Total removal due to both steps was calculated as well (reds and purples) and was shown to be slightly higher for the new suit than the re-used suit. As mentioned, this could be due to there being less of a difference calculated by ImageJ due to residual fluorescence, or the much higher contamination on the body surface. While disrobing was shown to be less effective when suits were re-used, this was understandably reversed

when decontamination is considered (pinks and greens). Decontamination after being protected by a new suit removed a smaller percentage of contamination than did decontamination after use of a re-used suit. Logically this is due to the much higher percentage of total body area contaminated when a re-used suit was used.

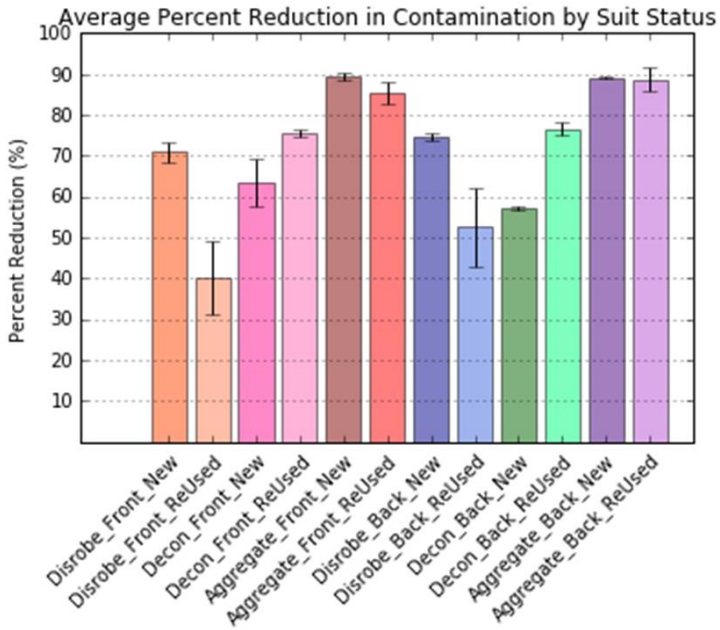

Figure 21. Summary of results from New vs Re-Used Suits.

Data was tested for normality when possible (Shapiro-Wilks test), equal variance (Levene's test), and then equal means (Welch's t-test) (Table 12). In addition, visualizing the data as boxplots helped show that reduction for Disrobe Front and Decon Back were statistically different (Figure 22). However, due to small sample sizes the power of the statistical tests conducted is limited. Aggregate decontamination was not statistically different between the new and re-used suits.

Table 12. P-values for Statistical Tests Conducted

	Shapiro-Wilks (Normality)	Levene's (Equal Variance)	Variance Ratio Rule of Thumb (Equal Variance)	Welch's t-test (Equal Means)
Disrobe Front, New	*	0.218	12.6^	0.0288~
Disrobe Front, Re-used	0.578			
Disrobe Back, New	*	0.113	112. 6^	0.0803
Disrobe Back, Re-used	0.470			
Decon Front, New	*	0.000581+	33.5^	0.275
Decon Front, Re-used	0.157			
Decon Back, New	*	0.183	7.0^	0.000826~
Decon Back, Re-used	0.246			
Total Front, New	*	0.195	13.3^	0.154
Total Front, Re-used	0.519			
Total Back, New	*	0.0941	153.9^	0.888
Total Back, Re-used	0.380			
	*Cannot test for normality on only 2 points. In addition, power of testing normality on 3 points is limited.	+Unequal variance, though due to small sample size these results should not be assumed to be absolute	^Variances are not equal. If the ratio is < 3, variances can be assumed to be equal	~Means are not equal. However, power is limited due to small sample sizes

Due to the statistical difference of 2 out of 6 sets of data, it was decided that further experiments would need to be performed either with only new or only re-used suits. Re-using suits for more than one trial raised questions of how many times a suit

would be able to be re-used without significantly impacting the results so the latter option was chosen and all subsequent testing was performed using new Tyvek suits for one run each and then discarding them as intended.

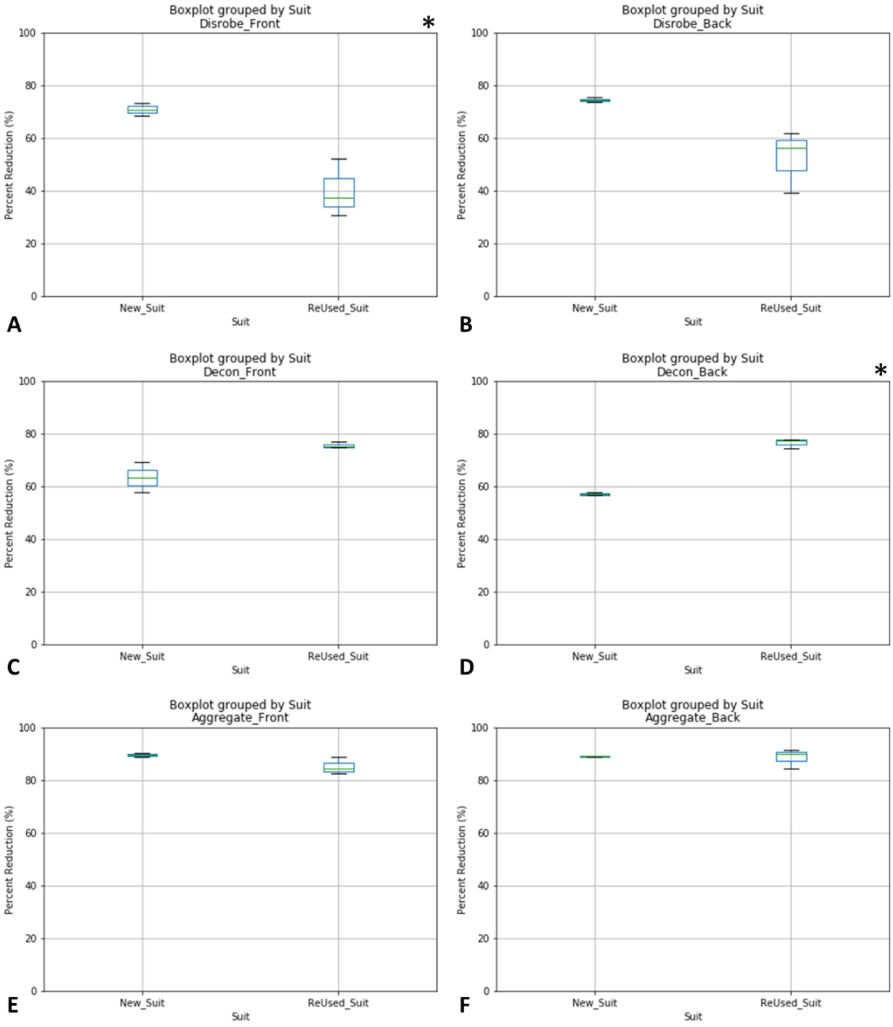

Figure 22. Summary of results from New vs Re-Used Suits. A) Disrobe Front, statistically different ($p = 0.0288$). B) Disrobe Back, not statistically different ($p = 0.0803$). C) Decon Front, not statistically different ($p = 0.275$). D) Decon Back, statistically different ($p = 0.000826$). E) Aggregate Front, not statistically different ($p = 0.154$). F) Aggregate Back, not statistically different ($p = 0.888$).

Tyvek Cuffs Open Trials

These trials were done in order to simulate an unprepared military population (wearing normal uniform but not protective gear) or a civilian population who would not have protective gear available. Representative images are shown in Figure 23.

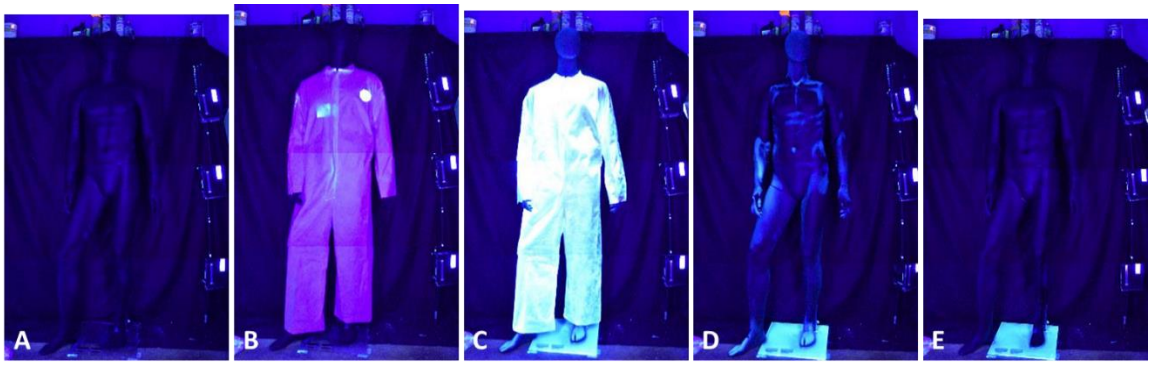

Figure 23. Representative Images from a trial with Tyvek, Cuffs Open. A) Unclothed mannequin, before exposure. B) Clothed mannequin, before exposure. C) Clothed mannequin, after exposure. D) Disrobed mannequin, after exposure. E) Unclothed mannequin, after decontamination.

The results of this experiment showed that disrobing alone removed 65-77% of contamination, while decontamination removed an additional 58-87% of contamination (Figure 24, Table 13). This resulted in an aggregate removal of contamination of 89-96% of contamination (Figure 24, Table 13).

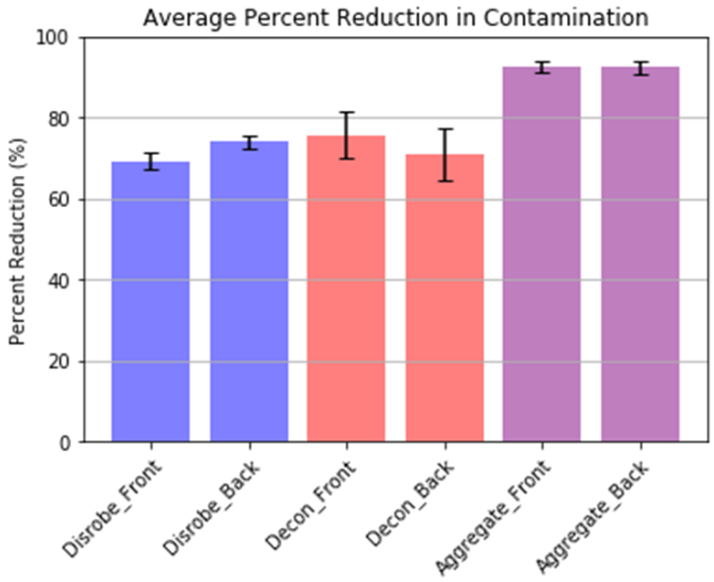

Figure 24. Summary of results from Tyvek, Cuffs Open Trials

Table 13. Summary Statistics for Percent Reduction for Tyvek, Cuffs Open Trials

	Mean Percent Reduction (%) (95% C.I.)	Standard Deviation (%)	Shapiro-Wilks Test p-value (Normality)
Disrobe Front	69.2 (64.9, 73.6)	2.22	0.845
Disrobe Back	73.9 (70.5, 77.2)	1.70	0.283
Decon Front	75.7 (64.3, 87.1)	5.81	0.00597*
Decon Back	70.7 (58.0, 83.4)	6.49	0.520
Aggregate Front	92.6 (89.7, 95.4)	1.46	0.0394*
Aggregate Back	92.3 (89.1, 95.6)	1.68	0.704

Standard deviations were higher for decontamination (5-7%) than for disrobing (1.5-2.5%) and total reduction (1-2%). This could be due to the fact that while exposure was completely hands-off and disrobing was minimally involved, decon was a very manual process. While every effort was made to perform the decontamination protocol in

the same manner, human behavior is variable and thus researcher behavior likely influenced the high variability and ranges evident in the decontamination step.

In addition, a Grubbs test was performed to determine if any outliers existed within the data. One was found in the Decon Front dataset (circled in red in Figure 25).

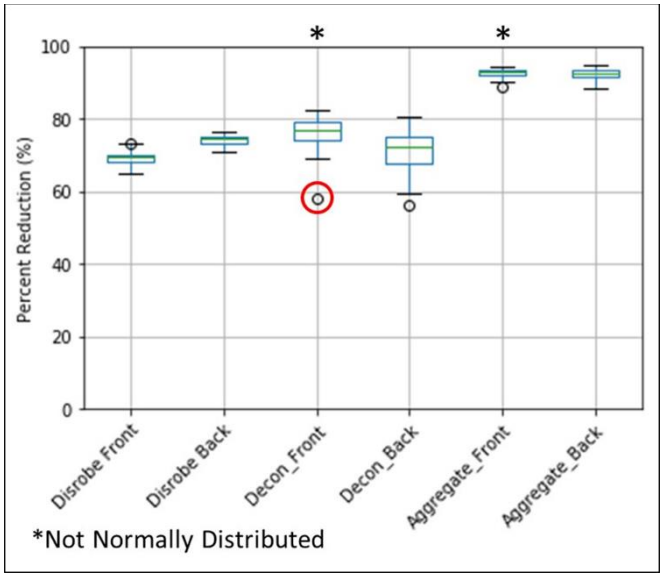

Figure 25. Summary of boxplot results from Tyvek, Cuffs Open Trials, outlier circled in red

Tyvek, Cuffs Taped Trials

These trials were done to simulate a military population which was prepared for a possible chemical warfare attack and would be dressed in full JSLIST suit. Representative images are shown in Figure 26. Visually, these results show that well-sealed Tyvek (when cuffs are secured by tape) is highly protective, even in situations with high aerosol concentration.

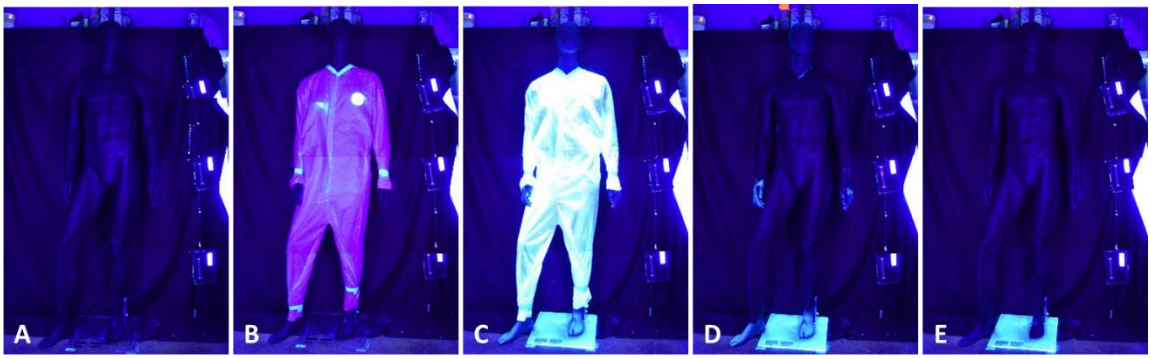

Figure 26. Representative Images from a trial with Tyvek, Cuffs Taped. A) Unclothed mannequin, before exposure. B) Clothed mannequin, before exposure. C) Clothed mannequin, after exposure. D) Disrobed mannequin, after exposure. E) Unclothed mannequin, after decontamination.

In addition to visual measures of area of contamination, the average total area of contamination (gray values 26-255) was calculated (Figure 27). Darker bars indicate front of the mannequin values, while lighter ones indicate the back of the mannequin. Red bars show the area of contamination on the Tyvek suit, while green bars show the area of contamination on the mannequin skin.

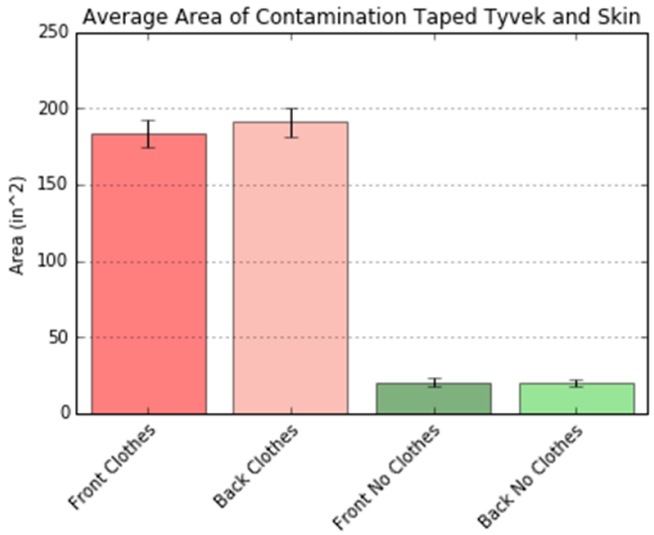

Figure 27. Average Total Area and Area of Contamination on Taped Tyvek.

The results of these trials show that variability is lower for disrobing and total removal than for decontamination (Figure 28). As previously mentioned, this is likely due to variations in researcher behavior during decontamination. In addition, the very small amount of contamination present on the body means that if a spot is left contaminated it is a larger percentage of the whole contaminated area than is the case when large areas of the body are contaminated to start with, such as in the Tyvek, Open Cuffs trials. As in the Tyvek, Open Cuffs trials, standard deviations are higher for decon (11-14%) than for disrobing (1-2%) or total reduction (1-2%) (Table 14). In addition, the Shapiro-Wilks test for normality showed that only one dataset, the Decon Front set was not normally distributed (Table 14).

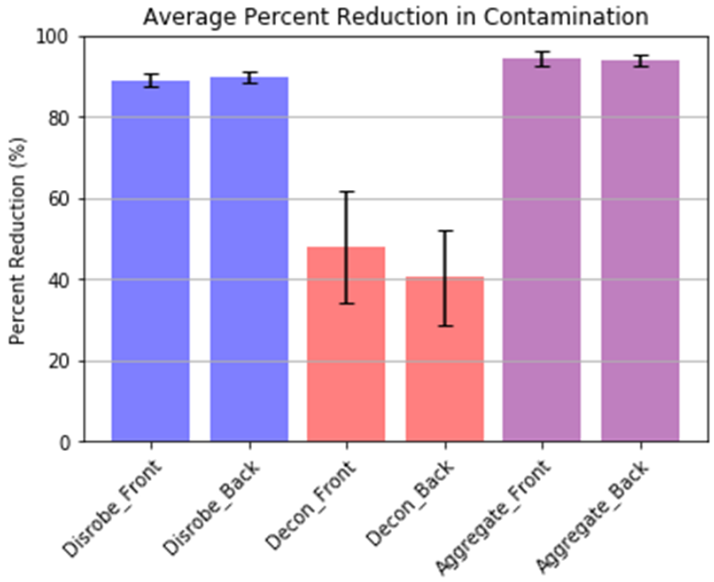

Figure 28. Summary of results from Tyvek, Cuffs Taped Trials

Table 14. Summary Statistics for Percent Reduction for Tyvek, Cuffs Taped Trials

	Mean Percent Reduction (%) (95% C.I.)	Standard Deviation (%)	Shapiro-Wilks Test p-value (Normality)
Disrobe Front	88.9 (85.7, 92.2)	1.65	0.690
Disrobe Back	89.7 (87.2, 92.3)	1.29	0.567
Decon Front	47.9 (20.9, 75.0)	13.8	0.0406*
Decon Back	40.4 (17.5, 63.3)	11.7	0.215
Aggregate Front	94.2 (90.8, 97.6)	1.74	0.0566
Aggregate Back	93.9 (91.0, 96.8)	1.48	0.260

The Grubbs test showed that one outlier existed within the dataset, in the Decon Front data (circled in red in Figure 29).

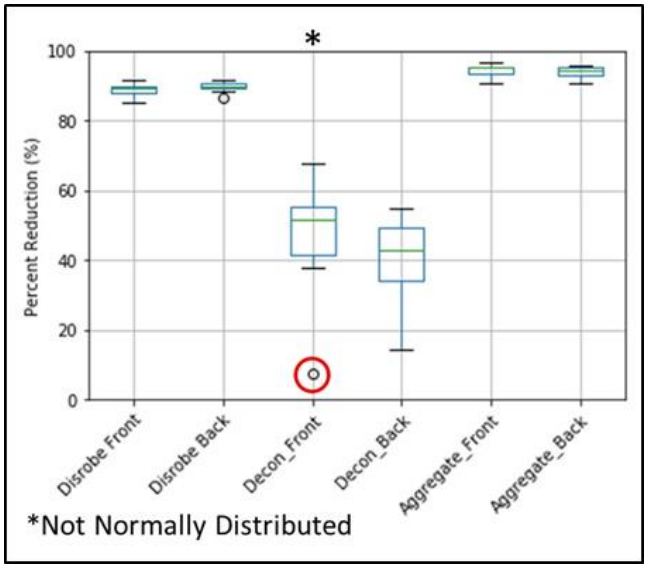

Figure 29. Summary of boxplot results from Tyvek, Cuffs Taped Trials, outlier circled in red

JSLIST Suit Trial

Since one JSLIST suit was available a trial was run using this suit. It was expected to be similar to the results of the taped Tyvek trials. As seen in Figure 30 however, contamination was seen on the skin surface at places that were covered by the uniform. Due to the thickness and absorbent charcoal lining of the JSLIST, it is more likely that the aerosol migrated through small openings at the neck, wrists, and ankles than through the fabric of the jacket though neither theory can be confirmed. However, this indicates that under conditions where personnel are exposed to high concentrations of hazardous aerosol for long periods of time that there is a possibility of aerosol penetrating even this protective equipment resulting in contamination to the warfighter.

Figure 30. Images from JSLIST suit trial. A) Unclothed mannequin, before exposure. B) Clothed mannequin, before exposure. C) Clothed mannequin, after exposure. D) Disrobed mannequin, after exposure. E) Disrobed mannequin, after decontamination.

These data show that disrobing is relatively effective at removing contamination (63-75% removal) while decon removes an additional 60-78% of contamination and aggregate removal reaches 92% (Figure 31). However, this is only one data point and no firm conclusions should be drawn from this point.

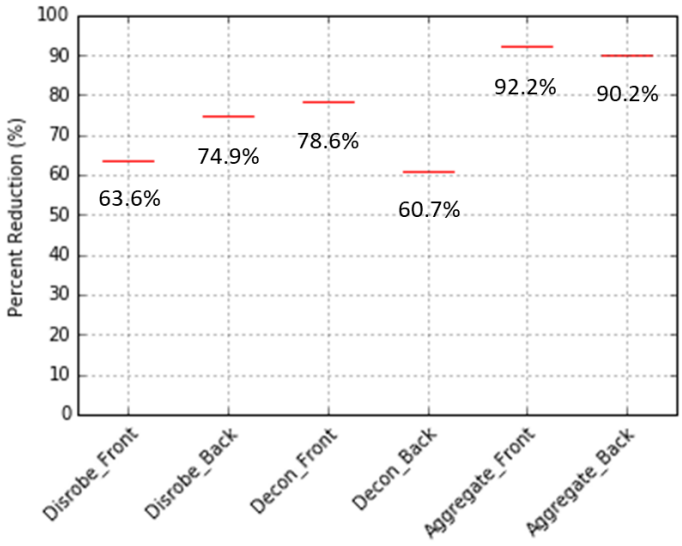

Figure 31. Summary of boxplot results from JSLIST Trial

Due to the visualization issues inherent in using fabric clothing, an analysis was run which considered the average amount of contamination on Tyvek (taped cuffs) to be a surrogate for the amount of contamination expected on the JSLIST (See Figure 27 above, Figure 32). Orange bars show the reduction calculated from the extent of contamination visualized on the JSLIST suit itself, while blue bars show the reduction that would be expected if the true contamination were the same as that visualized on taped Tyvek. Understandably, the reduction is higher using surrogate data than the JSLIST values, due to the nature of visualization on the clothing material (values increased from 64-75% to 77-85%).

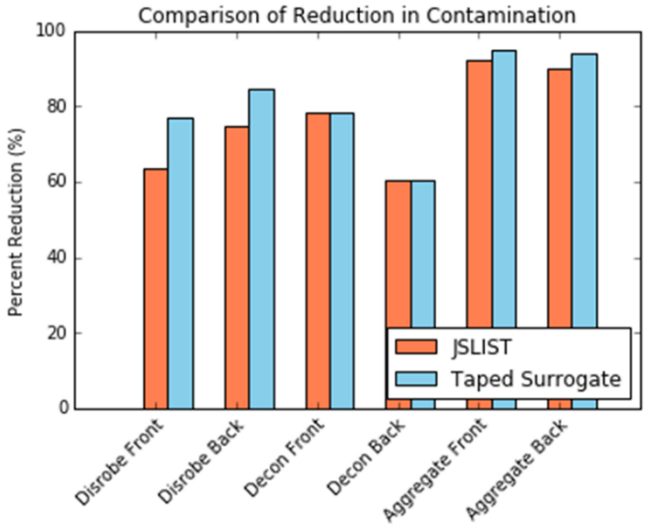

Figure 32. Comparison of Reduction in Contamination using Taped Tyvek Total Contamination as a Surrogate for JSLIS Contamination

As the taped Tyvek was intended to be a simulant for the JSLIST clothing scenario, several tests were conducted to determine whether the JSLIST data point could have from the Tyvek taped data set. First the Taped Tyvek dataset was plotted, with the JSLIST points overlayed to show where they fall in relation to the full dataset (Figure 33). Figure 33A shows the boxplot of the Taped Tyvek data, while B shows all points in the dataset as a scatter plot, showing that the JSLIST points are distant from the Taped Tyvek points. Then the JSLIST data point was added to the Taped Tyvek dataset and a Grubbs test was conducted to determine whether the JSLIST point was considered an outlier in the dataset, as well as considering the three standard deviations rule of thumb for outliers. The Grubbs test showed no outliers, which would indicate that the point may be considered part of the dataset, though the 3 standard deviations rule shows that the

JSLIST point is not part of either Disrobe dataset (Table 15). Further replicates would allow a t-test to be conducted which could give a better idea.

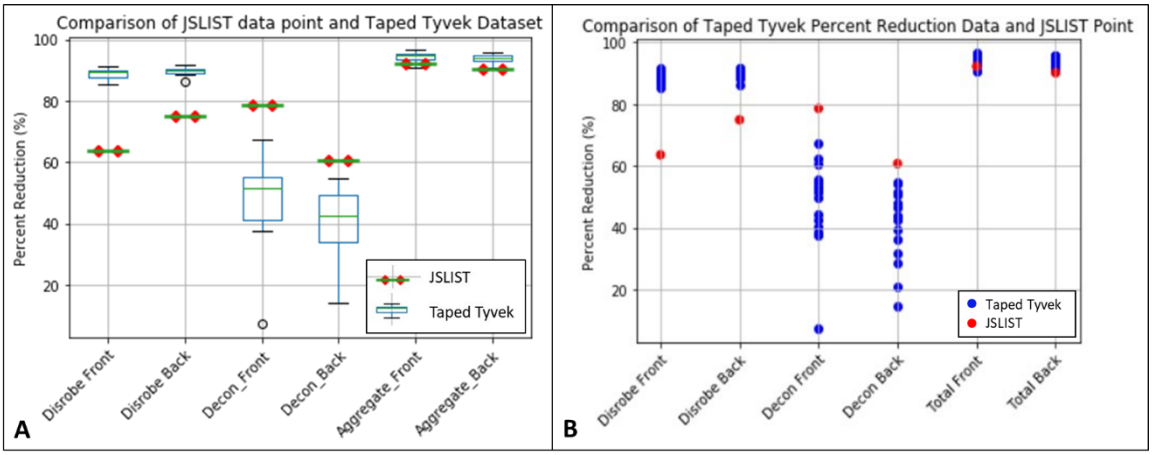

Figure 33. Plots for the JSLIST suit and the Taped Tyvek Dataset. A) Boxplot B) Scatter plot

Table 15. Taped Tyvek Mean and Standard Deviation plus JSLIST

	Mean Percent Reduction (%)	Standard Deviation (%)	Three Standard Deviation Range	JSLIST Datapoint	JSLIST within Tyvek?
Disrobe Front	88.9	1.65	83.95 – 93.85	63.6	No
Disrobe Back	89.7	1.29	85.83 – 93.57	74.9	No
Decon Front	47.9	13.8	6.5 – 89.3	78.6	Yes
Decon Back	40.4	11.7	5.3 – 75.5	60.7	Yes
Total Front	94.2	1.74	88.98 – 99.42	92.2	Yes
Total Back	93.9	1.48	89.46 – 98.34	90.2	Yes

While the JSLIST points were not considered outliers in the Taped Tyvek dataset, visually they did not appear similar, so the same procedure was followed but with the Open Tyvek dataset (Figure 34). The Grubbs test again indicated that the JSLIST points were not outliers in the dataset and visually they appear to align more closely with the

Open Tyvek dataset, indicating that the JSLIST point may have come from the Open Tyvek dataset as well. The three standard deviation rule of thumb also showed that the JSLIST data point was within the Open Tyvek data set (Table 16).

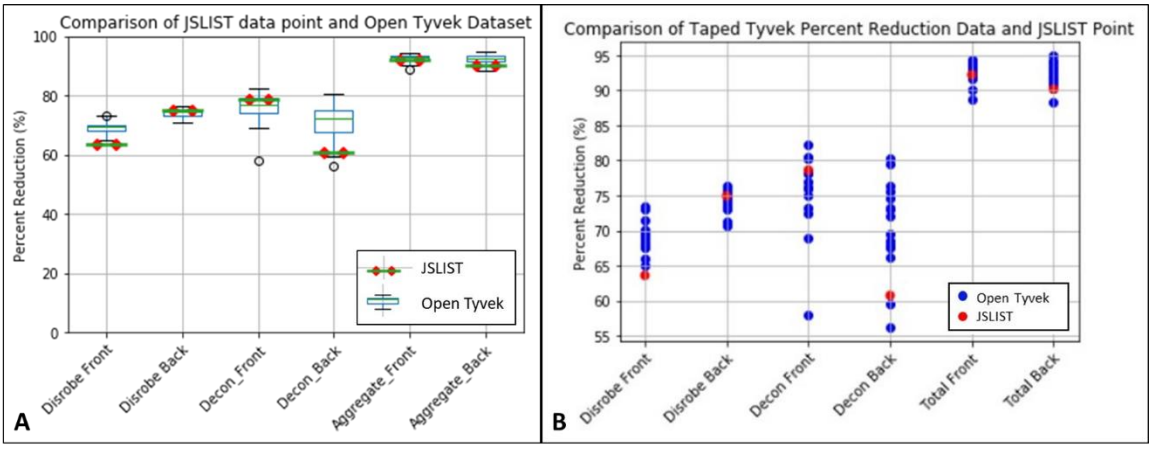

Figure 34. Plots for the JSLIST suit and the Open Tyvek Dataset. A) Boxplot B) Scatter plot

Table 16. Open Tyvek Mean and Standard Deviation plus JSLIST

	Mean Percent Reduction (%)	Standard Deviation (%)	Three Standard Deviation Range	JSLIST Datapoint	JSLIST within Tyvek?
Disrobe Front	69.2	2.22	62.54 – 75.86	63.6	Yes
Disrobe Back	73.9	1.7	68.8 – 79.0	74.9	Yes
Decon Front	75.7	5.81	58.27 – 93.13	78.6	Yes
Decon Back	70.7	6.49	51.23 – 90.17	60.7	Yes
Total Front	92.6	1.46	88.22 – 96.98	92.2	Yes
Total Back	92.3	1.68	87.26 – 97.34	90.2	Yes

Decontamination Efficacy

An analysis was conducted to see whether decontamination efficacy increased over time. The efficacy of decontamination was plotted by trial as shown in Figure 35.

Generally reduction due to decontamination was less for the Taped Tyvek trials than for the Open Tyvek trials and the JSLIST trial, which makes sense due to the lesser amount of contamination present on the skin during Taped Tyvek trials. However, there does not seem to be a trend upward over time meaning that decontamination efficacy is relatively constant over time.

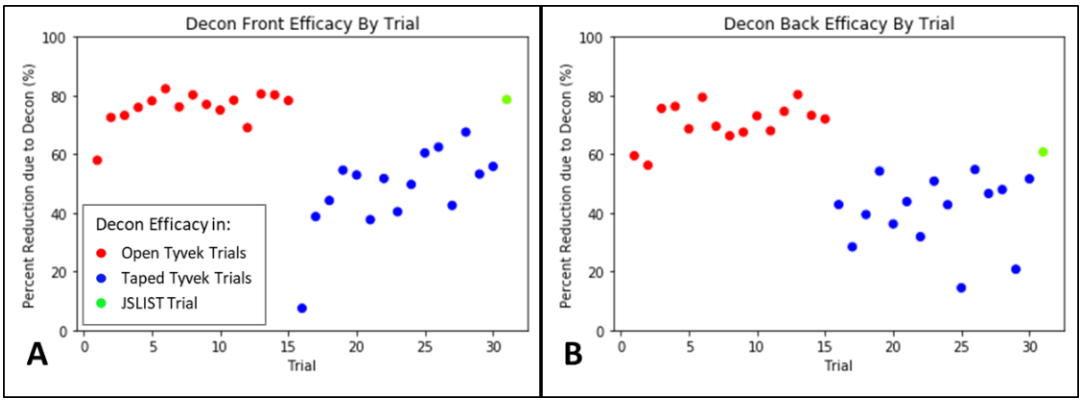

Figure 35. Decon efficacy by trial. A) Front B) Back

MURPHEE Aerosol Chamber Trials

Three trials were conducted using the MURPHEE aerosol test chamber as the exposure booth. Images of the front of the mannequin for all three trials are shown in Figure 36. The back of the mannequin is not shown as little contamination was visible on the back in any of the trials. As seen in Figure 36, deposition of the contaminant was not consistent between trials. Of note is the particularly small amount of contamination visible in Figure 36-1C, as the mannequin was lying on the floor of the chamber for most of this trial. This indicates that the aerosol likely remained suspended and thus did not deposit on the mannequin. In trials 2 and 3 the mannequin was more closely in line with the aerosol stream, allowing a larger quantity of aerosol to deposit.

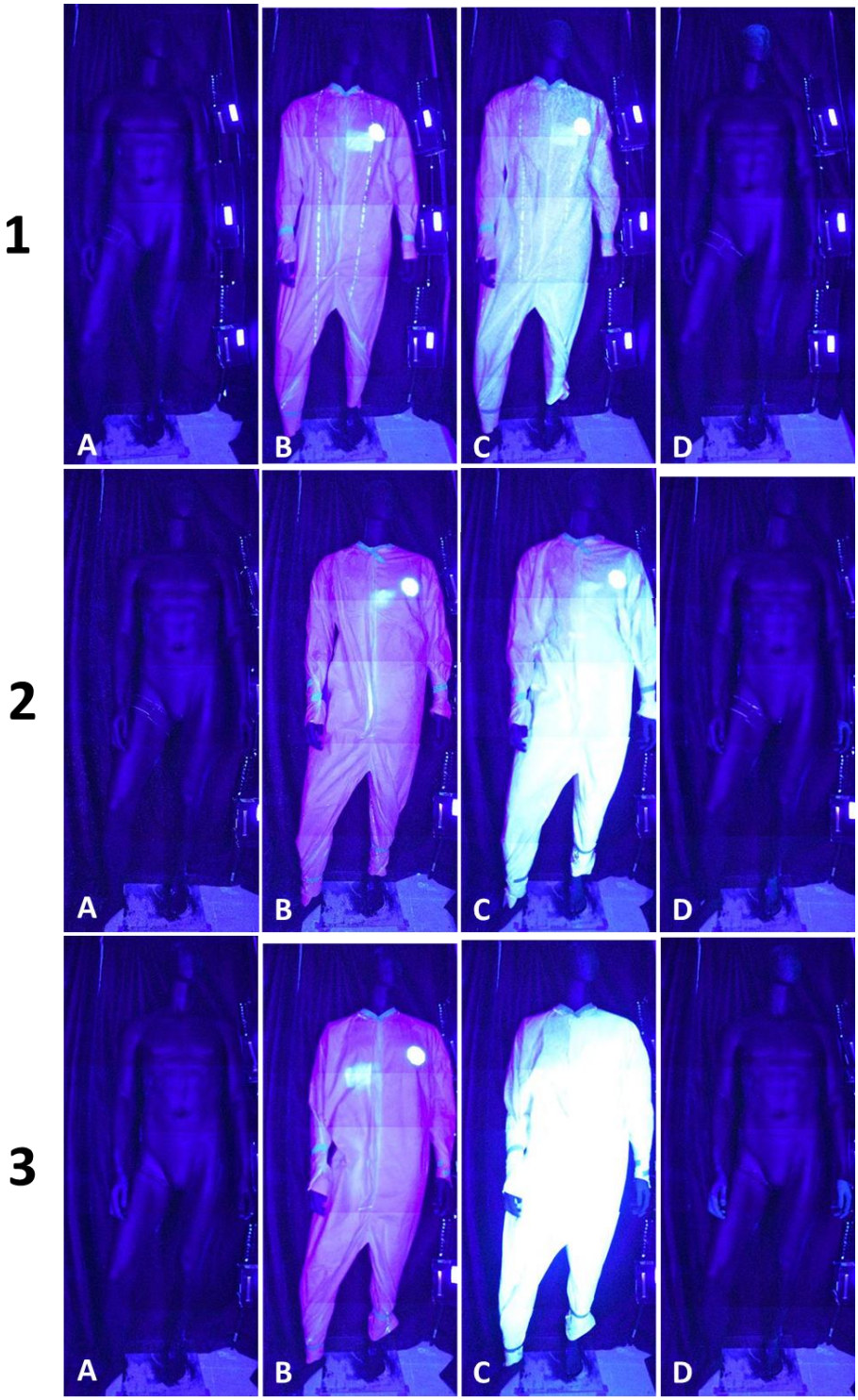

Figure 36. Images from all three trials in the MURPHEE aerosol chamber. A) Before exposure. B) Before exposure. C) After exposure. D) After exposure, disrobing.

Percent reduction in contamination due to disrobing was determined for the UES trials (Figure 37, Table 17). Figure 37A showed that reduction was much higher for the front than the back, due to the significantly higher amount of contamination present on the front of the mannequin than the back. Reduction for each trial is shown in Figure 37B and C. The range of reduction values are shown in Table 17. Ranges are presented in two ways, first being the range of values for all three trials, and the second being for only trials U2 and U3 since the mannequin was located on the floor of the chamber for the majority of trial U1.

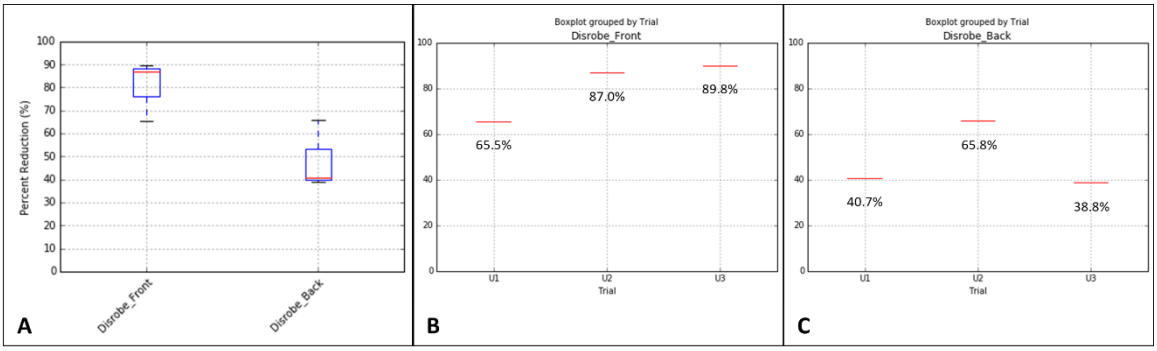

Figure 37. Summary of data from all three trials in the MURPHEE chamber.

Table 17. Summary Statistics for MURPHEE Chamber Trials

	Front Range (%)	**Back Range (%)**
All 3 Trials	65.5 – 89.8	38.8 – 65.8
Only U2 and U3	87.0 – 89.8	38.8 – 65.8

The results of these trials confirm that further troubleshooting is needed to refine the protocol in order to provide consistent results. Possible improvements to these protocols are found in the following sections.

Discussion and Conclusions

The results of these trials indicated several conclusions. First, that cotton clothing, even if black to promote contrast, provided a poor background for visualization of a liquid fluorescent aerosol. This could be due to the dye absorbing into the fibers and thus not being exposed to the UV light. Alternatively, it could be that the dye is exposed to the UV light, but that the fibers of the clothing reabsorb the emitted fluorescence, thus making it difficult to visualize fluorescence. In addition to the visualization issues with fabric, these studies showed that in high exposure conditions, such as those simulated here, that cotton clothing provides little protection from aerosol deposition onto skin surface.

While regular cotton clothing is not expected to be highly protective, Tyvek is a protective material. However, these studies show that wearing Tyvek may not be as protective as would be expected under conditions similar to those tested here. The conditions tested here are likely a conservative scenario due to the extremely high concentration of aerosol generated and the length of exposure time. While 70 minutes is much shorter than a standard workday, it is unlikely that personnel would be exposed to a cloud that dense for that period of time without some response to attempt to protect themselves. For these reasons, this is likely a highly conservative scenario. However, these results show that if such a scenario were to occur that even Tyvek clothing would likely not provide much protection to the skin due to migration of aerosol through openings in the garment (sleeves, pant legs, neckline).

The realization that Tyvek was only semi-protective due to aerosol was alleviated by the next set of trials in which the cuffs and neckline were tightly secured to the body. No contamination was found on parts of the body which were covered by the suit. This supports the assumption that aerosols were moving through openings in the sleeves, legs, and neck of the suit, rather than passing through the material of the Tyvek. While it should be noted as a concern that aerosols can easily migrate up sleeves of protective suits such as Tyvek, it should also be noted that in some (but not all) cases Tyvek is worn as a protective overgarment. Thus, the true amount of contamination on skin may be lower than shown in these experiments due to the presence of a second layer of clothing (whether that be a simple T-shirt and jeans, or other clothing).

The results of the JSLIST suit trial and analysis considering whether it would be part of either the taped or open Tyvek datasets showed that under these conditions the open Tyvek may be a more appropriate surrogate for the JSLIST than taped Tyvek. Observation of contamination under the JSLIST was discouraging due to the value placed on it as a piece of protective equipment. However, it should be noted that during an actual scenario, full coverage boots, gloves, and mask or respirator would be worn in conjunction with the suit. In addition, the hood would be tied around the face and head, rather than the neck as was done here. As well, the suit used was a retired training suit and should not necessarily be considered representative of a new one as it has likely been washed many times which can degrade the protectiveness of the suit.

While there are several reasons to expect the results gathered to be not representative of a real-world situation where the JSLIST would be worn, there are some

instances in which the suit might be worn in this or a similar manner. For instance, if an attack is considered possible but not expected imminently. In this situation, personnel may be wearing the suit pants and jacket but not hood, masks, or gloves in order to be prepared but still consider the comfort of personnel (particularly thermal stress).

Overall, the results of these experiments show that disrobing can remove up to 85-95% of contamination, though this is only in very specific cases where highly protective clothing is being worn. In these types of situations, such as a military population prepared for a possible CWA attack or rescue personnel responding to the scene of a CWA or other hazardous chemical incident and thus wearing protective equipment, it is likely that disrobing will remove a large percentage of the contamination. However, if enclosed protective clothing is not worn, such as in an unprepared military or civilian population, it is likely that much less contamination (65-75%) will be removed simply by disrobing. This work supports the oft stated assumption that 90% of contamination will be removed simply by disrobing, though with the caveat that this may only be true in highly specific circumstances.

This work also attempted to verify the effectiveness of a wet decontamination protocol. This work showed that decon is a much more variable process, and efficacy would likely be even more variable in situations where multiple personnel are conducting decontamination and in high pressure situations such as a mass casualty attack and decontamination line. With this variability in mind, decontamination removed an additional 56-82% of the remaining contamination for open Tyvek, and 7-68% for the taped Tyvek. While it has been discussed that the exposure scenario conducted in these

experiments is likely a high exposure scenario, the chemical warfare agent simulant used in these experiments is likely a best-case simulant, at least as far as wet decontamination is concerned. This is due to the high water-solubility of the dye used as a simulant. However, many chemical warfare agents tend to have hydrophobic properties (such as sulphur mustard, soman, and VX) [14], [43]. This is partly why they are so dangerous, as they are more likely to be able to pass through dermal barriers and are more difficult to wash off of skin. As discussed however, the oil-based simulant purchased caused both a visible stain and a fluorescent residue on surfaces similar to the aerosol test chamber. For this reason, it was determined that a water-based dye should be used unless a less permanent oil-based simulant could be found. Future research should consider the possibility of other oil-based simulants which may be more easily removed from lab equipment as a more appropriate simulant for chemical warfare agents.

Sources of Uncertainty and Bias

Several sources of uncertainty or error were identified during these experiments which are shown in Figure 38. The first source of error is the interaction of sunlight with the UV dye, causing a photobleaching effect. Although a Mann-Whitney U-test showed that there was a statistically significant difference between the means of the test and control coupons after the test coupon was placed in the shade during the decontamination process, the fact that the mean gray values only differed by 5 indicated that the magnitude of error imparted by this effect would be small. This effect would cause an overestimation of the efficacy of the decontamination protocol, rather than an

underestimation. Secondly, using the camping shower as an exposure booth meant that a very small enclosed space was created, with little to no airflow. This resulted in a fairly high concentration of aerosol building up in the booth over the exposure time. This would likely overestimate the exposure and could overestimate by a significant margin.

A third source of uncertainty was that the volume of the UV dye aerosolized in each trial varied slightly. The reason for this is unknown but could have been due to a variety of factors. In addition, this variability would contribute to differences in exposure during each trial and slight differences in the amount of deposition onto the mannequin. This effect was deemed to be small but could be in either direction.

A fourth source of uncertainty was the use of a hydrophilic dye as a simulant. Due to its ready solubility in water and the fact that a water-based decontamination method was used, the efficacy of decontamination could be overestimated by this dye, particularly when compared to a lipophilic simulant. However, as this dye was determined to be a reasonable sarin simulant, which is also hydrophilic, the magnitude of overestimation was determined to be small. In addition, the use of a detergent would aid removal of lipophilic agents as well as hydrophilic ones.

A fifth source of uncertainty was the use of Tyvek suits as clothing. Though they were extremely useful for being able to visualize the fluorescent dye after exposure, Tyvek is not an everyday clothing material. This makes it a somewhat unrealistic scenario to imagine that someone would be wearing Tyvek if they were exposed during a surprise CWA or HAZMAT incident. In addition, Tyvek is a protective clothing, so the amount of deposition onto skin is likely decreased somewhat from cotton clothing due to

the impossibility of penetration through the bulk clothing. This would slightly underestimate the amount of expected deposition onto skin. However, as shown in the Open Tyvek trials, small aerosols can move through openings in the clothing, so the effect is likely small.

Finally, the image analysis process could have been a source of error. Due to slight misalignment in images from one step of the process to the next, image subtraction could create artefacts. This could either artificially increase or decrease the number of pixels with gray values in the 26-255 range (the contamination threshold). While these artefacts are unlikely to significantly affect results, there is a potential for a medium magnitude effect which would over- or underestimate contamination.

Source		Magnitude/Bias
Photobleaching/Sun	Overestimate decon efficacy	
Tent as Exposure Booth	Overestimate exposure	
Volume of Simulant Aerosolized	Either over or underestimate exposure	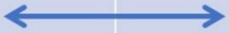
Simulant Used is Hydrophilic	Overestimate decon efficacy	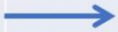
Tyvek Suits as Clothing	Aids visualization but may underestimate amount on skin	
Image Misalignment	Artefacts could either over or underestimate contamination	

Figure 38. Sources of Uncertainty Table.

V. Conclusions and Recommendations

Chapter Overview

This chapter summarizes the conclusions of the research described above, as well as makes recommendations for method improvements and directions of future research.

Conclusions of Research

The first chapter of this work described an extensive literature review into CBRN decontamination which was performed. This review identified several gaps in the decontamination literature, including a lack of a standard testing methodology for commercial decontaminants. Evaluation efforts vary from lab to lab which makes determining the efficacy of a particular product or method difficult. In addition, quantification of chemical contaminants is done in many different ways. While it is true that not all chemicals can be analyzed by the same methods, having standard methods to measure contamination would make understanding the research much easier. In addition, most studies only consider small volumes (such as swatch testing) of contaminants in a lab setting, there are very few world-scale studies that have been performed.

In addition to measurement and method gaps, there is very little literature which considers hazardous chemical incidents which are not chemical warfare agents. Chemical warfare agents are banned from being stored or produced so, while highly toxic, they are less likely to be utilized in bulk than a more widely available toxic industrial chemical.

Mass casualty literature highlights the need for continuous training to ensure that response teams would be prepared in the event of a disaster. However, in the civilian

world, that training rarely takes place with the frequency or depth that it should. Military populations are more likely to be trained, both in what to do if personnel are involved in an incident, as well as in how to respond on both a personal and medical team level, but the quality of training can vary as well. In addition, human nature is highly variable and can greatly impact the effectiveness of decontamination situations. Privacy is a huge concern, particularly for civilian populations who are much less likely to comply with guidelines, such as disrobing for decontamination. In addition, the stress and emotions involved in response to a mass casualty scenario makes it unlikely that decontamination is performed with the same care as it would be during training or in a lab experiment.

Considering this uncertainty as to how well decontamination will be performed under a high-stakes scenario makes it very important to be able to understand what CWA may be involved and the presence and extent of contamination on a patient. This means that detection of chemical weapons after a real-world incident is highly important, though it is a challenging endeavor. It is important that this becomes a focus of research however, as detection would give peace of mind to everyone involved in a mass casualty CBRN incident to know that someone is not contaminated and can freely move around. This is particularly important when releasing victims to return to their normal lives, or for healthcare personnel who are treating wounded victims. Secondary contamination has been well-documented anecdotally, but little studied.

Finally, this review identified the often-cited assumption that disrobing will remove 90% of contamination. However, no source was found which contained any data to support this claim. In fact, the most cited source for this statistic, a paper written in

1994 by Robert Cox, did not provide any evidence for the claim either [2]. This assumption is used as the basis for most military and civilian guidelines, so it is important to understand the veracity of this claim.

In addition to the CBRN decontamination literature review, an aerosol test chamber was designed and constructed for use in this and future research. After construction it was characterized by measuring air velocity at many points along the x-, y-, and z-axes. This allowed the visualization of airflows and the creation of a series of velocity maps for the chamber. In addition, solid aerosol particles were dispersed within the chamber and measured using real-time instruments at four planes within the chamber. Equal variance was determined across the x-y planes, though the magnitude of the variance was high. The considerable variance suggests that further tests are needed to characterize the variability of chamber performance, or that research taking place within the chamber requires large sample sets to ensure statistical significance can be obtained. In addition to the physical measurements, a computational fluid dynamics model was created to aid in prediction of flow behavior. Future work could be run through the model first to reduce the number of pilot tests needed. In addition, the full range of air speeds possible was not characterized for velocity profiles, and only one air speed was examined for aerosol behavior. Future research may rely on different settings than those studied so it would be prudent to perform further characterization at different air speeds.

The third section of this work describes the development of a reproducible, semi-quantitative method by which contamination (and subsequently decontamination efficacy) can be investigated. This method utilizes a UV fluorescent liquid aerosol as a

chemical warfare agent simulant. This work elucidated some of the challenges associated with working with such materials in this context, including issues with inherent fluorescence (such as dust or residual contamination from prior experiments) and visualization on porous surfaces (such as cotton clothing). However, once a suitable clothing surrogate was found, nonporous Tyvek suits, visualization provided many fewer problems. These experiments showed that deposition of aerosol was very repeatable with contamination area 95% confidence intervals being small (25 to 40 in^2). The results of these experiments showed that under certain conditions the statistic of 90% decontamination simply by disrobing may be an accurate amount, such as when highly protective clothing is being worn and openings are highly restricted (Taped Tyvek trials). However, it also confirmed suspicions that the assumption is likely not accurate in many cases, such as if protective clothing is worn but not tightly sealed (Open Tyvek trials, and JSLIST). These situations resulted in 65-75% of contamination removed by disrobing. However, it should also be noted that the exposure conditions tested herein are a high exposure scenario and thus contamination penetrating through clothing or moving through openings may be less of a possibility in a more realistic exposure scenario.

Limitations of Research and Recommendations for Future Work

While conclusions were able to be drawn from this work, several limitations of the methodology have been identified. First, visualization issues were encountered with the clothing used in initial trials which led to the use of Tyvek suits for the bulk of data

collection. While this use aided measurement and visualization, Tyvek is not a material which is commonly worn, making this a somewhat unrealistic scenario. Tyvek is non-porous and therefore more protective than regular clothing so it may not be an accurate representation of the amount of contamination that would be present on skin except in scenarios where similar protective gear is worn regularly. Future research could attempt using other clothing types such as standard military uniforms, polyester athletic clothing, or any clothing with a tighter weave than cotton. In addition, if cotton is still desired, a waterproofing spray might be able to be used to prevent penetration through the fabric, though this might then also be considered unrealistic to normal-wear clothing. Future work could also consider the addition of fluorescence microscopy or other high-resolution imaging technique to examine the fabric at high magnification after exposure. This could help elucidate the reason for challenges with visualization and may direct research to a different solution which has not been considered here.

In addition to the fact that Tyvek is not often worn, it is also not generally the only layer of clothing. In most cases Tyvek is worn over street clothing which would provide a mild second layer of protection from aerosols reaching the skin. Thus, visualizations on skin presented in these tests are likely an overestimation from what would be found in a real-world scenario. However, the amount of contaminant that passes through the clothing would be similar. The JSLIST suit may be worn as the primary uniform so the results above may be representative of exposures from real-world scenarios. Future work could include trials run where the mannequin is dressed in a layer

of street clothing underneath the Tyvek or JSLIST for a more realistic view of the contamination that would get to the skin.

In addition, future research should consider performing additional trials with JSLIST suits to determine the variability inherent in using this type of clothing. It would also be prudent to perform trials both with the suit worn in the same manner as here, as well as with the full accoutrements (boots, gloves, mask) to determine the variability and reproducibility. As well, supply cost can be a limiting factor to research and the number of trials possible. A few additional trials with JSLIST suits could confirm the suitability of using Tyvek suits as a surrogate which would both keep supply costs down and allow a greater statistical power from the number of tests run.

A second limitation of the research conducted is the CWA simulant used and its delivery method. Many agents tend to be hydrophobic, which can make removal from skin difficult and prolong contact. The simulant used in this research was highly water-soluble which was helpful from an experimental performance perspective as it was both easy to use and easy to clean. However, the difference in hydrophilicity between this simulant and live agents means that this dye may not be a particularly realistic simulant. This limitation likely does not significantly affect the first aim of the research (examining simulant deposition onto clothing and penetration through onto skin) as hydrophilicity would have little impact on interaction with clothing fibers or the mannequin surface material. However, the high water-solubility of the simulant may make the wet decontamination protocol utilized appear significantly more effective at removing contamination from the mannequin surface than would be seen with a hydrophobic

simulant. A mild detergent is employed during the decontamination protocol so that would aid removal of a hydrophobic simulant, but the extent is unknown. Future research should consider other fluorescent tracers such as oil-based which would have a more similar hydrophobicity to chemical warfare agents. Literature indicates that curcumin in methyl salicylate may be a possible candidate for a more hydrophobic simulant. In addition, the color of fluorescence should be considered. Dust in particular can interfere with visualization as it can reflect the UV light, appearing to fluoresce blue. Use of a simulant with fluorescent wavelength in the red or yellow range might aid in visualization. In addition, a fluorescent powder or bead could be used. This would likely have a larger diameter than the droplets generated in these studies which could act as a simulant for biological aerosols as well as possibly being more visible on clothing surfaces.

In combination with different aerosol types which could be used as a more appropriate surrogate for different types of contaminants comes the possibility for other research questions. Secondary contamination due to off-gassing of vapors or re-aerosolization of aerosol contaminants is a concern for responders, decontamination workers, and healthcare professionals after a CBRN or HAZMAT incident. Future work could consider this possibility by including air and breathing zone monitoring for researchers during the experimental process (particularly disrobing). Additionally, it would be interesting to take images of the researcher after handling the mannequin and disrobing to examine the possibility for cross contamination, both as a concern for the researchers and as a consideration of secondary contamination of responders.

In addition to physicochemical properties of the simulant used in these experiments, the delivery method utilized may be unrealistic. Unsurprisingly, no definitive guide was found for how chemical warfare agents may be employed in different situations. However, methods can vary. While it is unclear whether a similar method of dispersing fine aerosol droplets has been used, it is a possibility which should be considered during testing of protective gear to ensure effectiveness.

Thirdly, this research was performed using a mannequin as a test subject. While this aided research by being still during imaging and exposure periods, it is only a semi-realistic simulant for the human body. The mannequin surface was refinished using a matte spray paint to aid in the visualization process as well as cleaning. However, this surface is highly dissimilar to the skin that it was intended to mimic. While there are many ethical considerations to using humans or other animals during research, it would be beneficial in the future to consider using a mannequin with a different surface or skin samples to get a better idea of how the amount of simulant deposited on the skin may be different than the true exposure. This was not the aim of the research conducted here, though it is a worthwhile avenue to pursue in the future. In addition, the use of a mannequin meant that there was a smooth, hair-free surface, which aided imaging but is unrealistic. As hair can act as both a protective layer as well as a reservoir for additional exposure, future work could consider using a wig to examine how the presence of hair can affect contamination of the skin. In addition, any future tests conducted on volunteers or skin samples will have to contend with skin tone and inherent fluorescence of the human body, a complication which was not present in these trials.

Another limitation encountered during this research was the restricted access to lab equipment. While exposures were intended to be carried out in the MURPHEE aerosol chamber, current events and restricted access made that impossible. To that end, a makeshift exposure booth was used for the majority of experiments. This exposure booth likely had more variability inherent as its purpose is not to create a fully enclosed space for aerosol exposure, but rather provide privacy. Because of the original purpose of the camping shower, there is an ~4-inch mesh section at the bottom of the tent which allowed airflow through the booth. This introduced variability to the exposure conditions during the first set of trials and had to be covered in plastic to attempt to mitigate this. In addition, the roof of the tent, while covered with a rain fly, is also mesh so this was covered in the same manner. In addition to the issues with airflow, the booth was located outside during the exposure periods. This meant that air temperature was highly variable and the temperature inside the exposure booth variable as well. Temperature was monitored but could not be controlled which could affect aerosol characteristics. Higher relative humidity can extend the life of liquid droplets by reducing the rate of evaporation [35]. If the partial pressure of vapor at the droplet surface is greater than the saturation vapor pressure of the liquid then evaporation will not occur [35]. Conversely, higher temperatures may increase the evaporation rate due to an increase in the speed of gas molecules (more impacts with aerosol droplets may increase evaporation) as well as a increase in the viscosity of the air (also increases the likelihood of impacts between gas molecules and aerosols) [35].

Lastly, the lack of airflow, the volume of the booth, and the length of exposure time resulted in a very high concentration of aerosol inside the booth, though exact concentration was not able to be measured due to lack of access to instrumentation. This high concentration is likely unrealistic as an exposure scenario but provides a conservative estimate. Other limitations include the small space available and the close proximity of the aerosol nebulizer to the mannequin. In a real-world scenario it is highly unlikely that anyone would stand that close to a toxic source for that amount of time. As well as the proximity, the stand used to hold the nebulizer in place was created from cardboard boxes whose integrity degraded somewhat over the course of the experiments. In addition, it was not particularly sturdy and was subject to movement as the tent moved in the breeze which could have impacted the working of the nebulizer and thus aerosol generation.

A final limitation of this work was evident in the data analysis stage. Although the position of the mannequin stand, the mannequin on the stand, and the camera angle were all marked and every care was taken to ensure that objects were in the same location for every step of the process, it was nearly impossible to have all parts perfectly aligned every time. This created alignment issues which surfaced during the image analysis stage. When significant, misalignment created error in the measurement phase. This was corrected to the highest degree possible by the researcher, but was a time-consuming and manual process, which again could introduce error due to researcher judgement calls. Inter-person variability is not an issue in this instance, but in a broader research team could be a source of error that would need to be accounted for. Future work that includes

image analysis as part of the data and analysis methods should consider the creation of a different stand which may hold the mannequin more securely in place and be less subject to movement and jostling inherent in moving of the mannequin. One that would rotate so that the mannequin and stand did not have to be removed to image both sides of the mannequin would be immensely helpful. In addition, the use of a grid in the background of the mannequin might allow for better alignment, not only for the body position of the mannequin, but also in the viewfinder of the camera to ensure that the images are in alignment when they are collected.

In addition to the recommendations above, future work could also consider testing different decontamination methods. In situations where wet decontamination is not possible or is inadvisable (such as cold weather), there are other decon methods which can be used such as dry decontamination or so-called improvised decontamination. In addition, wet decontamination can be carried out using the ladder pipe system, which is used for ambulatory victims of an incident. A protocol to simulate this decontamination method could be tested as well. Efforts could also be made to improve the efficacy of the protocol described above by adjusting variables such as time, water temperature and pressure, detergents used, or other factors.

Most of these recommendations consider the work that was done in the makeshift exposure situation at the author's home. Due to time constraints only 3 trials were performed in the MURPHEE aerosol chamber, which was not enough to work out all of the issues presented. Thus the author would like to recommend some adjustments to the

protocol used and things to consider to make future research in the MURHPEE more successful.

First, although the concentration of aerosol was quite high in the exposure tent-booth, the concentration in the MURPHEE was much lower. This is due both to the significantly larger volume of the chamber (3'x3'x21', volume of 189 cubic feet, compared to 4'x4'x7', volume of 112 cubic feet), as well as the continuous flow of air moved by the fan attached to the MURPHEE chamber. Recommendations to combat these differences are multi-faceted. First, aerosol generation should likely be adjusted to increase the output of aerosol. This could be done by using a different aerosol generator which could handle a higher concentration, by increasing the air pressure to the Collison nebulizer to increase the aerosol output, or by using multiple nebulizers or aerosol generators. A home humidifier or fog machine might be appropriate, though research and testing would be needed to determine the suitability. In addition, while one draw of the MURPHEE chamber is the ability to conduct tests with moving air, tests could be run wholly or partially with the fan off. This could allow a higher aerosol concentration to accumulate before the fan was turned on to move air, or simply allow diffusion of aerosol through the chamber to occur. While these changes would be necessitated to achieve similar deposition to that experienced in the shower exposure booth, it should be noted that the conditions tested may be representative of a different exposure scenario and thus that no changes may be needed.

Another recommendation would be to test different locations of the nebulizer. For ease of conducting experiments and due to the thought that these fine aerosol droplets

might evaporate completely before reaching the mannequin, the nebulizer was only placed 2 feet upstream from the mannequin. It is possible that having the nebulizer so close to the mannequin created a directed stream of the aerosol which resulted in the aerosol cloud passing over the mannequin completely and depositing further downstream in the chamber.

In combination with both the placement of the aerosol generator and considering different types of aerosol generators, the size of aerosol generated should be considered. It is possible that larger aerosols would make deposition on the mannequin more likely or make any deposition that does occur more visible. As well as droplet size, particulate aerosols may aid both deposition and visibility.

Along with the aerosol, the mannequin itself could be adjusted to try and increase aerosol deposition for visualization purposes. Deposition of an aerosol from a moving airstream to a surface parallel to air movement is far less likely than deposition to a surface perpendicular to airflow. Thus, the mannequin could be propped into a more vertical position to increase the surface area in line with airflows.

In addition to changes in exposure methods, the imaging methods could be adjusted to be more effective. As discussed previously, a stand which holds the mannequin more securely in the same place, as well as rotates would greatly aid the imaging process. In addition, the size needed for an imaging booth was vastly underestimated by the author. The imaging booth created had dimensions of 3 feet by 5 feet by 7 feet tall. The first issue with this was that it did not allow sufficient room to move or position the mannequin on the stand. Secondly, there was very little room

available to work for fear of disturbing the UV lights and camera tripod. Because of these issues, the set-up was adjusted by removing curtains from the side nearest the camera as well as part of the long side and moving the frame ~1.5 feet from the wall to allow more room for maneuvering. By removing curtains in this way however, the author was forced to turn off the overhead lights in the room during all imaging steps. In addition, the shorter distance between the camera and the mannequin necessitated by the imaging booth dimensions made it so that the full range of the body required five imaging regions, rather than three. This created more opportunities for misaligning the camera during imaging. In addition, the camera can only write files so quickly, a time which increases as the memory card becomes fuller, so the imaging process was significantly extended by having to image five body regions.

As well as misalignment issues, the change in distance between the mannequin, camera, and UV lights could have caused some confounding of the results collected. The distance could change how the UV dye fluoresced to appear either brighter or dimmer. In this instance, as comparisons were not made between the MURPHEE trials and those conducted at home this is unlikely to affect conclusions drawn but should be considered if a similar situation arises in future.

As well as the modifications suggested, it was also impossible to perform wet decontamination in the lab due to lack of access to sufficient space and running water. These things may be able to be obtained in future but were not feasible on the short notice available during this collection period. For these reasons it may be necessary to consider other options for decontamination or alternate delivery methods for water.

While other changes and improvements could be made, in the author's opinion, these are the most likely to have the largest impact on the success of future work.

Appendix A

Original Article

Design and characterization of multi-use research for particulate hazards and environmental exposures (MURPHEE) aerosol test chamber

Megan L. Steele[a], Emily M. Titus[b], George P. Lemmer[b], Jacob M. Denney[c], Jeremy M. Slagley[c], Casey W. Cooper[c], Robert M. Eninger[d]

[a]Integrative Health & Performance Sciences, UES, Inc, Beavercreek, OH, USA, [b]Department of Systems Engineering and Management, Air Force Institute of Technology, Centauri Contractor, Wright-Patterson AFB, OH, USA, [c]Department of Systems Engineering and Management, Air Force Institute of Technology, Wright-Patterson AFB, OH, USA, [d]HQ Air Force Materiel Command, Office of the Command Surgeon, Wright-Patterson, AFB, USA

CONTACT Megan L. Steele msteele@ues.com Integrative Health & Performance Sciences, UES, Inc, Beavercreek, OH, 45432, USA.

ABSTRACT

Aerosol test chambers are used to contain aerosols during experiments to protect researchers and provide a stable research environment. This work describes the design and characterization of a novel test chamber, the Multi-Use Research for Particulate Hazards and Environmental Exposures (MURPHEE) Chamber. Design was made modular to accommodate current and future research needs, although it was not possible to ensure laminar airflow. Characterization methods consisted of air velocity mapping as well as spatial variability of ultrafine particulate aerosols. Air speeds within the chamber varied but were homogenous enough for confidence in data collection. Particulate size distributions were similar, but there was high variability in the counts, leading experiments to require large sample sizes. In addition, a computational fluid dynamics model was created and validated using the data to guide future work and allow planning and pilot tests to be conducted more swiftly and with less cost.

Introduction

Test chambers are used when conducting aerosol research to protect the health of researchers, prevent cross contamination of the lab and test environment, and maintain the aerosol in a well-defined space. Based on the ultimate aims of the research, chamber design must consider materials of construction, the point of introduction of study aerosols, and location of any sampling ports (Lidén et al. 1998; Lundgren 2006). Temperature, pressure, and relative humidity can all have substantial effects on aerosol characteristics so researchers must decide from the outset if the chamber should be designed to control these parameter or if it is sufficient to simply monitor them (Hagerman et al. 2014; Isaxon et al. 2013; Lidén et al. 1998; Lundgren 2006; Rønborg et al. 1996). Even after construction, work cannot begin without a thorough understanding of the chamber characteristics, to include the achievable air velocities, airflow patterns, spatial and temporal variability of particle movement, and air exchange rates and mixing behavior of the chamber (Isaxon et al. 2013; Lidén et al. 1998; Lundgren 2006; Lundgren et al. 2006; Pieretti and Hammad 2018).

Environmental test chambers are commonly characterized in conjunction with computational fluid dynamics (CFD) techniques to verify and validate models and code (Li et al. 2007; Lin et al. 2005; Lucci et al. 2018; Zhang et al. 2005). Computational fluid dynamics has been used to model fluid flow of indoor environments for several decades, with the work of Nielsen (1974) being the oft cited dissertation regarding flow in air-conditioned environments using full scale models and numerical solutions as the basis for CFD models in the present day. When considering any fluid flow, the fundamental set of equations used to describe the

conservation of momentum and mass transport are the Navier-Stokes equations, specifically in regard to incompressible turbulent flows (White 2011).

Common concerns when modeling fluid flow are turbulence intensity, fluid density and temperature, inlet velocity, and outlet conditions, along with other environmental impacts of concern (such as respiring workers, typically represented as heated manikins) (Elnahas 2005). Indoor environments are commonly modeled with comfort or contaminant mass transport as the subject of concern. Both issues are affected by fluid temperature, relative humidity, bulk air flow, contaminant source, room dimensions, room geometries, and locations of heat sinks and sources. A variety of works describe the construction and modeling of environmental test chambers validating CFD models using the above parameters.

Following the guidelines presented by Srebric and Chen (2002), CFD modeling requires verification, validation, and clear reporting of results. The verification process requires the correct choice of code for analysis of the turbulent air flow and corresponding mass and heat transfer. Validation requires the CFD user to generate a model with the verified code to create a representative simulation of experimental data. Reporting results communicates the usefulness of the model and allows the ability to reproduce the model.

Chamber design considerations

The chamber design focused on three near-term research projects: testing the operational parameters of the Institute of Occupational Medicine (IOM) inhalable samplers, measurement of airflows and aerosol transport around a litter-bound patient, and decontamination of the same litter-bound patient. As these projects had varied requirements and future needs are unknown,

design of the chamber was meant to maximize flexibility by modularity of design. Due to the size of a standard NATO litter (0.584 m wide) and space available at the research facility, it was decided that 0.762 m by 0.762 m would be the minimum cross section considered to avoid boundary effects (NATO 2013). Air velocities inside the chamber needed to be similar to those encountered in common indoor workplaces, from office spaces which approach calm environments (<0.3 m s^{-1}) to those spaces which require robust ventilation to protect against particulate hazards (≥ 0.5 m s^{-1}) (Baldwin and Maynard 1998; Bennett et al. 2018). Considering the desire to mimic workplace environments, it was determined that ambient air conditions would be suitable and no effort was made to control temperature or humidity.

Early designs aimed for laminar flow inside the chamber and basic fluid dynamics calculations were undertaken to determine if this would be possible within the space constraints. A range of air temperatures, air velocities, and chamber cross-sections were considered although ultimately, it was determined to be impossible to achieve laminar or fully developed turbulent flow. Further information on calculations and design are included in the Supplemental Information.

As calculations indicated that achieving laminar and fully developed turbulent flow would be impossible within the real-world space constraints, the final design was a rectangular chamber with dimensions of 0.914 x 0.914 x 6.401 meters. Polycarbonate was chosen as the material for the walls, to allow researchers to monitor experiments. Though the chamber was designed to operate under negative pressure, a 0.762 cm wall thickness was deemed adequate as the magnitude of the pressure would be small. The frame was constructed out of aluminum (80/20 Inc, Columbia City, IN). The final chamber design and fabrication was conducted by the

AFIT Model shop in three seven-foot sections which could be joined at the seams to form a single continuous chamber (Figure 1). The middle section included a door to allow access to the interior of the chamber. Air enters and is exhausted through banks of high efficiency particulate air (HEPA) filters. Air is moved through the chamber by a centrifugal fan equipped with a variable frequency drive located downstream (Model HDBI-120, Cincinnati Fans, Cincinnati, OH).

Figure 1 placement

After construction, all inside seams were caulked to seal them and the seams between chamber sections were sealed with Gorilla Tape® to facilitate detachment for cleaning or relocation. Once these activities were completed, characterization of the chamber could begin.

As turbulence was expected, some characterization was conducted with a flow straightener (Model: AS100, Ruskin, Kansas City, MO) in place. It was located just upstream of the door, at the seam between the first and middle chambers. All tests without the flow straightener included measurements from all three chambers, while those with the flow straightener only measured locations downstream of the flow straightener placement.

Chamber characterization methodology

Velocity mapping

Velocity mapping was done to understand the air speed characteristics along the face of each plane and longitudinally along the length of the chamber. Mapping was done using a VelGrid attached to an AirData Multimeter data logger (Model: ADM-880c, Shortridge Instruments, Inc, Scottsdale, AZ).

The VelGrid is designed to measure the face velocity profile by covering a 0.356 x 0.356 m^2 area and recording the average velocity from 16 points within this area. In this experiment, three VelGrids were stacked and used simultaneously to cover a vertical slice of a plane in the chamber (Figure S1 in the Supplemental Information). Data were recorded using the ADM-880c in automatic mode, which were downloaded from the device at regular intervals. The ADM-880c has the capability to automatically correct measured velocities for atmospheric temperature and pressure variations, although it cannot account for fluctuation in relative humidity. This was done manually (see Supplemental Information) by using the air temperature and relative humidity collected by a Kestrel 4000 Pocket Weather Tracker (KestrelMeter.com, Boothwyn, PA) which was set to record data every 20 minutes.

To measure the velocity in the aerosol chamber, it was divided into imaginary blocks of 0.305 m x 0.305 m x 0.305 m. Starting in chamber 1, the chamber was labelled in 0.305-meter (1-foot) increments along the z-axis (Figure 2). The chamber was lettered along the x-axis, with the cube on the side of the chamber furthest from the door being labelled ‘A’, the middle labelled ‘B’, and the one nearest the door labelled ‘C’. In addition, each VelGrid was given a number, used to designate the height it measured within the chamber, although the words ‘high’, ‘middle’, and ‘low’ are used for clarity.

Figure 2 placement

In the initial measurement of air velocity, the three VelGrids were stacked by attachment to a ring stand. The face of the VelGrids was positioned at each measurement location in the chamber, using tape marks on the chamber to ensure alignment. Once the VelGrids were

positioned, the ADM-880c data loggers were attached and turned on to begin recording data. The chamber door was closed, the two side seams were sealed with tape, and the fan was turned on. For each run, the fan was dialed up through the desired speeds using the variable frequency drive. In order to characterize the velocity across the full range of the fan, three frequencies were chosen: 16 Hz, 30 Hz, and 60 Hz. It was determined that 60 Hz would provide an air speed of 1 m s^{-1}, 30 Hz would provide 0.5 m s^{-1}, and 16 Hz would provide 0.2 m s^{-1}. From this point on, the fan settings will be referred to by the speed, rather than the frequency. The lower end was chosen to be slightly above the limit of detection of the ADM-880c data logger (0.127 m s^{-1}). For each run, the fan was dialed to 0.2 m s^{-1} and allowed to stabilize for a minute before a three-minute measurement period began. After the measurement period, the fan was dialed to 0.5 m s^{-1}, given a minute to stabilize and then measured for three minutes. Finally, the fan was dialed to 1 m s^{-1} and the stabilization and measurement periods were repeated. Once measurements were complete, the fan was turned off, the chamber opened, and the VelGrids were moved to the next measurement location along the x-axis. For the initial set of data, measurement locations were done sequentially (1A, 1B, 1C, 3A, 3B, 3C, etc.).

To validate the repeatability of measurements, certain locations within the chamber were selected for duplicate measurements on different days. One third of the original sampling locations were sampled for repeatability (14 of 39 without the flow straightener, and 9 of 27 with the flow straightener in place). Further information on sampling locations and methods are found in the Supplemental Information.

In addition to the initial air speed characterization, the air velocities were measured while clean air ran through the dust generator to ensure that the introduction of another air stream did

not significantly disrupt the established airflow patterns. Sampling planes were chosen based on those planes with the most consistent air velocities. Two planes were chosen for use when the flow straightener was not present (5 and 7) and two planes which could be used when the flow straightener was in place (8 and 10). These measurements were repeated with two different settings on the dust generator, a high and low flow, to ensure that the full operational range of the dust generator could be used without significant effect on the established airflow patterns. Final analysis showed no impact to the established patterns so aerosol studies commenced.

Spatial variability

Spatial variability of the chamber was examined using UltraFine Arizona Road Dust (ARD) (Particle Technology Inc., Arden Hills, MN) lofted by a rotating brush generator (RBG) 1000 dust generator (Palas GMBH, Karlsruhe, Germany) while real-time measurements were obtained with a particle counter. Measurements were taken in the same planes as were sampled with clean air (5 and 7 without the flow straightener, and 8 and 10 with the flow straightener in place).

Sampling probes channeled dust from the chamber to an optical particle sizer, OPS model 3330 (TSI, Inc., Shoreview, MN) to obtain particle distribution and concentration. One OPS reading was taken for two minutes, then the probe was moved to a new location (Figure 3). The end of the sampling probe was positioned in the center of each grid square. Sampling was not isokinetic as the opening of the probe was perpendicular to airflow, though any errors due to this would be equivalent for each location.

Figure 3 placement

For initial tests, the fan was set to 0.5 m s^{-1}. After the fan was turned on, the RBG dust generator was turned on. The compressed air line was set to 80 psi (5.51 x 105 Pa), and the pressure regulator on the RBG was set to 1 bar (105 Pa). The feed rate was set to 60 mm/hr. This gave a run time of approximately 40 minutes in most cases based on the amount of the reservoir filled. The brush speed was set to 1200 revolutions per minute per the manufacturer recommendation. Fifteen samples were taken per plane and experiments repeated on multiple days to capture inter-day variability.

Computational fluid dynamics model development

This study used COMSOL Multiphysics® (version 5.4), a multiphysics solver which uses a finite element method (COMSOL 2018). The model was a standard k-ε turbulence method with steady state conditions considering gravity. To account for hydrostatic pressure, a two-equation model using Reynolds Averaged Navier-Stokes (RANS) and wall functions was used. This model is recommended for used with high Reynolds numbers and low Mach numbers indicating incompressible flow, which is representative of the exposure chamber flow conditions (CFD Module User's Guide 2018). The standard k-ε model is robust and commonly used to model airflow around bluff bodies which is an important consideration for future work.

The aerosol chamber was imported to COMSOL software from a 3-dimensional computer-aided design (CAD) file that allowed for an accurate digital representation of the chamber as the computational domain. The model was created full size and used the HEPA filter bank as the inlets, one for each filter, with additional inlets at the door to account for improper seals. An 11-inlet model was designed which accounted for leaks in the door as recorded with

hot wire anemometer described below. This model was deemed to be the best representative model of the exposure chamber based on the velocity profile obtained during characterization. The model considered each of the 9 HEPA filters as an inlet boundary condition with the velocity determined by measuring face velocity at the filter exterior with a hot wire anemometer (Table 1). During the process of model development, the best results applied a 10% increase to the observed face velocity measurement. An additional 2 inlets were included at the bottom of the door to represent leaks. The outlet boundary condition was constant pressure set at the location of plane 21. The initial conditions were set by the experimentally determined conditions at plane 1 with pressure set to 0.971 atm, temperature set to 294 K and velocity of 0.51 m s^{-1} (representative of average chamber velocity).

Table 1 placement

The governing equations are the RANS equations with transport equations for k and ε shown (Equation 1 and 2). The experimental conditions reflected steady temperature as there were no heat sources or sinks within the exposure chamber. Gravity was considered to account for hydrostatic pressure and larger particle settling for applicability to future experiment. The geometry for the exposure chamber was created using CAD software with the design specifications and post-construction measurements. The mesh consisted of 1,262,836 elements with 1,040,112 tetrahedral, 11,418 pyramid, and 211,306 prism elements.

$$\rho \frac{\partial k}{\partial t} + \rho \boldsymbol{u} \cdot \nabla \mathrm{k} = \nabla \cdot \left(\left(\mu + \frac{\mu_T}{\sigma_k} \right) \nabla k \right) + P_k - \rho \varepsilon \quad (1)$$

$$\rho \frac{\partial \varepsilon}{\partial t} + \rho \boldsymbol{u} \cdot \nabla \varepsilon = \nabla \cdot \left(\left(\mu + \frac{\mu_T}{\sigma_\varepsilon} \right) \nabla \varepsilon \right) + C_{\varepsilon 1} \frac{\varepsilon}{k} P_k - C_{\varepsilon 2} \rho \frac{\varepsilon^2}{k} \quad (2)$$

Table 2 placement

The measured velocity profile was compared to numerical simulation by averaging the computed solutions across the face of the imaginary blocks (i.e. 1A-low, with 9 blocks per plane). The velocity field solutions were exported from COMSOL Multiphysics® and sorted, filtered, and averaged using Python (version 3.7.1, Jupyter Notebook version 5.7.4) to return the velocity profile average for each block. When comparing measured and simulated values, a total of 117 squares were considered from the characterization. The comparison was made based on the confidence interval (C.I.) of measurements from the ADM-880c. Locations that were measured multiple times were considered highly variable if repeated measurements fell outside the C.I. of the original measurement and thus were not considered ideal for model verification and validation. Locations where repeated measurements all fell within the respective C.I.s were considered good locations for validation and weighted more heavily in analysis. Locations that were only measured once were considered based on the C.I. of the single measurement.

Of 117 squares, 9 were considered highly variable based on the criteria (7.70%). There were a remaining 54 squares (46.15%) with multiple measurements and 54 (46.15%) with only a single measurement. For model validation purposes, if the simulated value fell within the observed range with C.I., it was considered a valid simulated value with less emphasis given to highly variable locations due to the larger inclusion range.

Analysis and results

Chamber measurement results

Velocity data were visualized as contour plots using the open source software R (Version 3.6.0). Breakpoints for the velocity were chosen based on the VelGrid's precision, ± 3% ± 7 fpm (± 3% ± 0.03556 m s^{-1}) (Shortridge Instruments 2015). When plotted, data for the entire chamber without a flow straightener showed unevenness of flow throughout the chamber, though the least variability was observed in the middle slice of the chamber, away from horizontal position C (Figure 4). Velocity plots for when the fan operated at 0.2 m s^{-1} and 1 m s^{-1} are available in the Supplemental Information. All three fan speeds showed velocity extremes at chamber locations 9 and 12, indicating gaps in the door.

Figure 4 placement

Plotted data for flow-straightened air followed the same pattern observed without the flow straightener (Figure 5). The straightener was placed at chamber position 7, in hopes that it would improve stability in sections 8 – 13, allowing for experiments to take place within easy reach of the only access point, the door. Despite the flow straightener, disturbances at chamber positions 9 – 12 persisted. For this reason, data are only presented moving forward for the cases when the flow straightener was not in place. Profiles for 0.2 m s^{-1} and 1 m s^{-1} and all other figures pertaining to measurements taken with the flow straightener in place are available in the Supplemental Information.

Figure 5 placement

Considering the uneven profiles collected along the chamber length, measurements were taken across different days to verify the repeatability of measurements. In Figure 6, the initial

measurements are shown as black dots. Measurements collected on subsequent days are shown as red and blue dots. The pink ribbon shows the uncertainty surrounding the initial measurements. The Grubbs' test was used to determine any data points that were outliers (α = 0.05). The only outliers found were in the 0.2 m s^{-1} data (see Supplemental Information). Results were similar for velocities measured with the flow straightener. Repeated measurements at 0.2 m s^{-1} and 1 m s^{-1} are available in the Supplemental Information. The variability observed was deemed controlled enough to proceed with further characterization without modification of the chamber.

Figure 6 placement

Velocity data were evaluated qualitatively and quantitatively for normality using quantile-quantile plots and the Shapiro-Wilkes test. Data collected without a flow straightener did not behave normally; however, those collected with the flow straightener in place did behave normally (Figure 7).

Figure 7 placement

Data were tested for equal variance using Levene's test for data procured without the flow straightener and Bartlett's test for those procured with the flow straightener. A significance of 0.05 was chosen as the cutoff. Table 2 shows the results of Levene's test for a variety of conditions: the longitudinal chamber position alone, the chamber position with regard to the vertical position, the chamber position with regard to the horizontal position, and the horizontal position with regard to the vertical position. Of these conditions, it was desirable to achieve either equal variance along the chamber length or equal variance within one plane at a specific

chamber position. With respect to only the chamber position, equal variance could not be assumed for fan speeds 0.5 and 1 m s^{-1}. The null hypothesis could not be rejected for any fan speed when considering the horizontal and vertical position, suggesting that in a plane at a specific chamber location, equal variance exists. While equal variance for chamber position with respect to the vertical or horizontal positions failed to reject the null, these conditions were not physically meaningful as they implied a long rectangular prism with equal variance, but unequal velocities. It is unlikely any sampling scenario would rely on that specific combination of conditions.

Table 3 placement

These results for the horizontal and vertical position interaction were qualitatively evaluated through boxplots (Figure 8). The conclusion remains the same though the extent of the variances is visually more apparent.

Figure 8 placement

Planes 5 and 7 without the flow straightener and planes 8 and 10 with the flow straightener were chosen for further characterization. Every two-minute sample at a single location in the plane was transformed from raw counts to the mass mean diameter through the process described below. Next, the geometric mean of each bin was computed (Equation 3) where di is the midpoint of the ith bin and ni is the number of particles in that bin. N represents the total number of bins.

$$\text{Geometric Mean} = \left(\prod_{i=1}^{N} d_i^{n_i}\right)^{\frac{1}{N}} \quad (3)$$

The midpoint for each particle size bin of the optical particle counter (OPC) was determined by averaging the extremes of the range. The volume of the particle this midpoint represented was calculated using Equation 4 where $d_{midpoint}$ is the diameter of the midpoint of the bin in meters, assuming a spherical particle shape.

$$\mathrm{V(m^3)} = \frac{\pi\left(d_{midpoint} * 10^{-6}\right)^3}{6} \tag{4}$$

The mass of the particles counted in each bin was computed with Equation 5, which assumed a particle density (ρ) of 500 kg/m3 per the manufacturer's safety data sheet (SDS).

$$\text{Mass (mg)} = (\rho * count * particle\ volume) * 10^6 \tag{5}$$

Each bin was normalized by dividing the mass by the bin width, resulting in a frequency/µm. The frequency was converted to a fraction by dividing the previous value by the total mass observed in all bins. The cumulative mass was calculated by dividing the mass per bin by the total mass of all bins.

The natural log of the midpoint diameter per bin was taken and this value multiplied by the number of particles in the bin. The average of this column was the count mean diameter (CMD) (Equation 6).

$$\text{CMD (µm)} = \frac{\sum_{i=1}^{N} n_{particles,bin\ i} * \ln\left(d_{midpoint\ of\ bin\ i}\right)}{N} \tag{6}$$

For the mass mean diameter (MMD), the natural log of the midpoint particle diameter for the bin was multiplied by the mass in the bin. The average of all the bin values was the MMD (Equation 7).

$$\text{MMD } (\mu\text{m}) = \frac{\sum_{i=1}^{N} mass_{particles,bin\ i} * \ln\left(d_{midpoint\ of\ bin\ i}\right)}{N} \tag{7}$$

The geometric standard deviation (GSD) for the CMD was calculated using Equation 8.

$$GSD_{CMD} = e^{\left(\frac{\sum_{i=1}^{N}\left(n_{particles,bin\ i}*\left(\ln\left(\frac{d_{midpoint,bin\ i}}{d_{CMD}}\right)\right)^2\right)}{\left(\sum_{i=1}^{N} n_{particles,bin\ i}\right)-1}\right)^{0.5}} \tag{8}$$

The GSD for the MMD followed a very similar process, with the exception of substituting in the MMD and mass instead of CMD and number of particles (Equation 9). Results of the preceding equations are shown in the Supplemental Information.

$$GSD_{MMD} = e^{\left(\frac{\sum_{i=1}^{N}\left(mass_{particles,bin\ i}*\left(\ln\left(\frac{d_{midpoint,bin\ i}}{d_{MMD}}\right)\right)^2\right)}{\left(\sum_{i=1}^{N} mass_{particles,bin\ i}\right)-1}\right)^{0.5}} \tag{9}$$

The MMD calculated from each reading was plotted by horizontal position, then vertical position to discern if aerosol distribution was more stable from side-to-side or top-to-bottom in the plane (Figure 9). The 0.5 m s^{-1} setting yielded the most consistent results though the MMD reported at any fan setting and any location only ranged from 3.5 – 4.25 µm. The boxplots for planes 7, 8, and 10 are available in the Supplemental Information.

Figure 9 placement

Considering the MMD boxplots, contours of the velocity and particle count profiles were generated to visualize airflow and aerosol patterns by plane (Figure 10). These final contours served as guidelines for follow-on research sampler placement. The complete set of contour maps by plane and fan setting are found in the Supplemental Information.

Figure 10 placement

All data gathered and analyzed confirmed initial design expectations, in that flow was turbulent and irregular along any plane of interest. Aerosol distribution data were encouraging as the distribution, if not the raw counts, were similar at all nine points sampled for each plane.

CFD Model Results

The simulation results (selected results in Table 3, see Supplemental Information for full results) fell within measurement confidence intervals as observed in experiments for 90/117 (76.92%) squares overall and 47/54 (87.04%) of the squares with multiple measurements. Four of the forty-five locations shown had model values which fell outside of the measurement C.I.s (shown in bold). Five of the nine highly variable locations (indicated by *) occurred in either plane 9 or 10, indicating the door leak was impacting consistent measurements in those locations. The model reasonably simulated the characterization based on velocity profile at each plane (Figure 11). In contrast to figures showing measured values, simulated values are only from a slice at the precise height indicated.

The mesh was left in free tetrahedral form generated by the software algorithm but had a finer mesh along the walls due to concerns with element size compared to the corners and inlet geometries. The mesh would need to be refined for future work that included more complex

geometries inside the chamber but was adequate for validation of velocity profiles at each chamber location.

Table 4 placement

Figure 11 placement

Conclusions and recommendations

A 6.401-m chamber with 0.835 m^2 cross-section was constructed to serve as a test space for aerosol studies. Air flow profiles were generated by measuring velocity at prescribed locations along the x-, y-, and z-axes. Aerosol size distribution profiles were created for the four planes identified as most stable with and without the flow straightener. Inter-day variability was deemed acceptable considering the limitations of the anemometer. This finding supports the use of the chamber for future studies without modification. While equal variance existed across x-y planes in the chamber, the magnitude of the variance was considerable. This considerable variance suggests researchers must either collect large sample sets to detect significance among the data or restrict their activities to a smaller, better defined subsection of a given plane.
The creation of a computational fluid dynamics model validated by physical measurements will be a great asset to future research projects. It will allow researchers to predict the impact to flow behavior when different sampling apparatus are in place prior to conducting pilot research. It is apparent that improvements to the door's seal could be made and CFD models could inform an improved design as well as behavior after modification. Finally, the air flow was only characterized at three fan settings, and aerosol behavior at a single fan speed. It stands to reason

that subsequent research may rely on intermediate velocities to achieve their research aims. Refinement of the current model would allow predictions to be made of flow behavior that could easily be validated with judicious sampling, rather than a repeat of the entire characterization outlined in this report. This CFD model will ultimately help save researchers time and funds. The data collected and analyzed in this study confirm the chamber performance is stable enough for a variety of research aims. Periodic confirmation of chamber performance is recommended. Any significant changes to the setup, including replacement of the access door require a complete recharacterization. With the present setup, researchers will need to conduct pilot studies to capture any bias inherent in the selected chamber location before proceeding to full scale studies, though use of the CFD model will aid this process.

Acknowledgments

We thank UES, Inc for their support in chamber assembly and for providing dedicated areas to support this research effort. In addition, Stephanie Ohms for her help in chamber assembly.

Funding

This work was supported by the United States Air Force, 711 Human Performance Wing, Airman Systems Directorate, Warfighter and Medical Optimization Division, under Grant #2019-073, and Grant #FA8650-17-C-6834.

Disclosure

No financial interest or benefit has arisen from the direct applications of this research.

References

Baldwin, P. E. J. and A. D. Maynard. 1998. A survey of wind speeds in indoor workplaces. Annals of Occupational Hygiene 42 (5):303–313. doi: https://doi.org/10.1016/S0003-4878(98)00031-3.

Bennett, J., D. Marlow, F. Nourian, J. Breay, A. Feng, and M. Methner. 2018. Effect of ventilation velocity on hexavalent chromium and isocyanate exposures in aircraft paint spraying. Journal of Occupational and Environmental Hygiene 15 (3):167-181. doi: 10.1080/15459624.2017.1401710.

CFD Module User's Guide. COMSOL Multiphysics®. (version 5.4). 2018. Stockholm, Sweden: COMSOL AB.

COMSOL Multiphysics®. (version 5.4). 2018. Stockholm, Sweden: COMSOL AB.

Elnahas, W. M. 2005. Effects of heating, breathing, hair style, posture, and air velocity on breathing zone concentrations for an anthropometrically-correct manikin in a wind tunnel. PhD diss., West Virginia University.

Engineers Edge, LLC. (no date) Viscosity of Air, Dynamic and Kinematic. Accessed January 3, 2020. https://www.engineersedge.com/physics/viscosity_of_air_dynamic_and_kinematic_14483.htm

Hagerman, I., C. Isaxon, A. Gudmundsson, A. Wierzbicka, K. Dierschke, M. Berglund, J. Pagels, J. Nielsen, E. Assarsson, U. B. K. Andersson, et al. 2014. Effects on heart rate variability by artificially generated indoor nano-sized particles in a chamber study. Atmospheric Environment 88:165–171. doi: 10.1016/j.atmosenv.2014.02.003.

Isaxon, C., K. Dierschke, J. H. Pagels, A. Wierszbicka, A. Gudmundsson, J. Löndahl, I. Hagerman, M. Berglund, E. Assarsson, U. B. Andersson, et al. 2013. Realistic indoor nano-aerosols for a human exposure facility. Journal of Aerosol Science 60:55–66. doi: 10.1016/j.jaerosci.2013.02.003.

Li, J., I. Yavuz, I. Celik, and S. Guffey. 2007. Predicting worker exposure—the effect of ventilation velocity, free-stream turbulence and thermal condition. Journal of occupational and environmental hygiene 4 (11):864-874. doi: https://doi.org/10.1080/15459620701665688.

Lidén, C., L. Lundgren, L. Skare, G. Lidén, G. Tornling, and S. Krantz. 1998. A new whole-body exposure chamber for human skin and lung challenge experiments - the generation of wheat flour aerosols. Annals of Occupational Hygiene 42 (8):541–547. doi: 10.1016/S0003-4878(98)00063-5.

Lin, C. H., K. H. Dunn, R. H. Horstman, J. L. Topmiller, M. F. Ahlers, J. S. Bennett, L. M. Sedgwick, and S. Wirogo. 2005. Numerical simulation of airflow and airborne pathogen transport in aircraft cabins – part I: numerical simulation of the flow field. ASHRAE Transactions 111 (1):755-763.

Lucci, F., N. D. Castro, A. A. Rostami, M. J. Oldham, J. Hoeng, Y. B. Pithawalla, and A. K. Kuczaj. 2018. Characterization and modeling of aerosol deposition in Vitrocell® exposure systems - exposure well chamber deposition efficiency. Journal of Aerosol Science 123:141-160. doi: https://doi.org/10.1016/j.jaerosci.2018.06.015.

Lundgren, L. 2006. Large organic aerosols in a human exposure chamber: Applications in occupational dermatology and lung medicine. Thesis, Karolinska Institutet.

Lundgren, L., L. Skare, C. Lidén, and G. Tornling. 2006. Large organic aerosols in a dynamic and continuous whole-body exposure chamber tested on humans and on a heated mannequin. Annals of Occupational Hygiene 50 (7):705–715. doi: 10.1093/annhyg/mel027.

NATO (National Atlantic Treaty Organization). 2013. Stretchers, bearing brackets and attachment supports. NATO Standard AMedP-2.1, NATO Standardization Agency.

de Nevers, N. 2005. Fluid Mechanics for Chemical Engineers. 3rd ed. New York, NY: McGraw-Hill Companies.

Nielsen, P. V. 1974. Flow in air conditioned rooms: Model experiments and numerical solution of the flow equations. Ph.D. thesis, Technical University of Denmark (Aalborg Universitet).

Pieretti, L. F. and Y. Y. Hammad. 2018. Performance of a whole-body human dust inhalation challenge exposure chamber. Toxicology Reports 5:793–799. doi: 10.1016/j.toxrep.2018.07.004.

Rønborg, S. M., H. Mosbech, C. R. Johnsen, and L. K. Poulsen. 1996. Exposure chamber for allergen challenge: The development and validation of a new concept. Allergy: European Journal of Allergy and Clinical Immunology 51 (2):82–88. doi: 10.1111/j.1398-9995.1996.tb04562.x.

Shortridge Instruments (2015) Airdata Multimeter ADM-880c Manual. Scottsdale, AZ: Shortridge Instruments, Inc.

Srebric, J. and Q. Chen. 2002. An example of verification, validation, and reporting of indoor environment CFD analyses (RP-1133). ASHRAE Transactions 108 (2):185-194.

White, F. M. 2011. Fluid Mechanics. 7th ed. New York, NY: McGraw-Hill.

Zhang, Y., Y. Sun, A. Wang, J. L. Topmiller, and J. S. Bennett. 2005. Experimental characterization of airflows in aircraft cabins, part II: results and research recommendations. ASHRAE Transactions 111 (2):53-59.

Captions

List of Figures

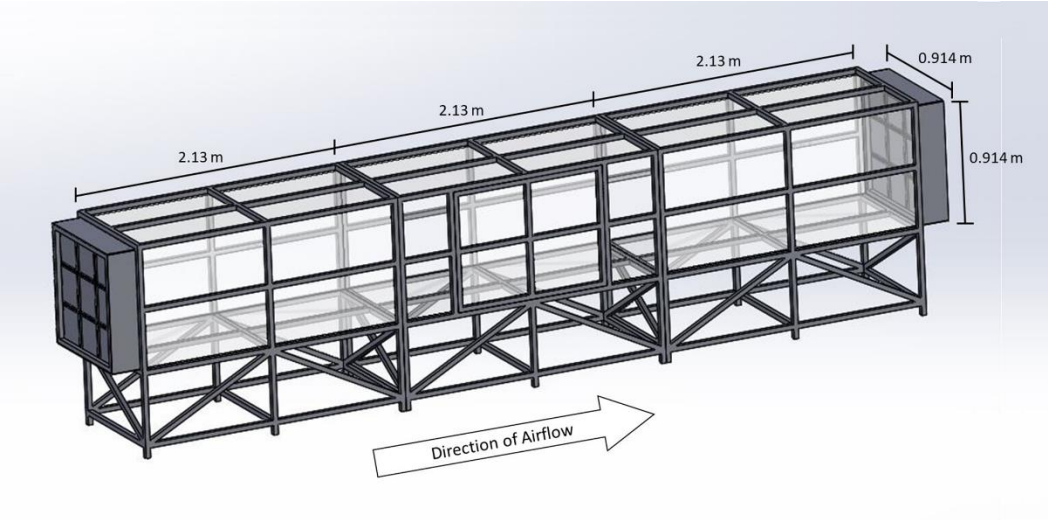

Figure 39. Final Chamber Design

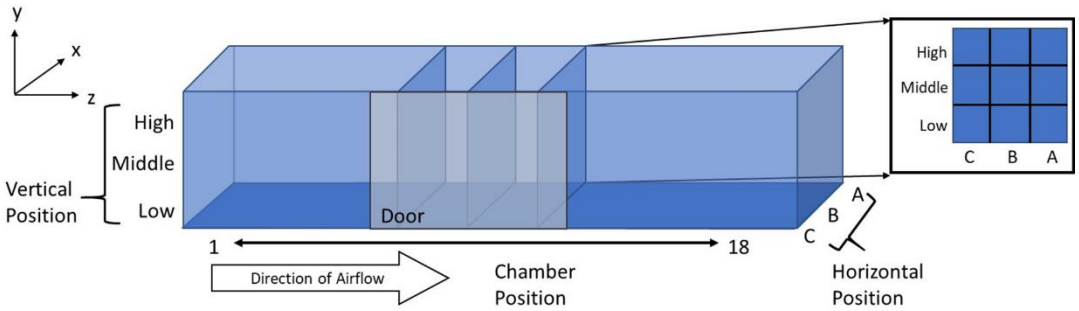

Figure 40. Chamber Measurement Locations

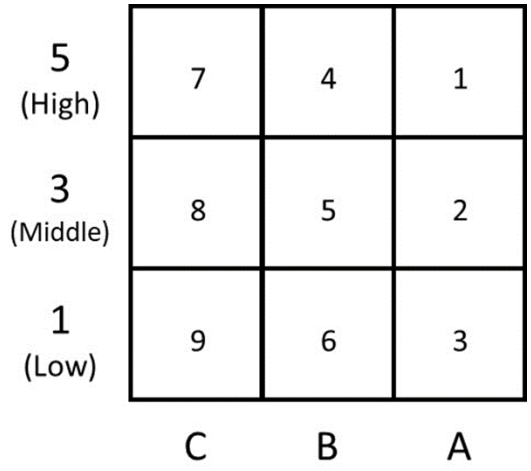

Figure 41. OPS Reading Positions in a Cross-Sectional Plane

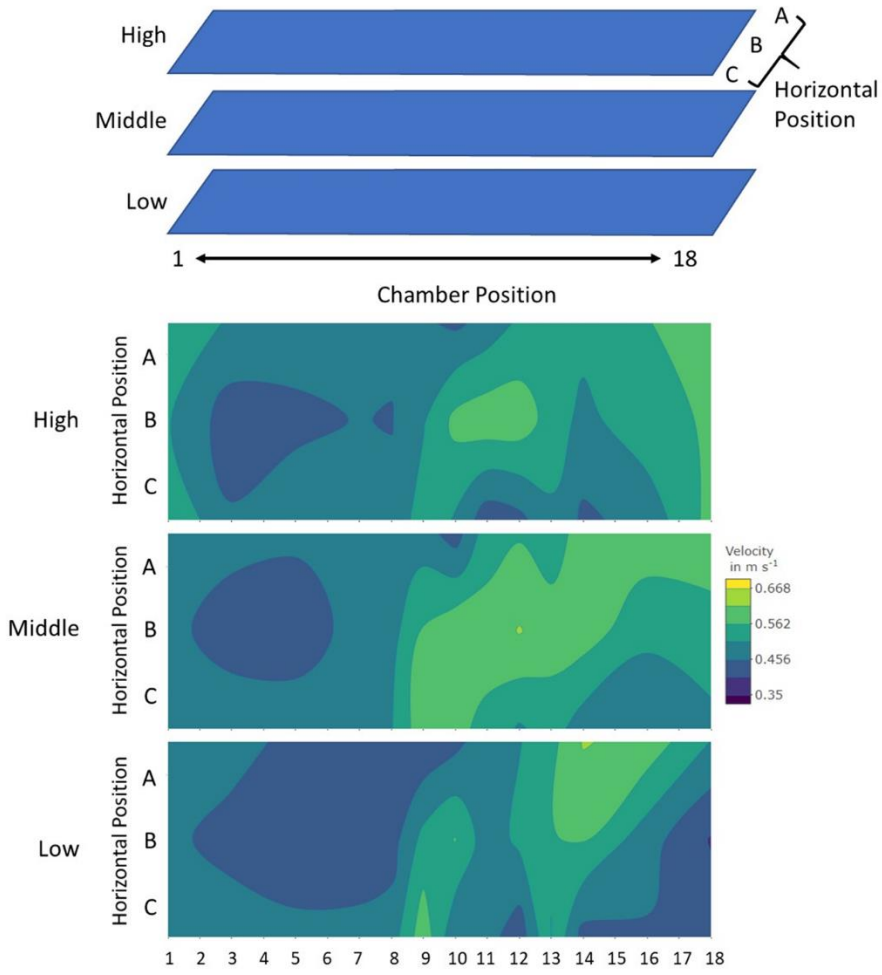

Figure 42. Vertical Velocity Profiles in the Chamber at 0.5 m s^{-1}, no Flow Straightener

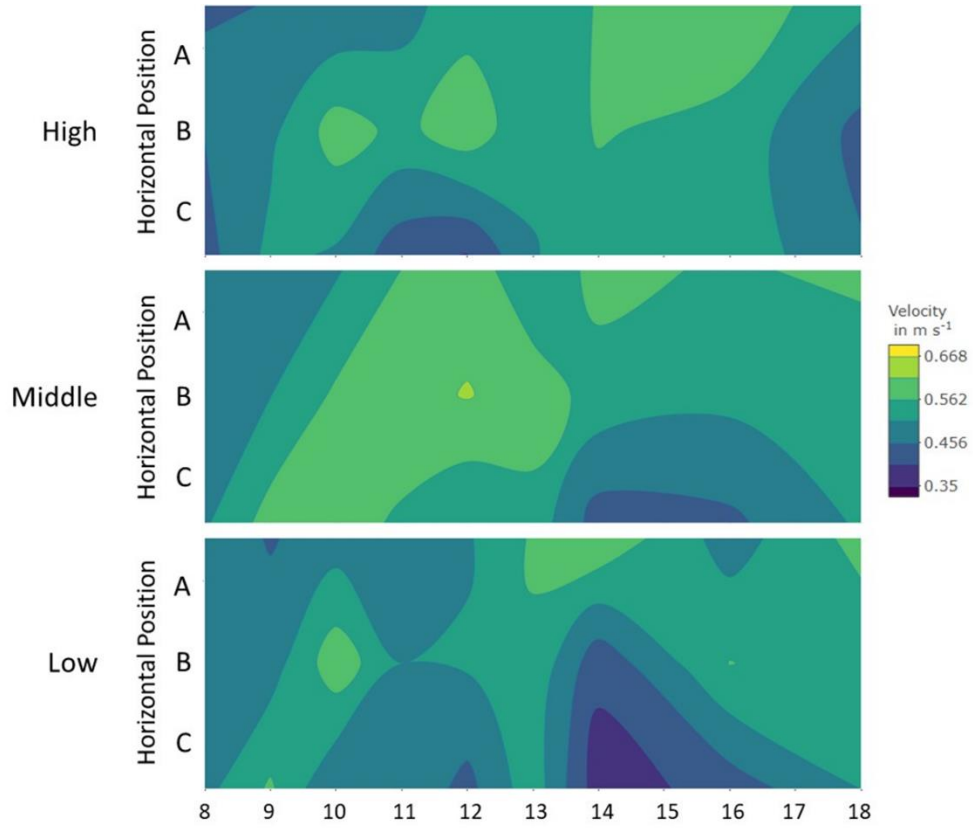

Figure 43. Vertical Velocity Profiles in the Chamber at 0.5 m s^{-1}, with Flow Straightener

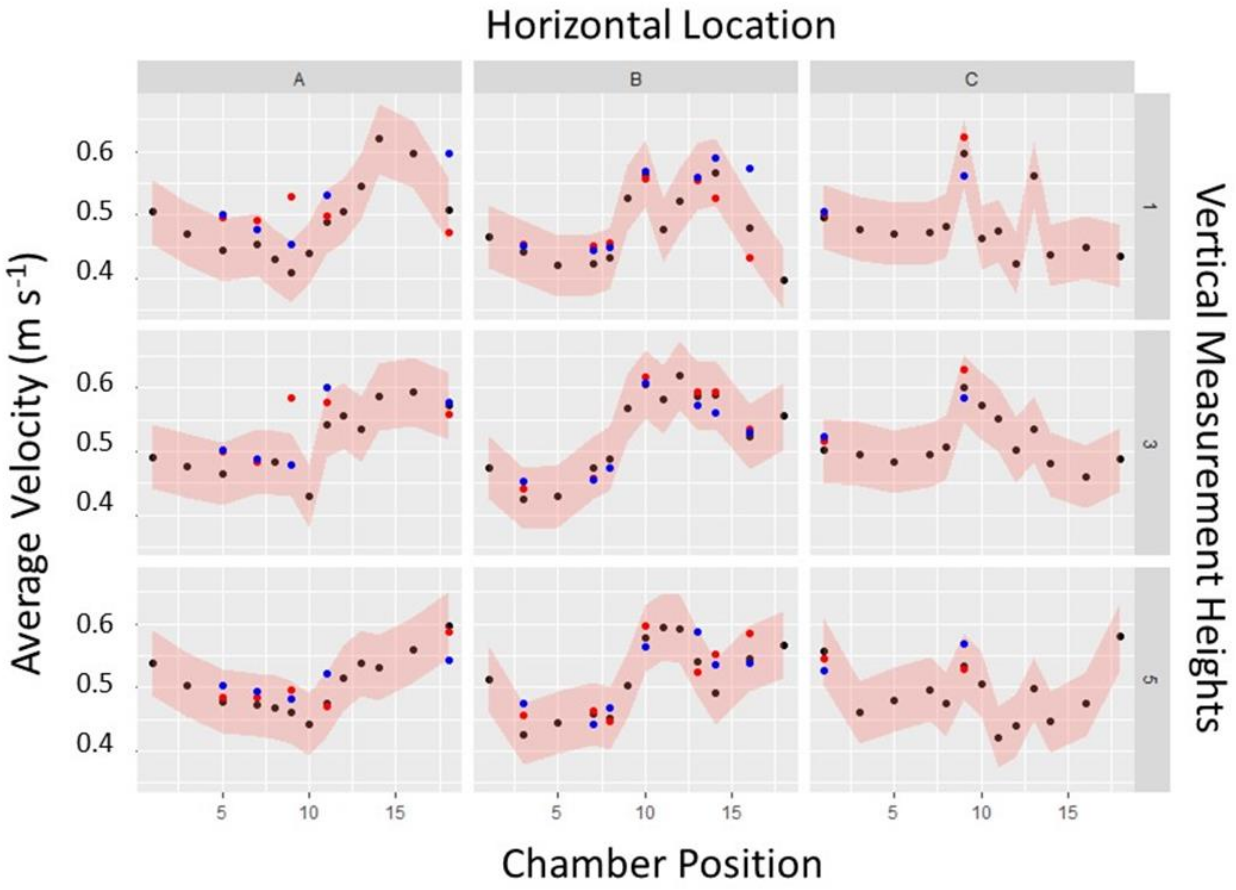

Figure 44. Day-to-Day Variability in Average Velocity at 0.5 m s^{-1}, no Flow Straightener

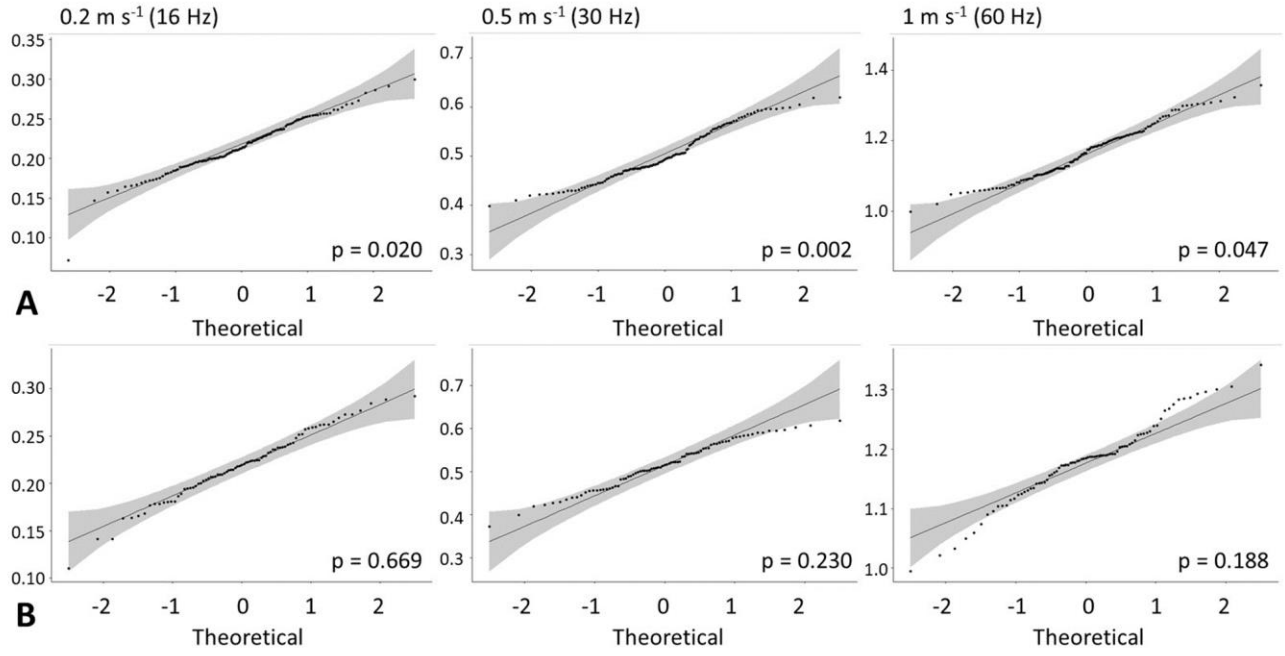

Figure 45. Quantile-Quantile Plots of Velocity Measurements: A) no Flow Straightener; B) with Flow Straightener

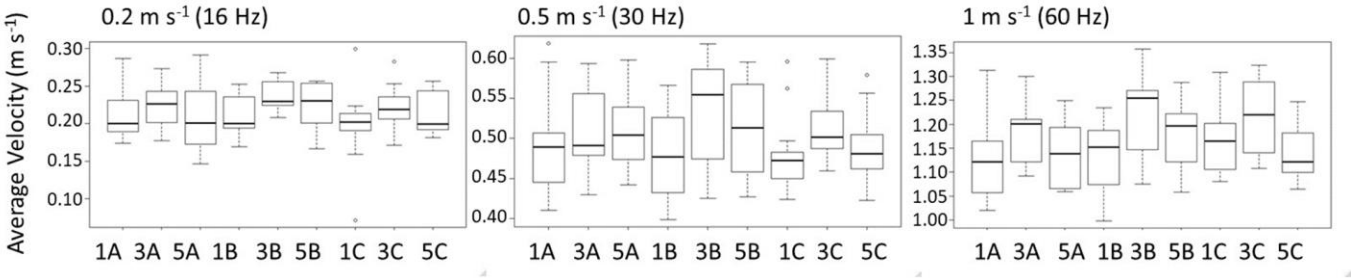

Figure 46. Variance of Velocity Profiles for without Flow Straightener Data

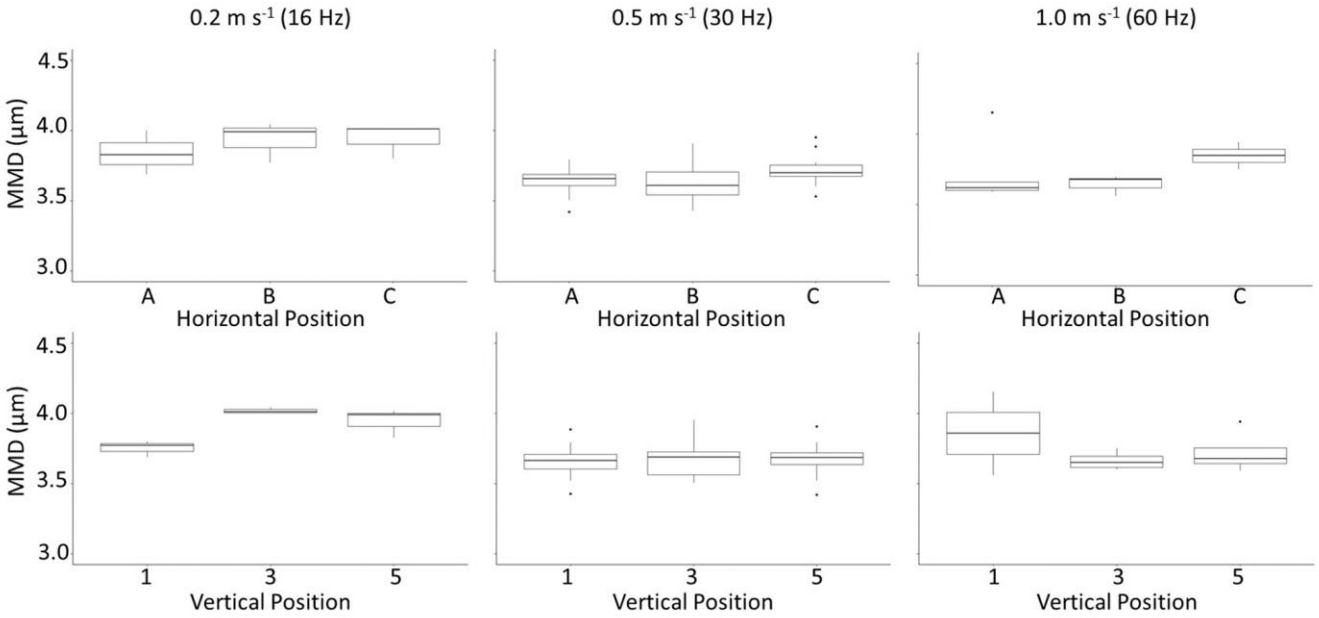

Figure 47. MMD Boxplots for Plane 5

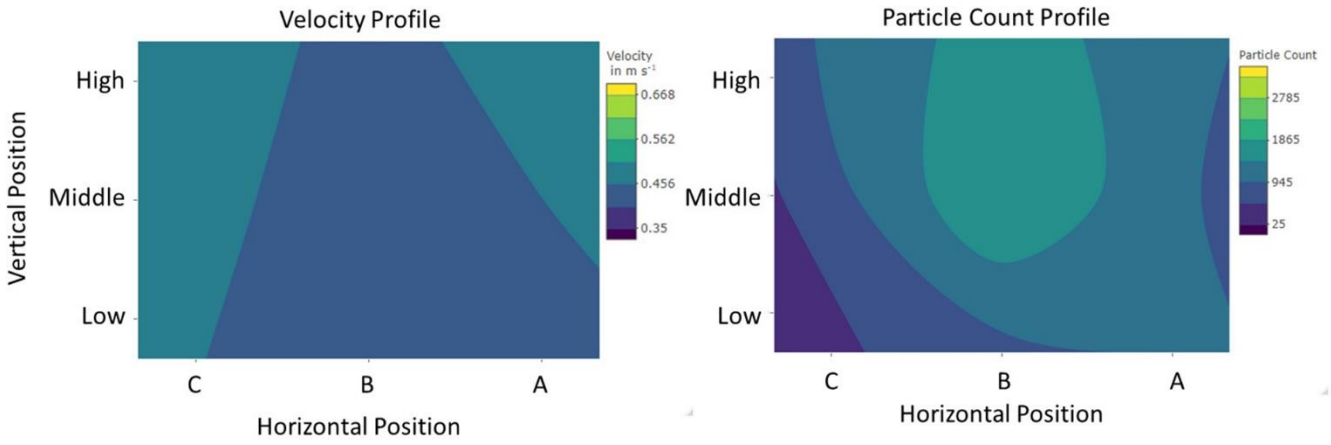

Figure 48. Velocity and Particle Count Profiles in Plane 5 at 0.5 m s^{-1}

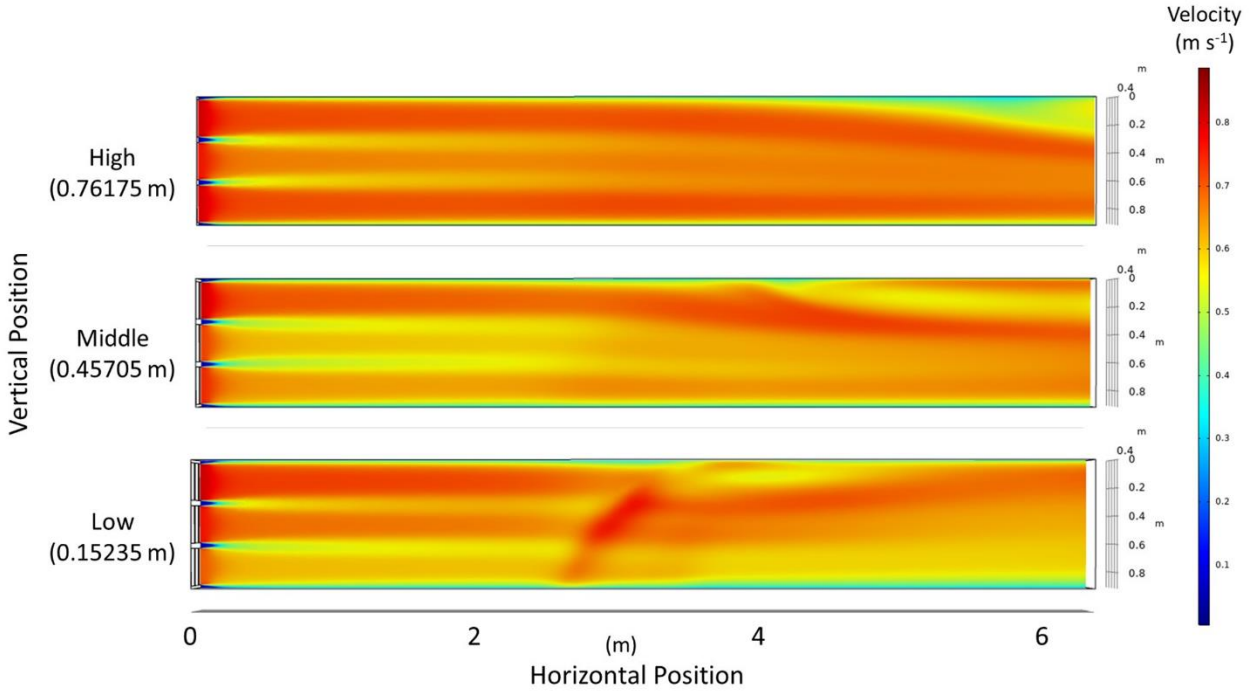

Figure 49. Airflow Visualization from CFD Model

List of Tables

Table 18. Exterior Filter Face Velocity

Filter Location	**Average Velocity**		**Standard Deviation**
	(fpm)	**[m s^{-1}]**	
A-Low	144.6	[0.735]	1.67
B-Low	136.0	[0.691]	2.12
C-Low	124.0	[0.630]	1.22
A-Middle	126.0	[0.640]	2.35
B-Middle	112.4	[0.571]	1.14
C-Middle	116.0	[0.589]	2.24
A-High	130.8	[0.664]	3.63
B-High	123.2	[0.626]	1.10
C-High	130.0	[0.660]	1.22

Table 19. Nomenclature for Equation 1 and 2

Variable	**Definition**	**Equation/Value**
μ_T	Turbulent Viscosity	$\mu_T = \rho * C_\mu \left(\frac{k^2}{\epsilon}\right)$
ρ	Fluid Density - depends on temperature, pressure, and fluid	Constant for incompressible flow
C_μ	Constant	0.09
k	Turbulent Kinetic Energy	Equation 1
ε	Turbulent Dissipation Rate	Equation 2
u	Velocity Field	User Input
∇	Gradient/Partial Differential	
μ	Fluid Dynamic Viscosity - relates the shear stress and shear rates of a liquid	

σ_k	Constant	1.0
P_k	Production Term	$P_k = \mu_T \left(\nabla \mathbf{u} : (\nabla \mathbf{u} + (\nabla \mathbf{u})^T) - \frac{2}{3}(\nabla \cdot \mathbf{u})^2 \right) - \frac{2}{3} \rho k \nabla \cdot \mathbf{u}$
T	Temperature - user defined reference temperature or calculated from other model inputs	
σ_ε	Constant	1.3
$C_{\varepsilon 1}$	Constant	1.44
$C_{\varepsilon 2}$	Constant	1.92
B	Surface roughness (Constant or user defined)	5.2
κ_v	von Kárman constant	0.41

Table 20. Results of Levene's Test for Equal Variance for Velocity Data without Flow Straightener

Air Velocity, m s^{-1} (Fan Frequency, Hz)	Chamber Position only			Chamber Position, Vertical Position			Chamber Position, Horizontal Position		
	Df	F	Pr(>F)	Df	F	Pr(>F)	Df	F	Pr(>F
0.2 (16)	12	1.7	0.077	38	0.502	0.990	38	0.502	0.990
0.5 (30)	12	3.200	0.0006	38	0.597	0.959	38	0.597	0.959
1.0 (60)	12	2.705	0.0032	38	0.528	0.984	38	0.528	0.984

Table 21. Validation Points for Planes of Interest

Plane	Grid Square	Velocity ($m\ s^{-1}$)				Percent Difference
		Measured Velocity	Min (Lower C.I.)	Max (Upper C.I.)	Model Value	
5	A-Low	0.445	0.396	0.550	0.546	23%
	A-Middle	0.464	0.415	0.554	0.536	15%
	A-High	0.478	0.423	0.568	0.464	-3%
	B-Low	0.420	0.372	0.555	0.492	17%
	B-Middle*	0.430	0.381	0.605	0.496	15%
	B-High	0.446	0.397	0.562	0.451	1%
	C-Low*	0.471	0.293	0.521	0.492	4%
	C-Middle	0.483	0.433	0.573	0.484	0%
	C-High	0.481	0.431	0.551	0.487	1%
7	A-Low	0.455	0.405	0.545	0.539	19%
	A-Middle	0.484	0.408	0.542	0.533	10%
	A-High	0.473	0.403	0.546	0.458	-3%
	B-Low	0.423	0.375	0.523	0.496	17%
	B-Middle	0.474	0.405	0.577	0.505	6%
	B-High	0.458	0.393	0.534	0.457	0%
	C-Low	0.472	0.364	0.522	0.491	4%
	C-Middle	0.495	0.444	0.562	0.484	-2%
	C-High	0.497	0.414	0.547	0.488	-2%
8	A-Low	0.430	0.381	0.546	0.531	24%
	A-Middle	0.483	0.398	0.533	0.520	8%
	A-High	0.469	0.365	0.519	0.435	-7%
	B-Low	0.432	0.383	0.552	0.504	17%
	B-Middle	0.489	0.424	0.556	0.511	4%
	B-High	0.453	0.398	0.518	0.461	2%
	C-Low	0.483	0.433	0.586	0.492	2%
	C-Middle	0.506	0.453	0.580	0.492	-3%
	C-High	0.474	0.395	0.524	0.485	2%
9	A-Low*	0.410	0.362	0.579	0.522	27%
	A-Middle*	0.479	0.428	0.636	0.468	-2%
	A-High	0.462	0.412	0.548	**0.694**	50%
	B-Low	0.526	0.475	0.578	0.502	-5%
	B-Middle	0.568	0.516	0.621	0.525	-8%

	B-High	0.504	0.453	0.554	0.480	-5%
	C-Low	0.596	0.509	0.676	**0.492**	-17%
	C-Middle	0.599	0.530	0.684	**0.496**	-17%
	C-High	0.534	0.478	0.622	0.495	-7%
10	A-Low*	0.440	0.391	0.656	0.515	17%
	A-Middle*	0.429	0.381	0.616	0.534	24%
	A-High	0.442	0.393	0.545	0.533	21%
	B-Low	0.565	0.488	0.696	0.513	-9%
	B-Middle	0.605	0.533	0.678	0.546	-10%
	B-High	0.577	0.468	0.651	0.487	-16%
	C-Low*	0.464	0.360	0.602	0.498	7%
	C-Middle	0.572	0.519	0.671	**0.501**	-12%
	C-High	0.505	0.439	0.559	0.497	-2%

Supplemental Information

Design and characterization of multi-use research for particulate hazards and environmental exposures (MURPHEE) aerosol test chamber – Supplemental Information

Megan L. Steele[a], Emily M. Titus[b], George P. Lemmer[b], Jacob M. Denney[c], Jeremy M. Slagley[c], Casey W. Cooper[c], Robert M. Eninger[d]

[a]Integrative Health & Performance Sciences, UES, Inc, Beavercreek, OH, USA, [b]Department of Systems Engineering and Management, Air Force Institute of Technology, Centauri Contractor, Wright-Patterson AFB, OH, USA, [c]Department of Systems Engineering and Management, Air Force Institute of Technology, Wright-Patterson AFB, OH, USA, [d]HQ Air Force Materiel Command, Office of the Command Surgeon, Wright-Patterson, AFB, USA

CONTACT Megan L. Steele msteele@ues.com Integrative Health & Performance Sciences, UES, Inc, Beavercreek, OH, 45432, USA.

S2. Chamber Design Considerations

Early designs aimed for laminar flow inside the chamber and basic fluid dynamics calculations were undertaken to determine if this would be possible within the space constraints. First, the effect of temperature was considered, and the Reynolds number (Re) was determined for a range of temperatures from 55-85°F, as this represented what could reasonably be expected in indoor workplaces. For each temperature, the appropriate density and dynamic viscosity were used (Engineers' Edge no date). The square cross-section of 2.5 feet was converted to equivalent

pipe diameter and air velocities from 0.1-1 m s^{-1} were considered. The Re was calculated using Equation S1.

Equation S8. Reynolds Number

$$\mathrm{Re} = \frac{Du\rho}{\mu}$$

where,

$\mathrm{Re} = Reynolds\ number$

$D = the\ pipe's\ diameter\ (m)$

$u = fluid\ velocity\ \left(\frac{m}{s}\right)$

$\mu = the\ fluid's\ \ viscosity\ (\frac{N * s}{m^2})$

$\rho = the\ fluid's\ \ density\ (\frac{kg}{m^3})$

This resulted in Reynolds number ranging from 4,265 to 59,468 (conditions of T = 85°F, u = 0.1 m s^{-1} and T = 55°F, u = 1 m s^{-1} respectively). No conditions considered resulted in laminar flow, thus turbulent flow equations were used for subsequent design iterations.

While lacking the consistent uniformity of laminar flow, it has been documented that turbulent flow can fully develop to approximate predictable behavior. For the purpose of this design, flow was considered fully developed if the boundary layers converged (de Nevers 2005). In order to determine if this condition could be met, boundary layer calculations for smooth surface with 2.5-foot cross-section were carried out. A simplified equation for boundary layer

thickness on a flat plate was used, due to the difficulties involved in determining numerical solutions for turbulent airflow (Equation S2) (de Nevers 2005). Air temperature was assumed to be 21°C (the midpoint of the range tested for the Re), giving air a kinematic viscosity of 1.156 x 10-5 m2/s. The same air velocities were used as for the Re calculations and the value of z was varied from 0.5 to 12 feet.

Equation S9. Boundary Layer Thickness

$$\delta = 0.37z\left(\frac{\upsilon}{u_{infinity}z}\right)^{\frac{1}{5}}$$

where,

$\delta = boundary\ layer\ thickness\ (m)$

$z = distance\ along\ z-axis\ (m)$

$\upsilon = kinematic\ viscosity\ of\ the\ fluid\ (\frac{m^2}{s})$

$u_{infinity} = final\ velocity\ (\frac{m}{s})$

These conditions resulted in boundary layer thicknesses ranging from 0.35 to 7.08 inches (corresponding to u = 1 m s^{-1}, z = 0.5 feet and u = 0.1 m s^{-1}, z = 12 feet respectively). These calculations show that fully developed flow does not occur by the midpoint of a 2.5 ft square chamber, which adds an additional degree of difficulty, due to the need to carefully characterize all locations within the chamber in order to conduct reproducible experiments.

S3.1. Velocity Mapping

The VelGrid consists of two crossed pieces, each with a smaller crossed piece near the end of each arm which covers an area 14 x 14 inches2. There are 16 holes to capture air, four on each arm of the device as shown in Figure S1.

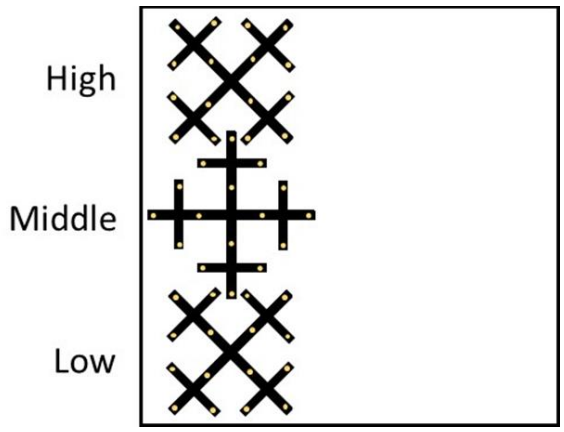

Figure S50. VelGrid Configuration in Chamber Cross-Section

The VelGrid poles were clamped at the break between the second and third sections to avoid any backwash turbulence from disturbing the velocity measurements. This was done for all measurement locations except 18 as the poles were too long so the third section was removed and the pole was clamped a third of the way from the end. For A and C positions, the middle VelGrid was positioned to touch the wall. For B position, the lowest VelGrid was positioned so the two cross arms were centered on the lower support bar of the chamber.

To determine which locations would be measured multiple times, measurement locations were sequentially assigned a number and then Excel was used to generate a random number which was then used as the location. For the third round of measurements, the same locations

were sampled a third time, by sequentially assigning each one a number and then using Excel to generate a random number for the sample order.

The automatic data logging mode of the ADM-880c records data points as quickly as the machine can process them, no more than 10 seconds apart. The ADM-880c automatically corrects for temperature as shown in Equation S3.

Equation S10. Temperature Correction for Velocity

$$Local\ Density\ Velocity = Velocity\ in\ local\ density\ mode * \sqrt{\frac{460 + °F}{530}}$$

S3.1.a. Chamber Characterization Data Processing

In order to know where the three-minute measurement period started and ended in the Excel file, the data line off the ADM-880c display was recorded. The data line was recorded in an Excel sheet both when the thee-minute timer was started and when it finished.

For the initial measurements, data was downloaded from the ADM-880c after every plane (the location was known because locations were always sampled A to C). For the random measurements, data was downloaded after every location in order to maintain data integrity. Downloaded files were named by the location (distance from inlet, horizontal letter, and height, i.e. 18A-3).

There were several steps taken during the data processing. First, the CSV files retrieved from the ADM-880c were converted to Excel files and the unused columns were deleted (mainly those for other ADM-880c recording functionalities). Then the data file was cross-referenced

with the data lines recorded during measurement and the measurement rows were highlighted. During this process the time for the first and last measurements were compared to ensure that a 3-minute window had been recorded. In all cases at least a 3-minute window was recorded. In a couple of instances, the end timer was not heard due to environmental noise and more than 3-minutes of data were collected. In these cases, the start time was used to determine an end row of 3-minutes.

After all of the measurement rows were marked, they were copied to a third Excel workbook to consolidate all data in one place. The location and fan setting information were input manually from the file name and then all data were copied to the new workbook. The columns containing only units were deleted as they were captured in the column headings.

Next, the recorded velocities were corrected for the relative humidity of the workspace. This was done by inserting 7 columns between the existing Temperature (°F) column and the Abs Pres (in Hg) column. These were used to convert temperature to degrees Celsius, calculate the Saturation Vapor Pressure (P_{sat}) and Vapor Pressure (P_{vapor}), contain the relative humidity data, and then calculate the corrected velocity (Equations S4, S5, and S6). The relative humidity data was copied from the downloaded Kestrel data sheet or from manually recorded points. The Kestrel was set to log data every 20 minutes. The following convention was used to assign relative humidity data to velocity readings. If a Kestrel reading was taken at 9:20:00, it was associated with ADM-880c readings between 9:20:00 and 9:39:59. Then the Kestrel reading for 9:40:00 was associated with velocity readings taken between 9:40:00 and 9:59:59. In addition, a column was added to capture the difference between the original value and the corrected value. The calculation of P_{sat} was done by using the equation behind the National Weather Services

Vapor Pressure Calculator (Equation S11) (Brice and Hall No Date). After the saturation vapor pressure was calculated, it was used to calculate the vapor pressure by the relationship between relative humidity and P_{sat} (Equation S12) (Engineering Toolbox 2004). Finally, the barometric pressure (Abs Pres, recorded by the ADM-880c), recorded velocity, and vapor pressure were used to determine the corrected velocity (Equation S13).

Equation S11. Saturation Vapor Pressure

$$\mathrm{P_{sat}} = 6.11 * 10^{\frac{7.5*T}{237.3+T}}, \;\; P_{sat} = [mbar]$$

$$\mathrm{P_{[inHg]}} = 0.0295300 * P_{[mbar]}$$

Equation S12. Relative Humidity, Vapor Pressure, and Saturation Vapor Pressure Relationship

$$\mathrm{RH} = \left(\frac{P_{vapor}}{P_{sat}}\right) * 100\% \rightarrow P_{vapor} = \left(\frac{\mathrm{RH}}{100}\right) * P_{sat}$$

Equation S13. Corrected Velocity for Moist Air

$$\mathrm{V_{moist\ air}} = \frac{P_b * V_{dry}}{P_b - P_{vapor}},$$

Where:

$V_{moist\ air}$ = velocity corrected for moist air

P_b = local barometric pressure,

V_{dry} = velocity corrected for local density (T & barometric pressure)

P_{vapor}=vapor pressure

S4.1. Chamber Characterization Data Processing

Velocity Profiles at 16 and 60 Hz

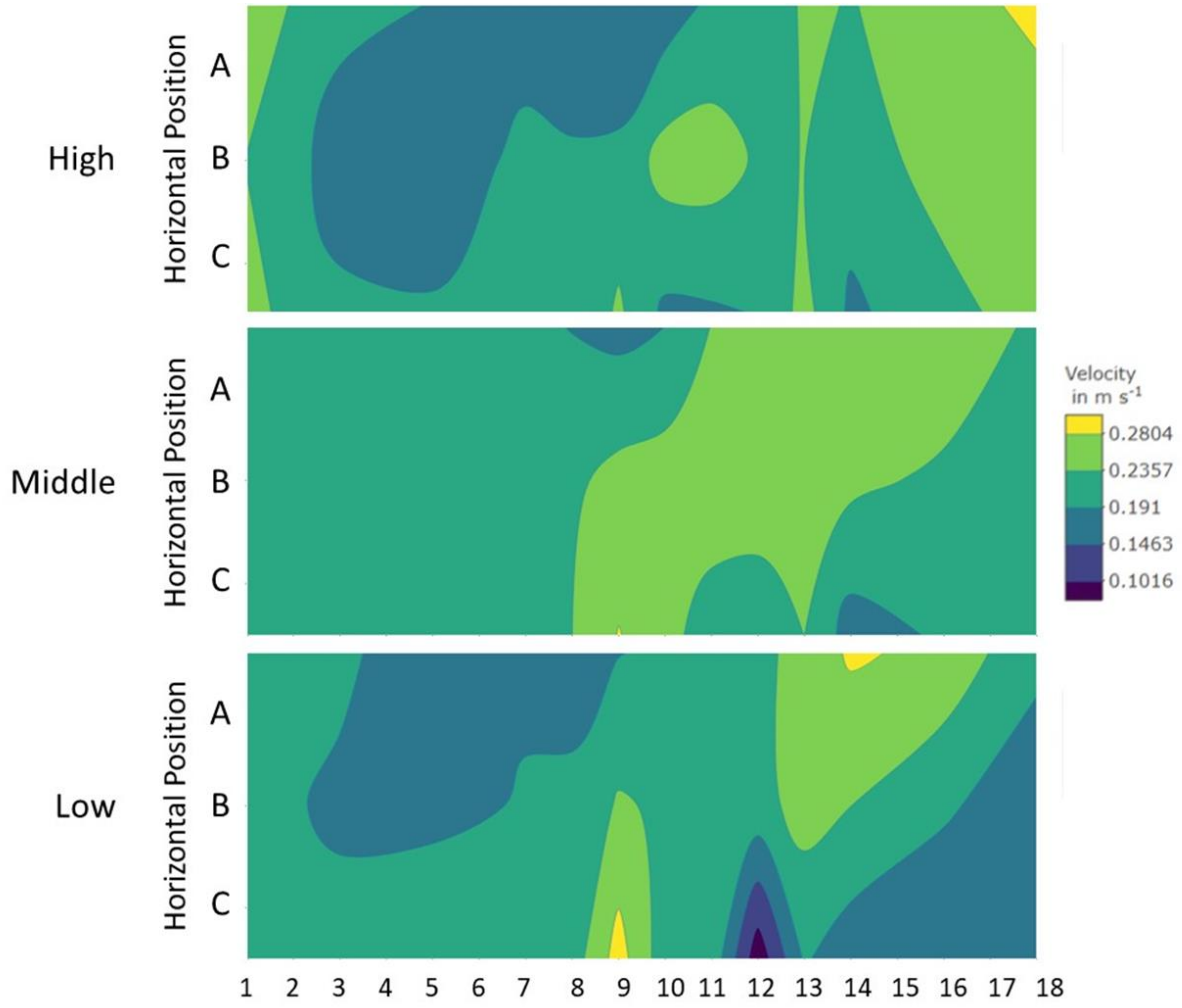

Figure S51. Vertical Velocity Profile of the Chamber at 0.2 m s^{-1} (16 Hz), no Flow Straightener

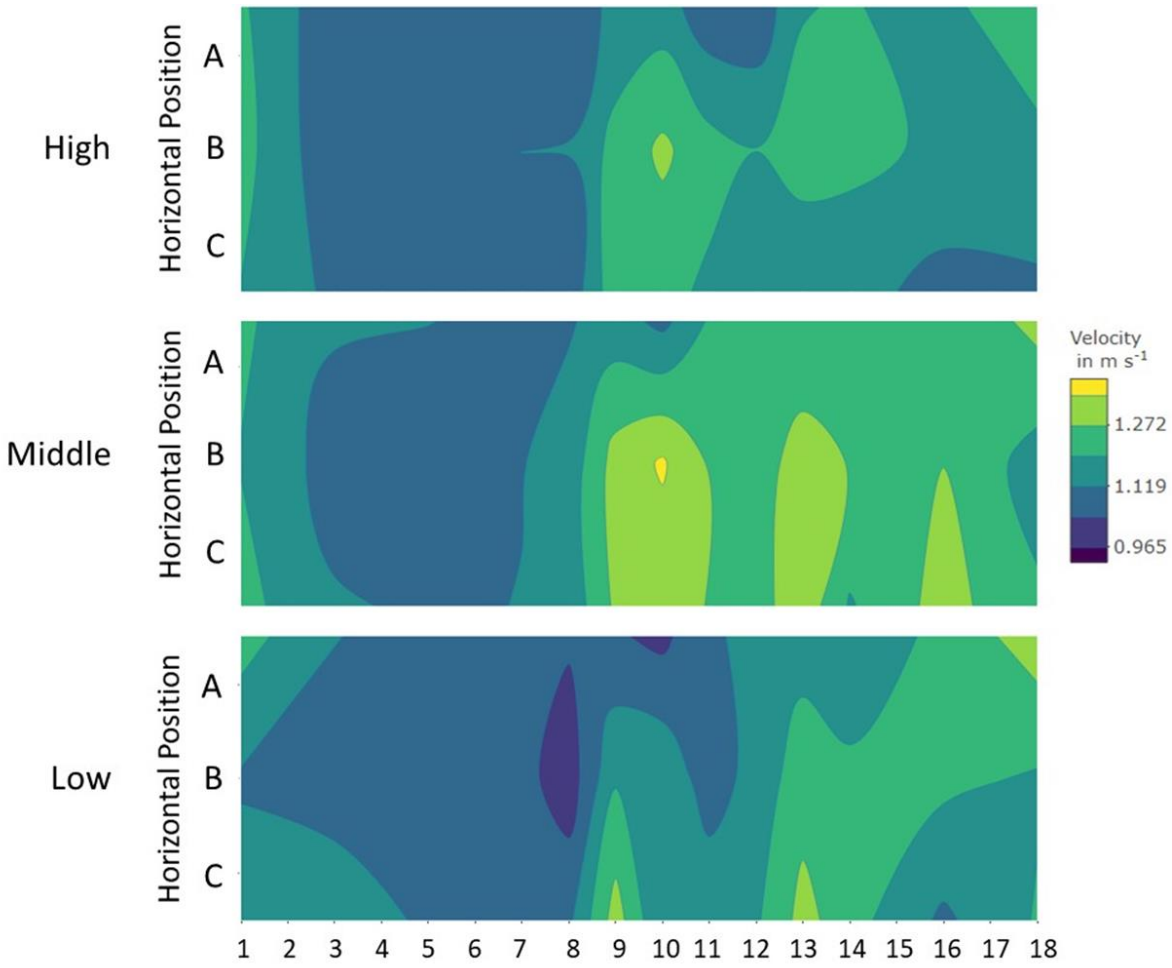

Figure S52. Vertical Velocity Profile of the Chamber at 1.0 m s^{-1} (60 Hz), no Flow Straightener

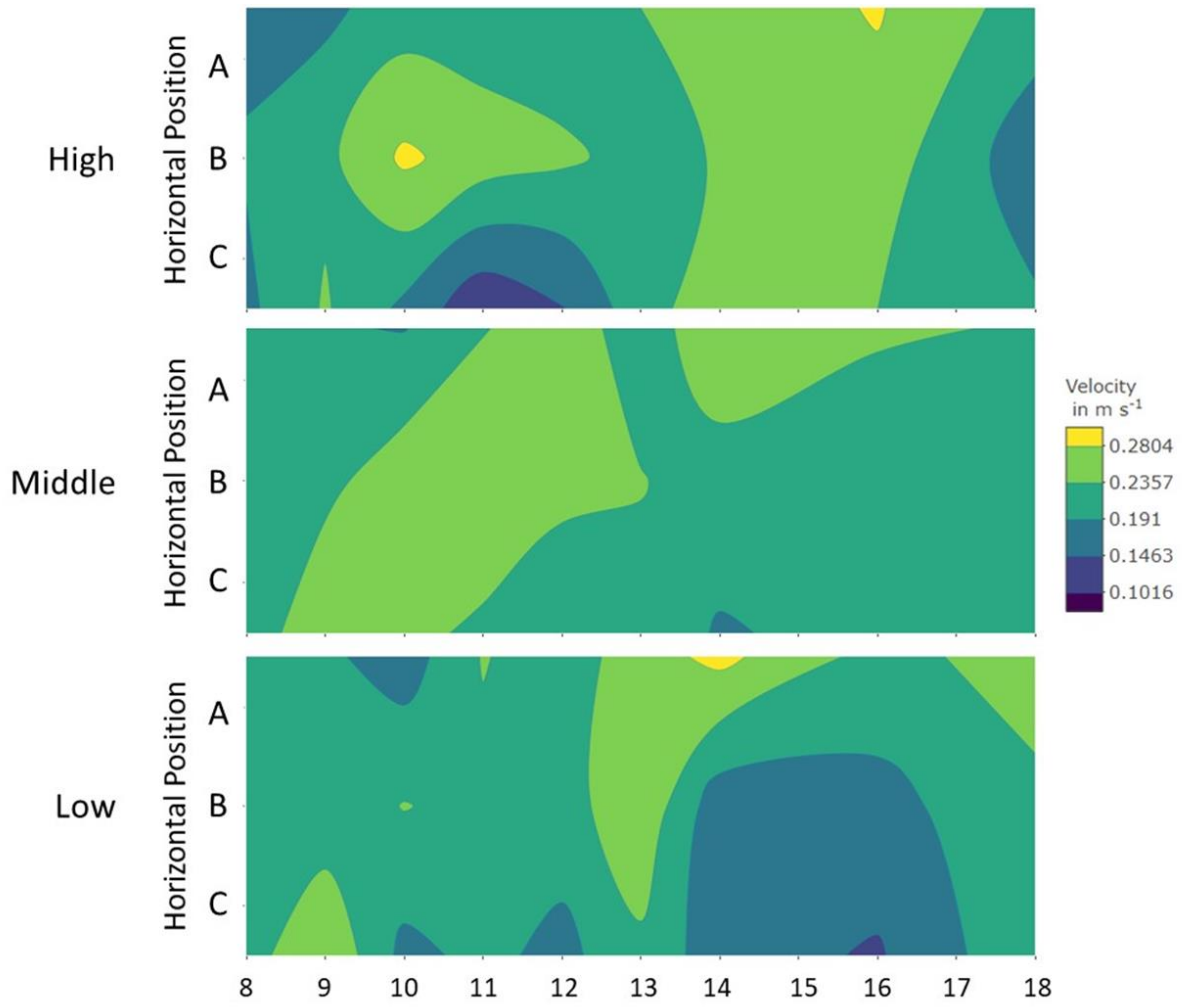

Figure S53. Vertical Velocity Profile of the Chamber at 0.2 m s^{-1} (16 Hz), with Flow Straightener

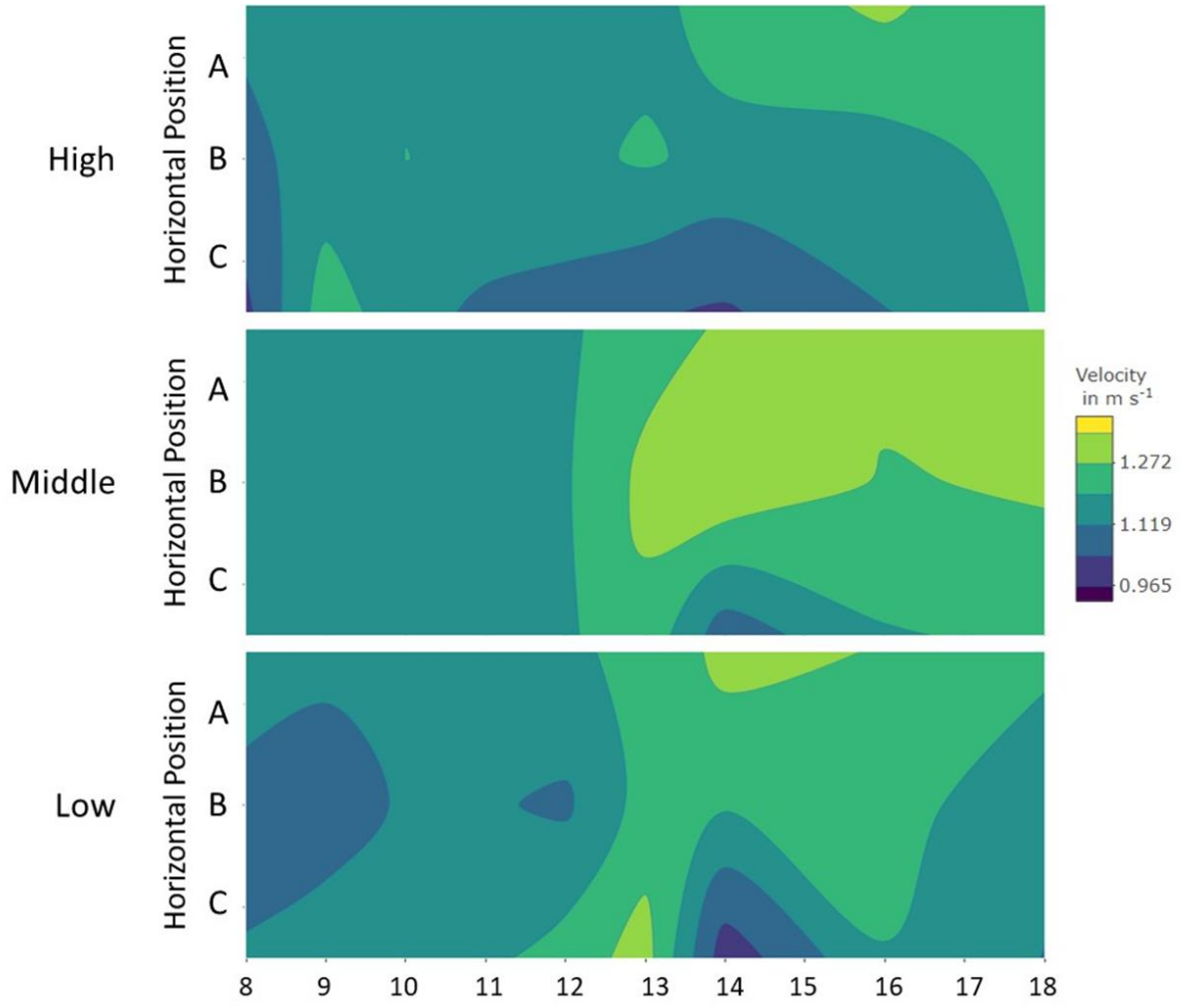

Figure S54. Vertical Velocity Profile of the Chamber at 1.0 m s^{-1} (60 Hz), with Flow Straightener

Day-to-Day Variability in Velocity Measurements

Grubbs' test was used to determine whether there were any outliers in the velocity data. One data point was shown to be an outlier at chamber position 16, suggesting transient slow velocities (Figure S6).

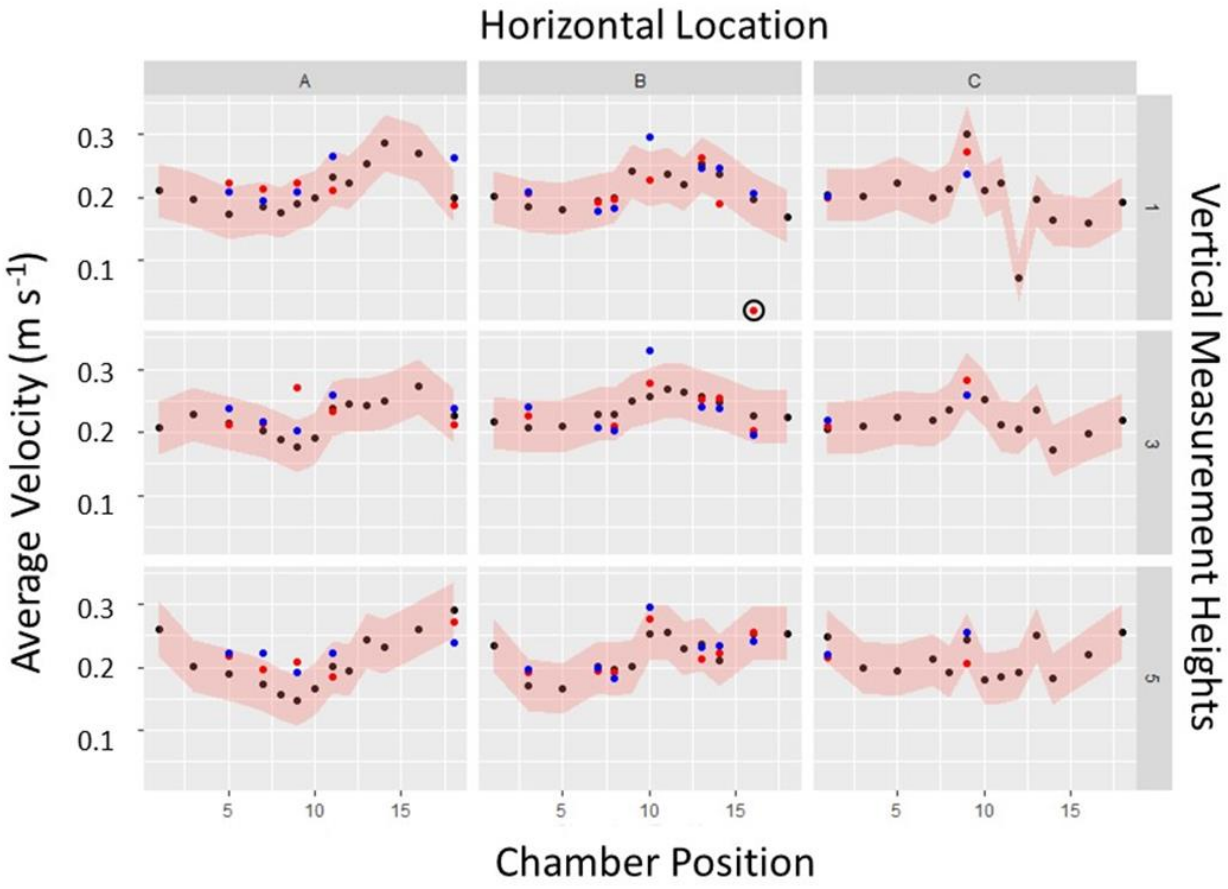

Figure S55. Day-to-Day Variability in Average Velocity at 0.2 m s^{-1}, no Flow Straightener

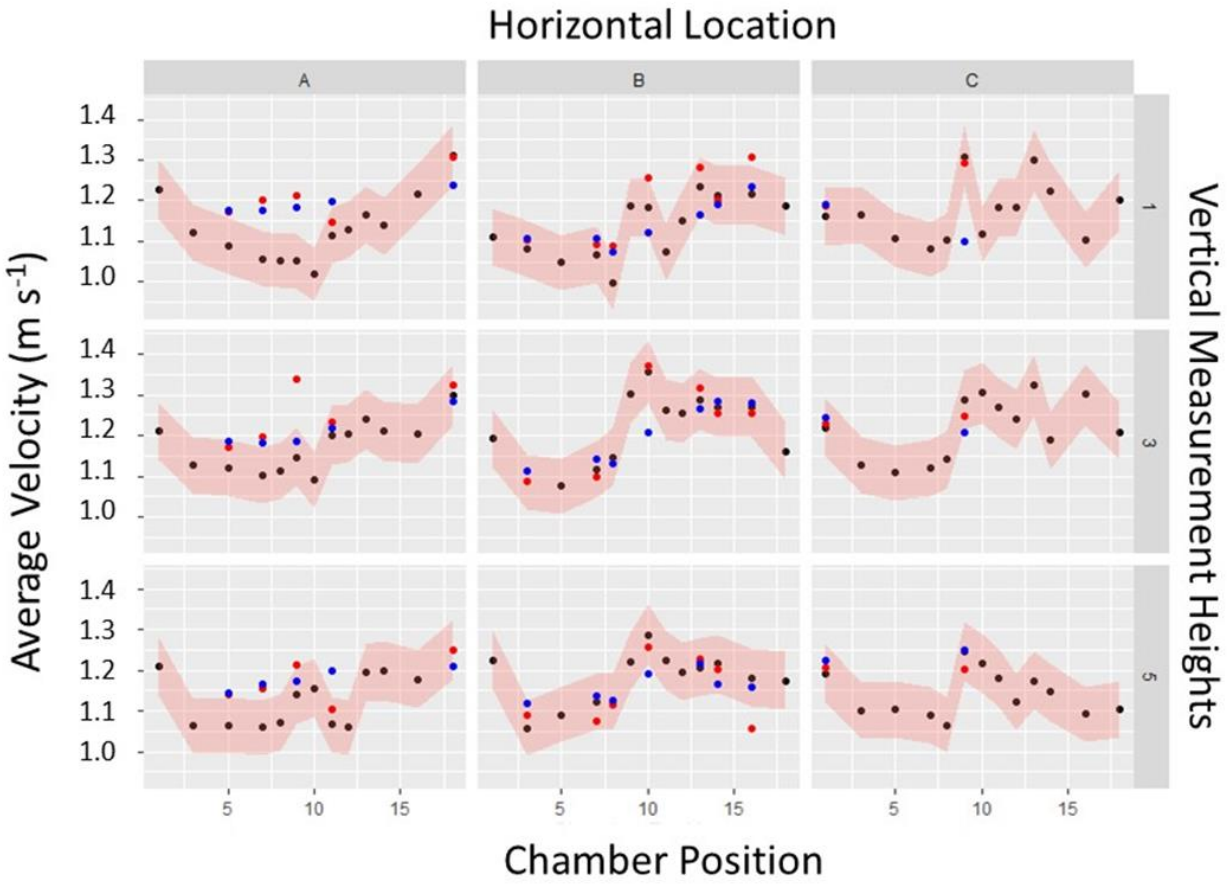

Figure S56. Day-to-Day Variability in Average Velocity at 1.0 m s^{-1}, no Flow Straightener

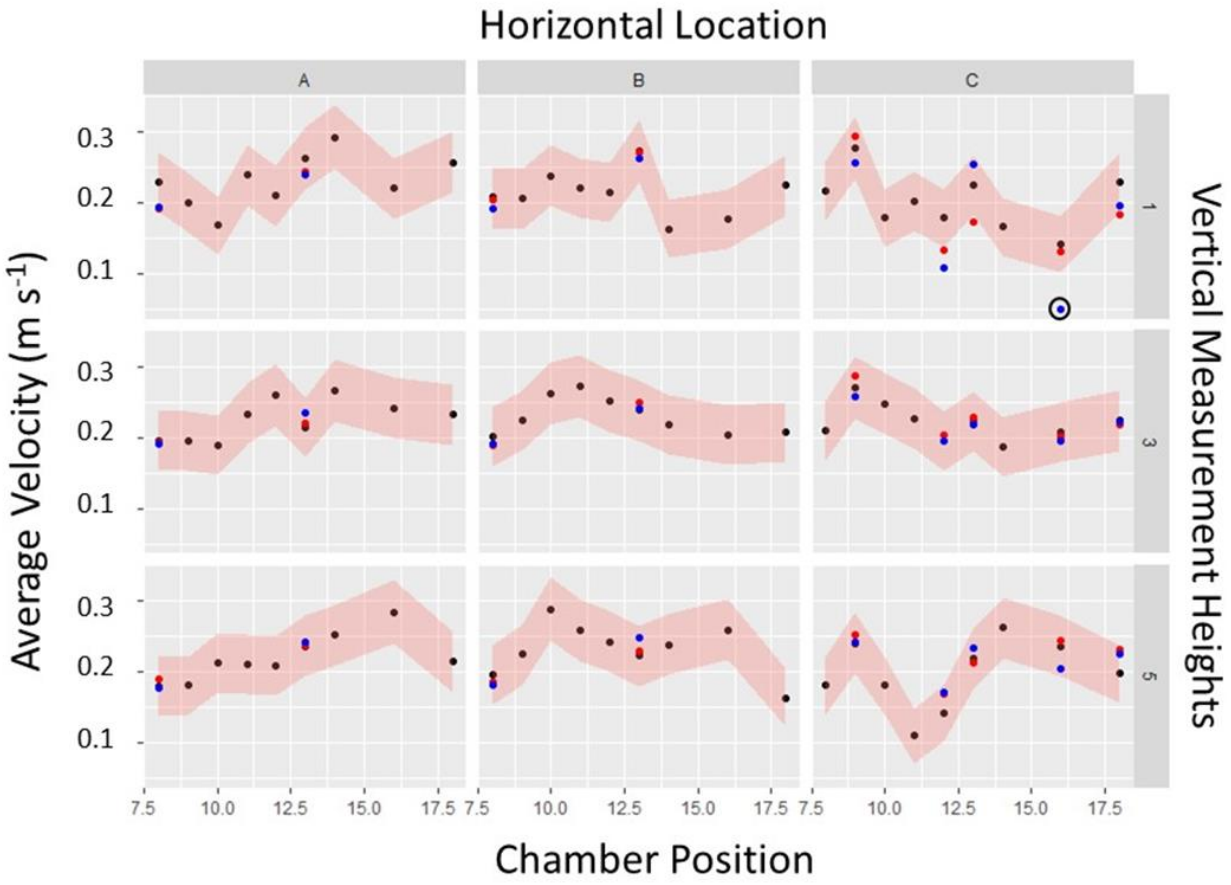

Figure S57. Day-to-Day Variability in Average Velocity at 0.2 m s^{-1}, with Flow Straightener

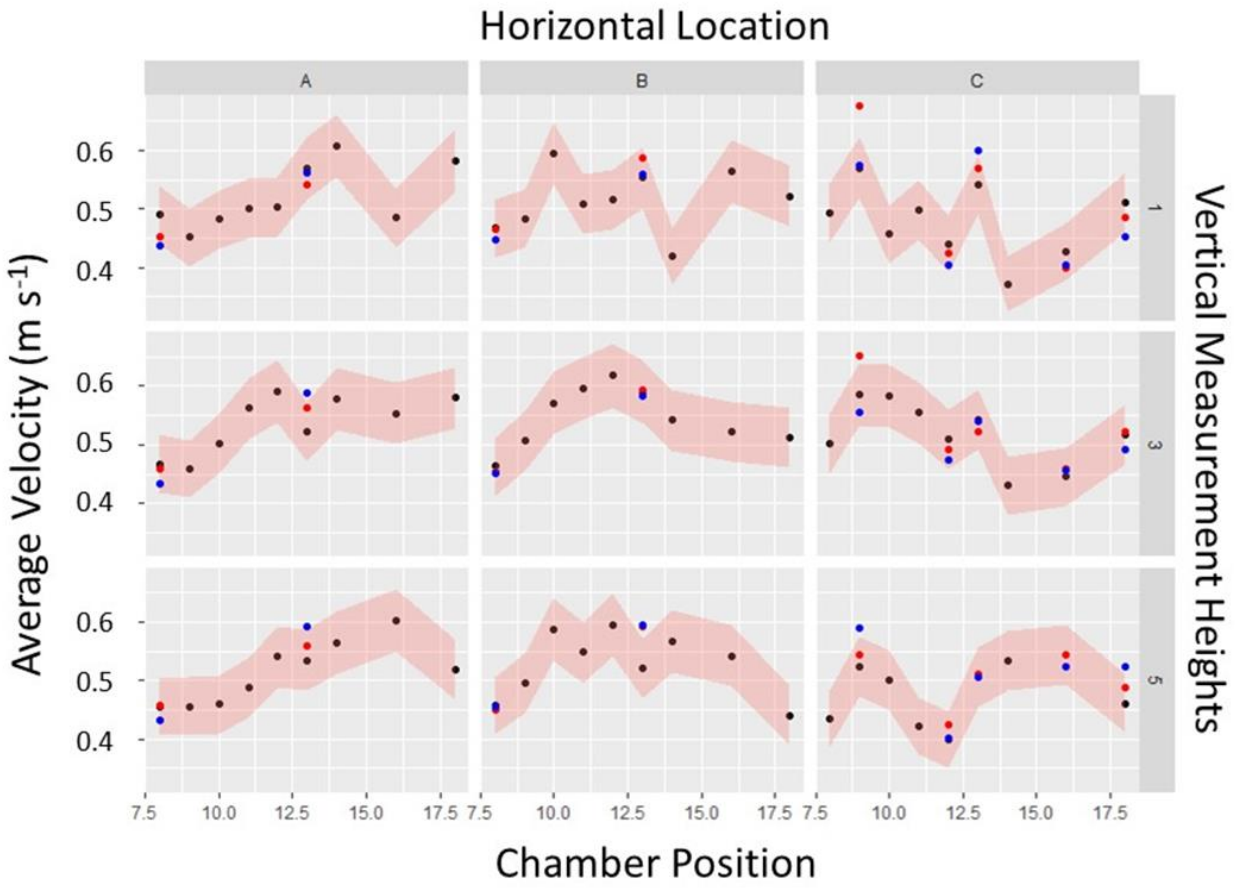

Figure S58. Day-to-Day Variability in Average Velocity at 0.5 m s^{-1}, with Flow Straightener

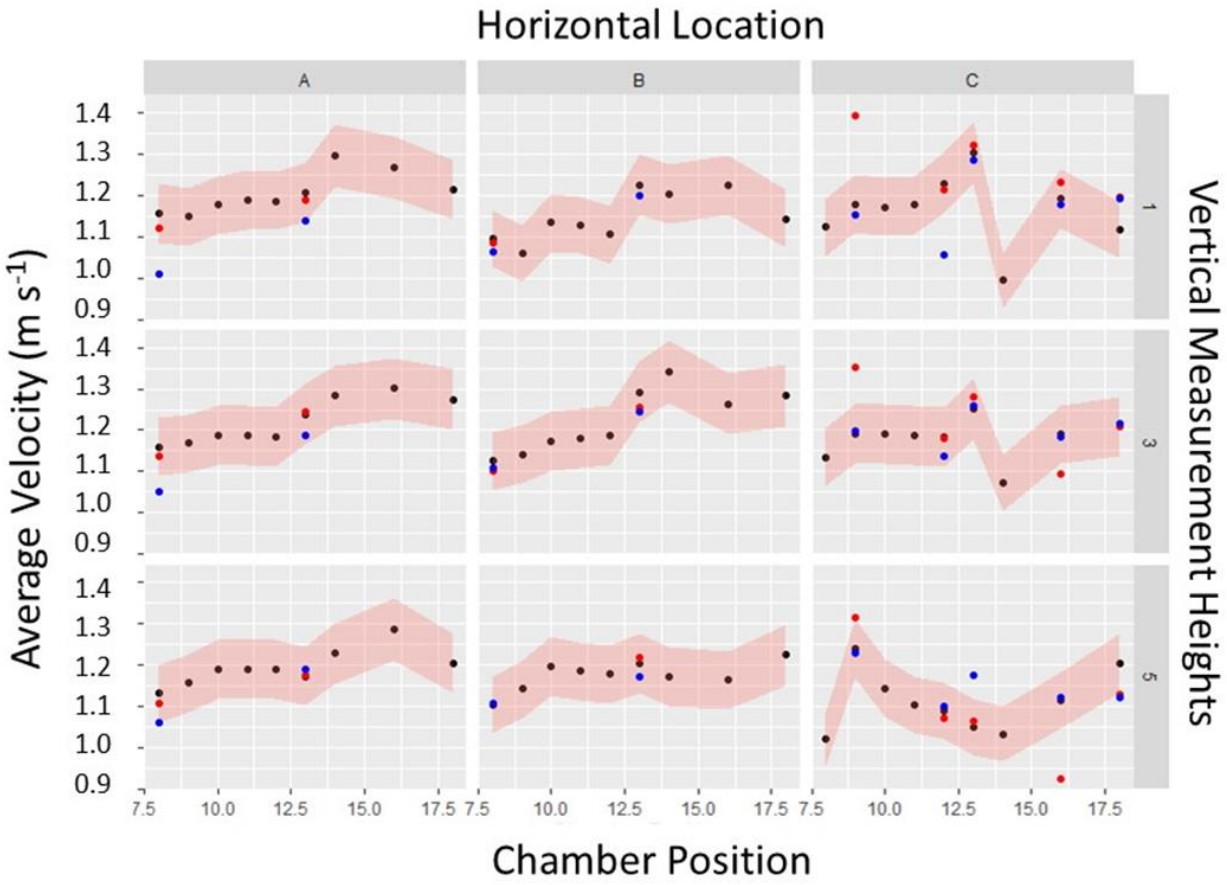

Figure S59. Day-to-Day Variability in Average Velocity at 1.0 m s^{-1}, with Flow Straightener

S4.1.a. Chamber Measurement Results and Analysis

Data collected without the flow straightener were tested for equal variance using Levene's test. In Levene's test, Pr(>F) should be less than the chosen cutoff value to reject the null hypothesis of equal variance. In this study, a significance of 0.05 was chosen as the cutoff. Data were tested for equal variance using Bartlett's test for data procured with the flow

straightener. For Bartlett's test, the p-value must be less than the specified cutoff to reject the null. Data were analyzed for the same interactions as data collected without the flow straightener.

Data collected with the flow straightener, when analyzed with Bartlett's test for equal variance, generated results similar to those found in the data without the flow straightener. Only chamber position alone resulted in p-values that necessitated the rejection of the null hypothesis (Table S1).

Table S22. Results of Bartlett's Test for Equal Variance for Velocity Data with Flow Straightener

Air Velocity, m s^{-1} (Fan Frequency, Hz)	Chamber Position only			Chamber Position, Vertical Position			Chamber Position, Horizontal Position			Horizontal Position, Vertical Position		
	K^2	df	p	K^2	df	p	K^2	df	p	K^2	df	p
0.2 (16)	14.59	8	0.067	32.42	26	0.18	25.53	26	0.489	5.59	8	0.69
0.5 (30)	19.43	8	0.013	34.74	26	0.12	33.58	26	0.15	0.45	8	0.99
1.0 (60)	31.15	8	0.0001	51.07	26	0.002	47.81	26	0.006	9.76	8	0.28

Results for the horizontal and vertical position interaction were again qualitatively evaluated through boxplots (Figure S11). Variances remained large overall.

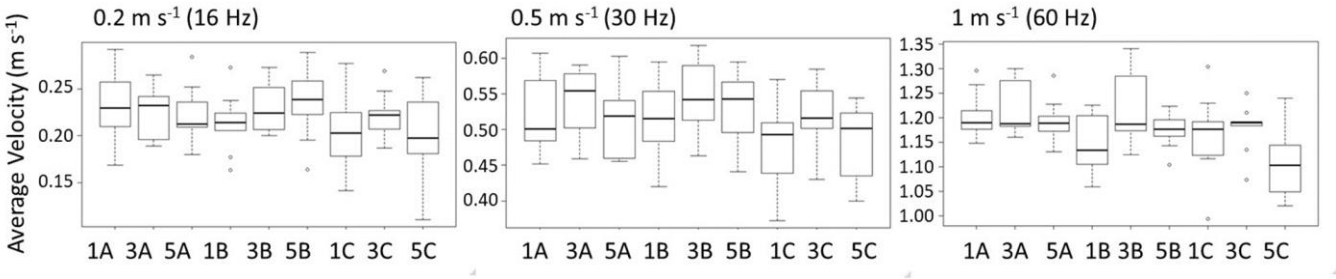

Figure S60. Variance of Velocity Profiles, with Flow Straightener

Example Determination of CMD, MMD, and GSD for Aerosol Data

Table S23. Size Distribution Calculations of Aerosol Data

Bin Width	Size Range (µm)	Midpoint	Volume (m^3)	Count	Mass (mg)	Frequency/µm	Fraction/ µm	Cumulative Mass	LN(d_i)	n_i*LN(d_i)	d_i/d_g	CMD	CMD (d_i/d_g)
0.074	0.3 - 0.374	0.337	2.00E-20	21789	2.18E-07	2.95E-06	0.119	1%	-1.09	-2.37E-07	1.20E-06	-23699.3	2802.2
0.091	0.374 - 0.465	0.420	3.87E-20	11158	2.16E-07	2.37E-06	0.095	2%	-0.87	-1.87E-07	9.79E-07	-9692.5	217.6
0.114	0.465 - 0.579	0.522	7.45E-20	5694	2.12E-07	1.86E-06	0.075	3%	-0.65	-1.38E-07	7.75E-07	-3701.6	35.5
0.142	0.579 - 0.721	0.650	1.44E-19	1951	1.40E-07	9.88E-07	0.040	3%	-0.43	-6.04E-08	4.02E-07	-840.5	173.6
0.176	0.721 - 0.897	0.809	2.77E-19	637	8.82E-08	5.01E-07	0.020	4%	-0.21	-1.87E-08	1.92E-07	-134.9	170.2
0.220	0.897 - 1.117	1.007	5.35E-19	2408	6.44E-07	2.93E-06	0.118	6%	0.01	4.49E-09	1.01E-06	16.8	1304.7
0.274	1.117 - 1.391	1.254	1.03E-18	1077	5.56E-07	2.03E-06	0.082	8%	0.23	1.26E-07	5.96E-07	243.7	982.8
0.341	1.391 - 1.732	1.562	1.99E-18	688	6.85E-07	2.01E-06	0.081	11%	0.45	3.05E-07	4.56E-07	306.4	948.7
0.424	1.732 - 2.156	1.944	3.85E-18	990	1.90E-06	4.49E-06	0.181	19%	0.66	1.27E-06	6.78E-07	657.8	1922.4
0.529	2.156 - 2.685	2.421	7.43E-18	722	2.68E-06	5.07E-06	0.204	30%	0.88	2.37E-06	3.82E-07	638.6	1879.7
0.658	2.685 - 3.343	3.014	1.43E-17	407	2.92E-06	4.43E-06	0.179	41%	1.10	3.22E-06	7.31E-08	449.1	1366.6
0.819	3.343 - 4.162	3.753	2.77E-17	256	3.55E-06	4.33E-06	0.174	56%	1.32	4.69E-06	1.31E-08	339.0	1078.9
1.020	4.162 - 5.182	4.672	5.34E-17	154	4.12E-06	4.04E-06	0.163	72%	1.54	6.36E-06	3.23E-07	238.1	796.2
1.269	5.182 - 6.451	5.817	1.03E-16	68	3.49E-06	2.75E-06	0.111	86%	1.76	6.14E-06	8.69E-07	119.2	419.7
1.580	6.451 - 8.031	7.241	1.99E-16	21	2.07E-06	1.31E-06	0.053	95%	1.98	4.10E-06	1.07E-06	41.2	152.9
1.969	8.031 - 10	9.016	3.84E-16	2	4.50E-07	2.28E-07	0.009	96%	2.20	9.89E-07	3.95E-07	5.2	20.1
10.000	10 - 20	15.000	1.77E-15	1	8.84E-07	8.84E-08	0.004	100%	2.71	2.39E-06	1.85E-06	2.7	11.8
			TOTAL:	48023	2.48E-05								

MMD Distribution Boxplots

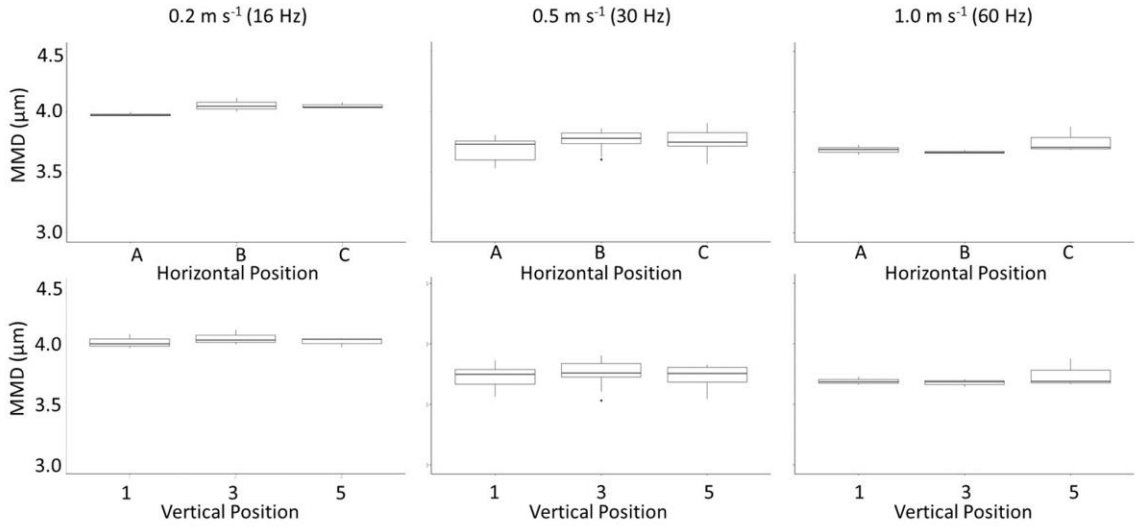

Figure S61. MMD Boxplots for Plane 7

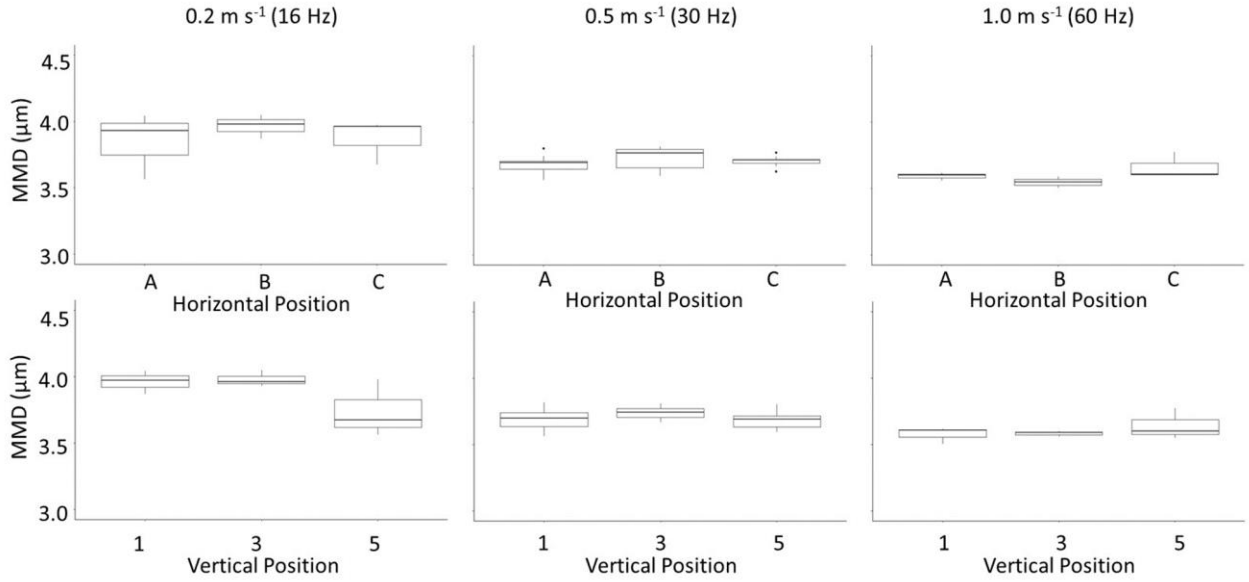

Figure S62. MMD Boxplots for Plane 8

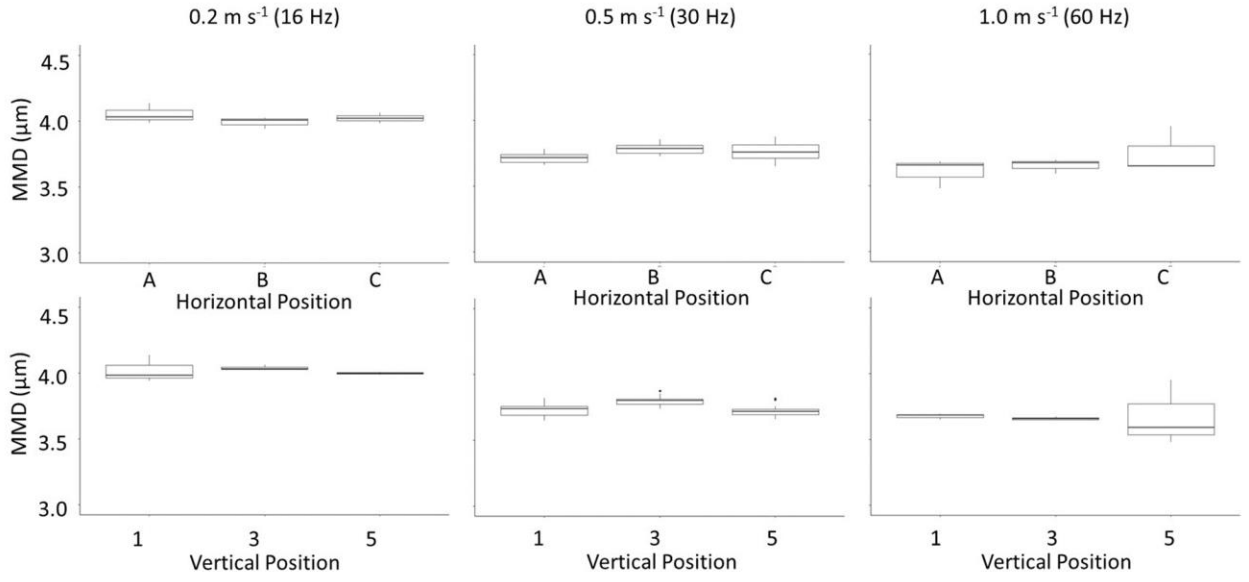

Figure S63. MMD Boxplots for Plane 10

S4.1.b. Chamber Measurement Results

Velocity and Particle Count Profiles

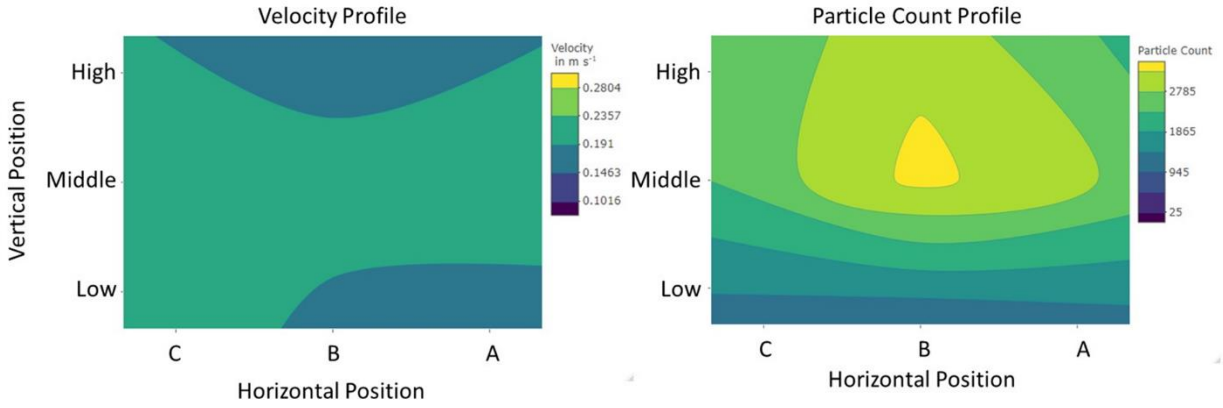

Figure S64. Velocity and Particle Count Profiles in Plane 5 at 0.2 m s^{-1}

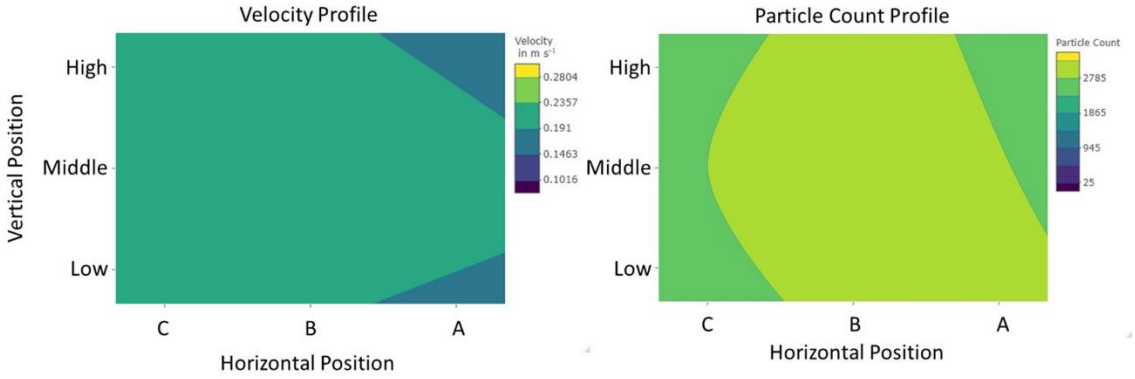

Figure S65. Velocity and Particle Count Profiles in Plane 7 at 0.2 m s^{-1}

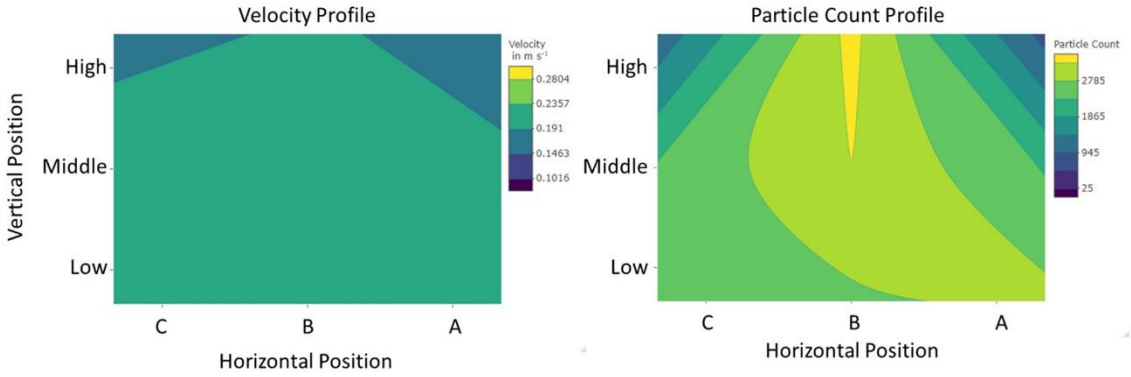

Figure S66. Velocity and Particle Count Profiles in Plane 8 at 0.2 m s^{-1}

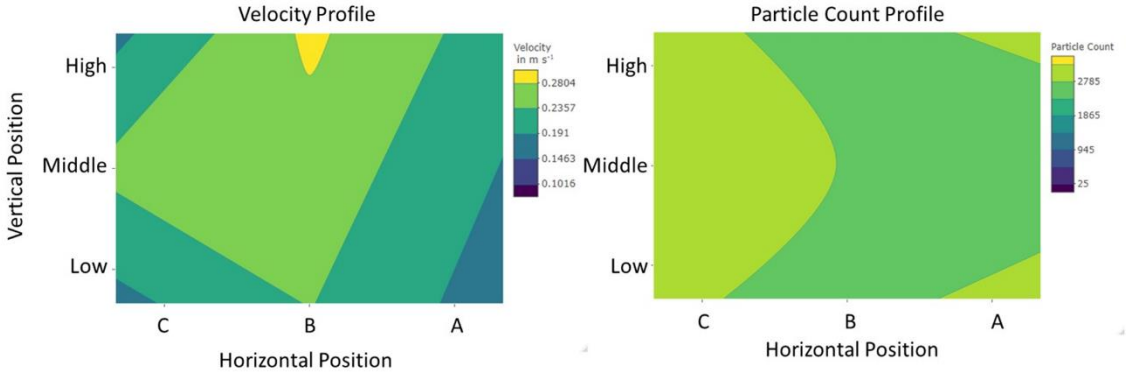

Figure S67. Velocity and Particle Count Profiles in Plane 10 at 0.2 m s^{-1}

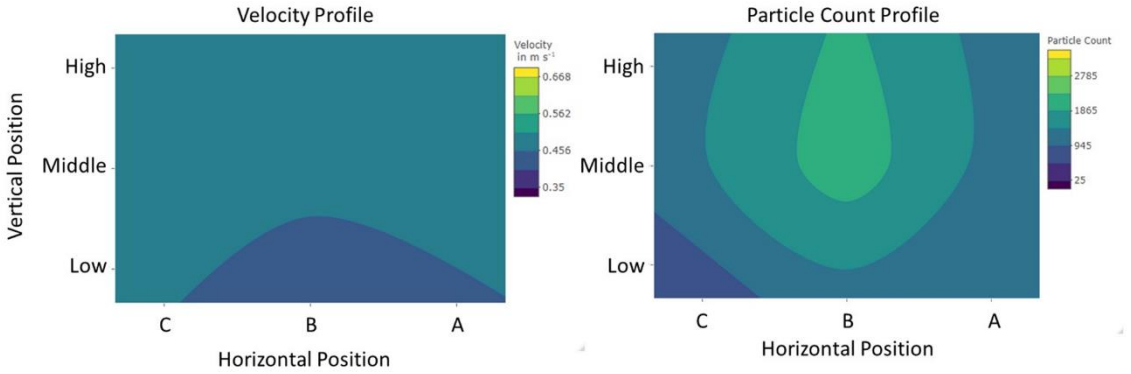

Figure S68. Velocity and Particle Count Profiles in Plane 7 at 0.5 m s^{-1}

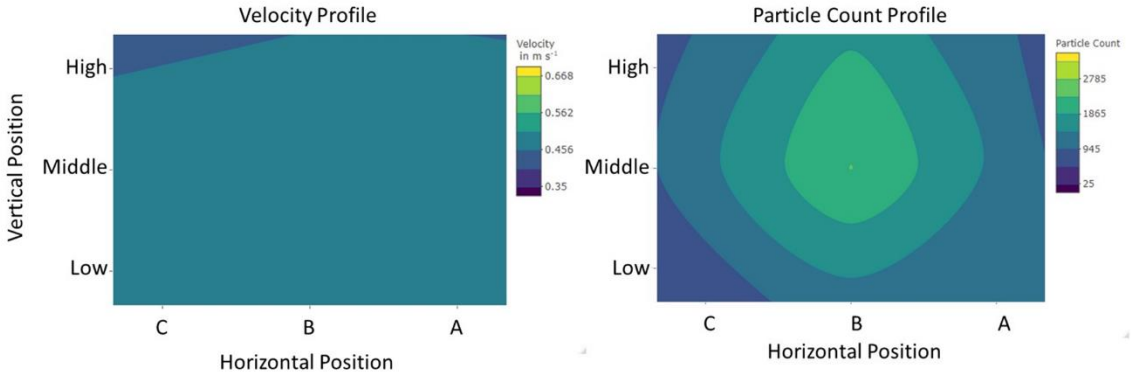

Figure S69. Velocity and Particle Count Profiles in Plane 8 at 0.5 m s^{-1}

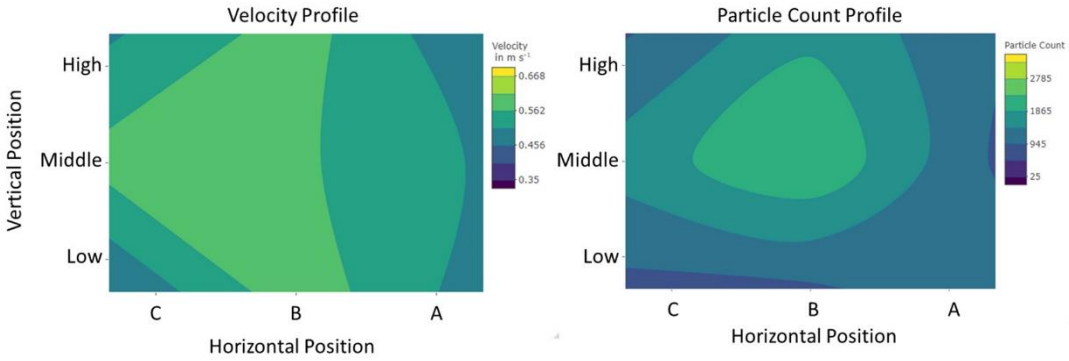

Figure S70. Velocity and Particle Count Profiles in Plane 10 at 0.5 m s^{-1}

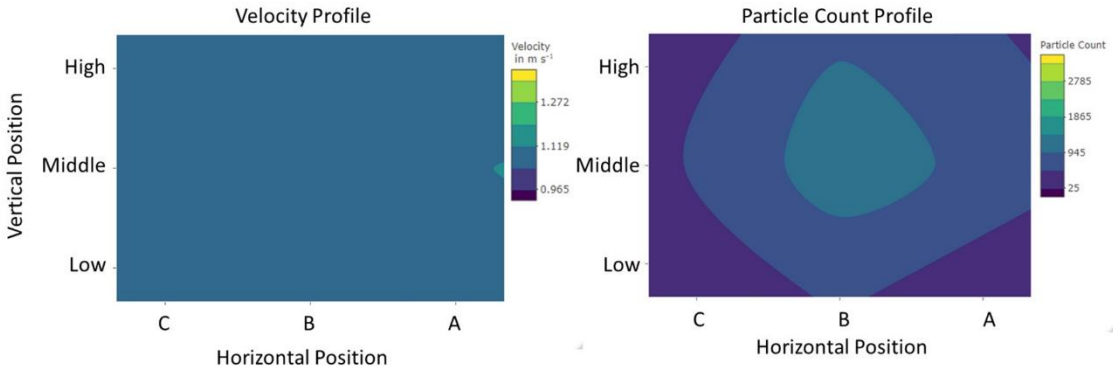

Figure S71. Velocity and Particle Count Profiles in Plane 5 at 1.0 m s^{-1}

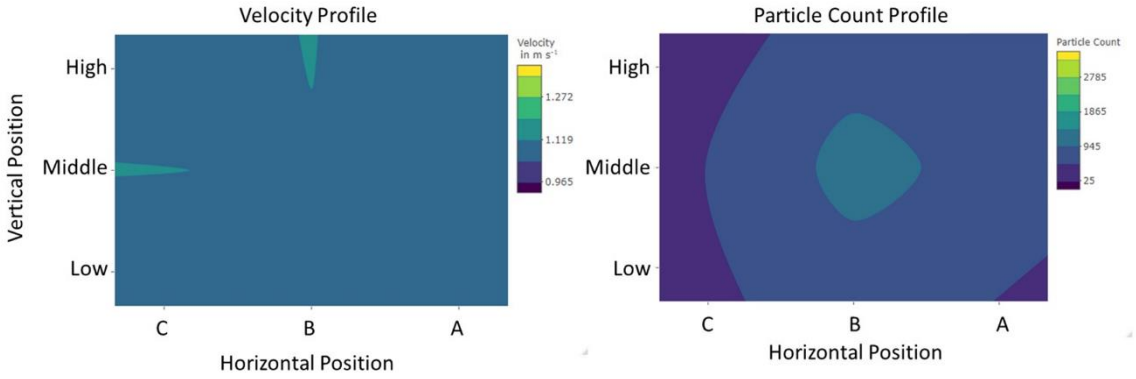

Figure S72. Velocity and Particle Count Profiles in Plane 7 at 1.0 m s^{-1}

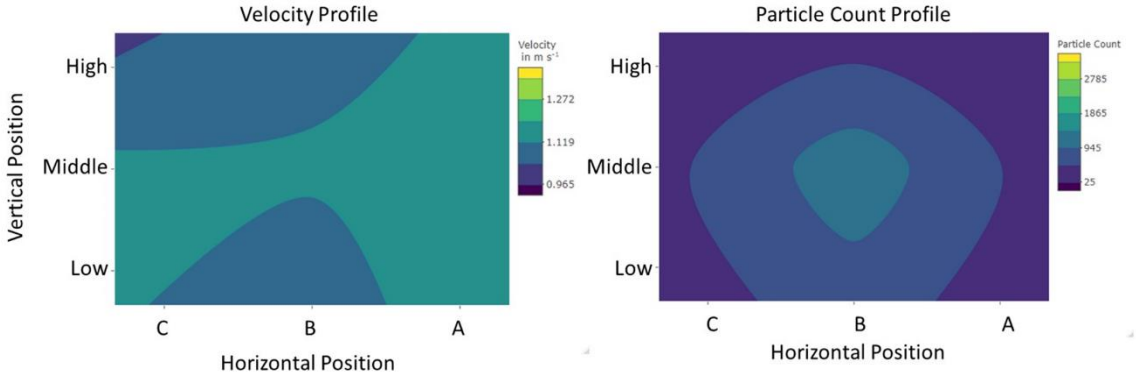

Figure S73. Velocity and Particle Count Profiles in Plane 8 at 1.0 m s^{-1}

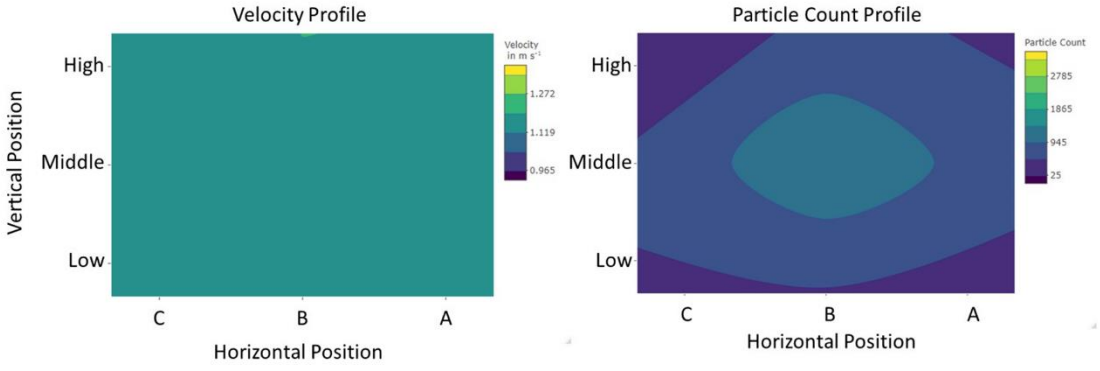

Figure S74. Velocity and Particle Count Profiles in Plane 10 at 1.0 m s^{-1}

S4.2. CFD Model Results

Table S24. Validation Points for Chamber CFD Model

Plane	Grid Square	Velocity (m s^{-1})				Percent Difference
		Measured Velocity	Min (Lower C.I.)	Max (Upper C.I.)	Model Value	
1	A-Low	0.504	0.454	0.555	0.521	3%
	A-Middle	0.491	0.441	0.542	0.522	6%
	A-High	0.539	0.488	0.591	**0.443**	-18%
	B-Low	0.465	0.415	0.514	0.461	-1%
	B-Middle	0.474	0.424	0.524	0.473	0%
	B-High	0.513	0.462	0.564	**0.428**	-17%
	C-Low	0.497	0.447	0.557	0.468	-6%
	C-Middle	0.502	0.451	0.573	0.456	-9%
	C-High	0.557	0.477	0.609	**0.470**	-16%
3	A-Low	0.470	0.421	0.520	**0.543**	15%
	A-Middle	0.477	0.427	0.527	**0.541**	13%
	A-High	0.504	0.454	0.555	0.467	-7%
	B-Low	0.441	0.393	0.502	0.502	14%
	B-Middle	0.425	0.377	0.502	0.485	14%
	B-High	0.427	0.379	0.525	0.452	6%
	C-Low	0.478	0.428	0.528	0.488	2%
	C-Middle	0.496	0.446	0.547	0.485	-2%
	C-High	0.462	0.413	0.512	0.490	6%
5	A-Low	0.445	0.396	0.550	0.546	23%
	A-Middle	0.464	0.415	0.554	0.536	15%
	A-High	0.478	0.423	0.568	0.464	-3%
	B-Low	0.420	0.372	0.555	0.492	17%
	B-Middle*	0.430	0.381	0.605	0.496	15%
	B-High	0.446	0.397	0.562	0.451	1%
	C-Low*	0.471	0.293	0.521	0.492	4%
	C-Middle	0.483	0.433	0.573	0.484	0%
	C-High	0.481	0.431	0.551	0.487	1%

7	A-Low	0.455	0.405	0.545	0.539	19%
	A-Middle	0.484	0.408	0.542	0.533	10%
	A-High	0.473	0.403	0.546	0.458	-3%
	B-Low	0.423	0.375	0.523	0.496	17%
	B-Middle	0.474	0.405	0.577	0.505	6%
	B-High	0.458	0.393	0.534	0.457	0%
	C-Low	0.472	0.364	0.522	0.491	4%
	C-Middle	0.495	0.444	0.562	0.484	-2%
	C-High	0.497	0.414	0.547	0.488	-2%
8	A-Low	0.430	0.381	0.546	0.531	24%
	A-Middle	0.483	0.398	0.533	0.520	8%
	A-High	0.469	0.365	0.519	0.435	-7%
	B-Low	0.432	0.383	0.552	0.504	17%
	B-Middle	0.489	0.424	0.556	0.511	4%
	B-High	0.453	0.398	0.518	0.461	2%
	C-Low	0.483	0.433	0.586	0.492	2%
	C-Middle	0.506	0.453	0.580	0.492	-3%
	C-High	0.474	0.395	0.524	0.485	2%
9	A-Low*	0.410	0.362	0.579	0.522	27%
	A-Middle*	0.479	0.428	0.636	0.468	-2%
	A-High	0.462	0.412	0.548	**0.694**	50%
	B-Low	0.526	0.475	0.578	0.502	-5%
	B-Middle	0.568	0.516	0.621	0.525	-8%
	B-High	0.504	0.453	0.554	0.480	-5%
	C-Low	0.596	0.509	0.676	**0.492**	-17%
	C-Middle	0.599	0.530	0.684	**0.496**	-17%
	C-High	0.534	0.478	0.622	0.495	-7%
10	A-Low*	0.440	0.391	0.656	0.515	17%
	A-Middle*	0.429	0.381	0.616	0.534	24%
	A-High	0.442	0.393	0.545	0.533	21%
	B-Low	0.565	0.488	0.696	0.513	-9%
	B-Middle	0.605	0.533	0.678	0.546	-10%
	B-High	0.577	0.468	0.651	0.487	-16%
	C-Low*	0.464	0.360	0.602	0.498	7%
	C-Middle	0.572	0.519	0.671	**0.501**	-12%
	C-High	0.505	0.439	0.559	0.497	-2%
11	A-Low	0.489	0.439	0.583	0.498	2%
	A-Middle	0.542	0.490	0.654	0.527	-3%
	A-High	0.474	0.420	0.574	0.541	14%
	B-Low	0.477	0.427	0.527	0.521	9%
	B-Middle	0.582	0.529	0.635	0.566	-3%

	B-High	0.596	0.542	0.649	**0.494**	-17%
	C-Low	0.475	0.425	0.525	0.497	5%
	C-Middle	0.551	0.499	0.603	0.508	-8%
	C-High	0.422	0.374	0.470	**0.495**	17%
12	A-Low	0.506	0.455	0.557	0.499	-1%
	A-Middle	0.556	0.504	0.608	0.518	-7%
	A-High	0.515	0.464	0.566	**0.461**	-11%
	B-Low	0.522	0.471	0.573	0.537	3%
	B-Middle	0.618	0.564	0.673	0.572	-8%
	B-High	0.593	0.540	0.646	**0.491**	-17%
	C-Low	0.424	0.375	0.472	**0.502**	18%
	C-Middle	0.502	0.451	0.552	0.511	2%
	C-High	0.440	0.391	0.489	**0.496**	13%
13	A-Low	0.545	0.493	0.597	**0.478**	-12%
	A-Middle	0.536	0.484	0.587	0.525	-2%
	A-High	0.539	0.488	0.591	0.492	-9%
	B-Low	0.560	0.503	0.612	0.544	-3%
	B-Middle	0.586	0.519	0.653	0.575	-2%
	B-High	0.540	0.472	0.642	0.494	-8%
	C-Low	0.563	0.510	0.615	**0.497**	-12%
	C-Middle	0.534	0.482	0.585	0.514	-4%
	C-High	0.498	0.447	0.548	0.497	0%
14	A-Low	0.619	0.565	0.673	**0.459**	-26%
	A-Middle	0.585	0.532	0.639	0.538	-8%
	A-High	0.530	0.479	0.582	0.496	-6%
	B-Low	0.567	0.475	0.643	0.536	-5%
	B-Middle	0.589	0.507	0.648	0.582	-1%
	B-High	0.493	0.443	0.604	0.488	-1%
	C-Low	0.437	0.388	0.485	**0.496**	14%
	C-Middle	0.481	0.431	0.531	0.510	6%
	C-High	0.446	0.397	0.495	0.493	10%
16	A-Low	0.596	0.542	0.649	**0.445**	-25%
	A-Middle	0.593	0.540	0.647	0.557	-6%
	A-High	0.560	0.507	0.612	**0.488**	-13%
	B-Low*	0.479	0.384	0.625	0.524	10%
	B-Middle	0.523	0.472	0.588	**0.589**	13%
	B-High	0.546	0.488	0.638	0.492	-10%
	C-Low	0.449	0.400	0.498	0.484	8%
	C-Middle	0.459	0.410	0.509	**0.509**	11%
	C-High	0.474	0.425	0.524	0.482	2%
18	A-Low*	0.507	0.422	0.651	0.473	-7%

	A-Middle	0.572	0.506	0.630	0.567	-1%
	A-High	0.598	0.492	0.652	**0.484**	-19%
	B-Low	0.398	0.351	0.446	**0.484**	21%
	B-Middle	0.555	0.503	0.607	0.598	8%
	B-High	0.568	0.515	0.620	**0.496**	-13%
	C-Low	0.435	0.387	0.484	0.481	11%
	C-Middle	0.487	0.437	0.538	0.512	5%
	C-High	0.580	0.527	0.633	**0.480**	-17%

References

Brice, T. and T. Hall. No Date. Vapor Pressure. National Weather Service, NOAA, El Paso, TX. Accessed January 3, 2020. https://www.weather.gov/media/epz/wxcalc/vaporPressure.pdf.

Engineers Edge, LLC. (no date) Viscosity of Air, Dynamic and Kinematic. Accessed January 3, 2020. https://www.engineersedge.com/physics/viscosity_of_air_dynamic_and_kinematic_14483.htm

Engineering Toolbox. 2004. Relative Humidity in Air. Accessed January 3, 2020. https://www.engineeringtoolbox.com/relative-humidity-air-d_687.html.

de Nevers, N. 2005. *Fluid Mechanics for Chemical Engineers*. 3rd ed. New York, NY: McGraw-Hill Companies.

Bibliography

[1] K. L. Koenig *et al.*, "Health care facility-based decontamination of victims exposed to chemical, biological, and radiological materials," *Am. J. Emerg. Med.*, vol. 26, no. 1, pp. 71–80, 2008.

[2] R. D. Cox, "Decontamination and Management of Hazardous Materials Exposure Victims in the Emergency Department," *Ann. Emerg. Med.*, vol. 23, no. 4, pp. 761–770, 1994.

[3] A. B. Wolbarst, A. L. Wiley, J. B. Nemhauser, D. M. Christensen, and W. R. Hendee, "Medical Response to a Major Radiologic Emergency: A Primer for Medical and Public Health Practitioners," *Radiology*, vol. 254, no. 3, pp. 660–677, 2010.

[4] H. Matar *et al.*, "Design and characterisation of a novel in vitro skin diffusion cell system for assessing mass casualty decontamination systems," *Toxicol. Vitr.*, vol. 28, no. 4, pp. 492–501, 2014.

[5] R. P. Chilcott, "Managing mass casualties and decontamination," *Environ. Int.*, vol. 72, pp. 37–45, 2014.

[6] USAF, "Home Station Medical Response to Chemical, Biological, Radiological, and Nuclear (CBRN) Incidents," 2013.

[7] R. P. Chilcott, J. Larner, and H. Matar, "Primary Response Incident Scene Management (PRISM): Guidance for the Operational Response to Chemical Incidents, Volume 1: Strategic Guidance for Mass Casualty Disrobe and Decontamination," Hertfordshire, UK, 2018.

[8] S. M. Cibulsky, M. A. Kirk, J. S. Ignacio, A. D. Leary, and M. D. Schwartz, "Patient Decontamination in a Mass Chemical Exposure Incident: National Planning Guidance for Communities," Washington, DC, 2014.

[9] E. Titus, G. Lemmer, J. Slagley, and R. Eninger, "A review of CBRN topics related to military and civilian patient exposure and decontamination," *Am. J. Disaster Med.*, vol. 14, no. 2, pp. 137–149, 2019.

[10] P. Rolland, M.-A. Bolzinger, C. Cruz, S. Briançon, and D. Josse, "Human scalp permeability to the chemical warfare agent VX," *Toxicol. Vitr.*, vol. 25, pp. 1974–1980, 2011.

[11] H. Matar, S. C. Price, and R. P. Chilcott, “Further studies of the efficacy of military, commercial and novel skin decontaminants against the chemical warfare agents sulphur Mustard, Soman and VX,” *Toxicol. Vitr.*, vol. 54, pp. 263–268, 2019.

[12] M. Schultz, J. Cisek, and R. Wabeke, “Simulated Exposure of Hospital Emergency Personnel to Solvent Vapors and Respirable Dust During Decontamination of Chemically Exposed Patients,” *Ann. Emerg. Med.*, vol. 26, no. 3, pp. 324–329, 1995.

[13] J. M. Slagley, H. Paschold, and J. M. Engler, “Evaluation of coverall field dry aerosol decontamination methods using a manikin,” *J. Occup. Environ. Hyg.*, vol. 14, no. 7, pp. 502–509, 2017.

[14] R. P. Chilcott *et al.*, “Evaluation of US Federal Guidelines (Primary Response Incident Scene Management [PRISM]) for Mass Decontamination of Casualties During the Initial Operational Response to a Chemical Incident,” *Ann. Emerg. Med.*, vol. In Press, pp. 1–14, 2018.

[15] C. A. Moore, S. C. Wilkinson, P. G. Blain, M. Dunn, G. A. Aust, and F. M. Williams, “Percutaneous absorption and distribution of organophosphates (chlorpyrifos and dichlorvos) following dermal exposure and decontamination scenarios using in vitro human skin model,” *Toxicol. Lett.*, vol. 229, pp. 66–72, 2014.

[16] L. Thors, M. Koch, E. Wigenstam, B. Koch, L. Hagglund, and A. Bucht, “Comparison of skin decontamination efficacy of commercial decontamination products following exposure to VX on human skin,” *Chem. Biol. Interact.*, vol. 273, pp. 82–89, 2017.

[17] W.-K. Loke, S.-H. U, S.-K. Lau, J.-S. Lim, G.-S. Tay, and C.-H. Koh, “Wet Decontamination-induced Stratum Corneum Hydration - Effects on the Skin Barrier Function to Diethylmalonate,” *J. Appl. Toxicol.*, vol. 19, no. 4, pp. 285–290, 1999.

[18] M. Spiandore *et al.*, “Efficacy of scalp hair decontamination following exposure to vapours of sulphur mustard simulants 2-chloroethyl ethyl sulphide and methyl salicylate,” *Chem. Biol. Interact.*, vol. 267, pp. 74–79, 2017.

[19] R. A. Fenske, S. M. Wong, J. T. Leffingwell, and R. C. Spear, “A Video Imaging Technique for Assessing Dermal Exposure II. Fluorescent Tracer Testing,” *Am. Ind. Hyg. Assoc. J.*, vol. 47, no. 12, pp. 771–775, 1986.

[20] B. A. Archibald, K. R. Solomon, and G. R. Stephenson, “Estimation of Pesticide Exposure to Greenhouse Application Using Video Imaging and Other Assessment Techniques,” *Am. Ind. Hyg. Assoc. J.*, vol. 56, no. 3, pp. 226–235, 1995.

[21] L. Oudejans *et al.*, “Decontamination of personal protective equipment and related materials contaminated with toxic industrial chemicals and chemical warfare agent surrogates,” *J. Environ. Chem. Eng.*, vol. 4, pp. 2745–2753, 2016.

[22] R. P. Chilcott, H. Mitchell, and H. Matar, “Optimization of Nonambulant Mass Casualty Decontamination Protocols as Part of an Initial or Specialist Operational Response to Chemical Incidents,” *Prehospital Emerg. Care*, vol. 23, no. 1, pp. 32–43, 2019.

[23] B. Poller *et al.*, “‘VIOLET’: a fluorescence-based simulation exercise for training healthcare workers in the use of personal protective equipment,” *J. Hosp. Infect.*, vol. 99, pp. 229–235, 2018.

[24] E. L. Beam, S. G. Gibbs, K. C. Boulter, M. E. Beckerdite, and P. W. Smith, “A method for evaluating health care workers’ personal protective equipment technique,” *Am. J. Infect. Control*, vol. 39, pp. 415–420, 2011.

[25] R. A. Fenske, J. T. Leffingwell, and R. C. Spear, “A Video Imaging Technique for Assessing Dermal Exposure I. Instrument Design and Testing,” *Am. Ind. Hyg. Assoc. J.*, vol. 47, no. 12, pp. 764–770, 1986.

[26] “UVGLASS1 UV Enhancing Amber Yellow Black Light Protective Glasses,” *Risk Reactor Website*, 2020. [Online]. Available: https://www.riskreactor.com/black-lights/uv-safety-glasses/uvglass1-uv-enhancing-amber-yellow-black-light-protective-glasses/. [Accessed: 04-Sep-2020].

[27] “IFWB-C0 Clear Blue Tracer.” Risk Reactor Inc., Santa Ana, CA, pp. 1–3, 2019.

[28] A. A. Fatah, R. D. Arcilesi, A. K. Judd, L. E. O’Connor, C. H. Lattin, and C. Y. Wells, “Guide for the Selection of Chemical, Biological, Radiological, and Nuclear Decontamination Equipment for Emergency First Responders,” Washington, DC, 2007.

[29] USMC, USN, and USAF, “Potential Military Chemical/Biological Agents and Compounds,” 2005.

[30] National Library of Medicine and NIH, “Methyl salicylate | C8H8O3 - PubChem,”

PubChem. [Online]. Available: https://pubchem.ncbi.nlm.nih.gov/compound/Methyl-salicylate#section=Vapor-Pressure. [Accessed: 26-Aug-2020].

[31] C. Technologies, "Collison Nebulizer - Instructions." CH Technologies (USA), Westwood, NJ, pp. 1–10, 2017.

[32] "DETAILED SPECIFICATION: JOINT SERVICE LIGHTWEIGHT INTEGRATED SUIT TECHNOLOGY (JSLIST) COAT AND TROUSER, CHEMICAL PROTECTIVE," 2002.

[33] EPA and N. C. for E. Assessment, "Chapter 7 of the Exposure Factors Handbook: Dermal Exposure Factors," Washington, DC, 2011.

[34] "Test Operations Procedures (TOP) 10-2-022A, Chemical Vapor and Aerosol System-Level Testing of Chemical/Biological Protective Suits." Test and Evavluation Capabilities and Methodologies Integrated Process Team (TECMIPT), Dugway Proving Ground, Utah, pp. 1–188, 2013.

[35] W. C. Hinds, *Aerosol Technology: Properties, Behavior, and Measurement of Airborne Particles*, 2nd ed. Hoboken, NJ, USA: John Wiley & Sons, Inc., 1999.

[36] E. Ibrahim, D. Harnish, K. Kinney, B. Heimbuch, and J. Wander, "An experimental investigation of the performance of a Collison nebulizer generating H1N1 influenza aerosols," *Biotechnol. Biotechnol. Equip.*, vol. 29, no. 6, pp. 1142–1148, 2015.

[37] S. A. Grinshpun *et al.*, "Evaluation of personal inhalable aerosol samplers with different filters for use during anthrax responses," *J. Occup. Environ. Hyg.*, vol. 14, no. 8, pp. 583–593, 2017.

[38] K. R. May, "THE COLLISON NEBULIZER: DESCRIPTION, PERFORMANCE AND APPLICATION," *Aerosol Sci.*, vol. 4, pp. 235–243, 1973.

[39] D. LLC, "IPPD Lesson 4 Decon Process." DECON LLC, pp. 1–37, 2017.

[40] J. Glarum, D. Birou, and E. Cetaruk, "Decontamination," in *Hospital Emergency Response Teams*, Burlington, MA: Butterworth-Heinemann, 2010, pp. 157–189.

[41] R. P. Moody and H. I. Maibach, "Skin decontamination: Importance of the wash-in effect," *Food Chem. Toxicol.*, vol. 44, pp. 1783–1788, 2006.

[42] J. Schindelin *et al.*, “Fiji - an Open Source platform for biological image analysis,” *Nat. Methods*, vol. 9, no. 7, pp. 1–15, 2007.

[43] L. Thors *et al.*, “RSDL decontamination of human skin contaminated with the nerve agent VX,” *Toxicol. Lett.*, vol. 269, pp. 47–54, 2017.

REPORT DOCUMENTATION PAGE

Form Approved
OMB No. 074-0188

1. REPORT DATE *(DD-MM-YYYY)*	2. REPORT TYPE	3. DATES COVERED *(From – To)*
11-09-2020	Master's Thesis	September 2018 – September 2020

TITLE AND SUBTITLE
Development of a Semi-Quantitative Methodology for Evaluation of Whole-Body Chemical, Biological, Radiological, and Nuclear Decontamination Using an Ultraviolet Fluorescent Aerosol

5a. CONTRACT NUMBER

5b. GRANT NUMBER
2018-178R, 2019-073

5c. PROGRAM ELEMENT NUMBER

6. AUTHOR(S)

Titus, Emily M., Contractor

5d. PROJECT NUMBER

5e. TASK NUMBER

5f. WORK UNIT NUMBER

7. PERFORMING ORGANIZATION NAMES(S) AND ADDRESS(S)

Air Force Institute of Technology
Graduate School of Engineering and Management (AFIT/ENV)
2950 Hobson Way, Building 640
WPAFB OH 45433-8865

8. PERFORMING ORGANIZATION REPORT NUMBER

AFIT-ENV-MS-20-S-081

9. SPONSORING/MONITORING AGENCY NAME(S) AND ADDRESS(ES)

711 HPW/RHBAF
2510 Fifth Street
WPAFB, OH 45433-7765
(937) 938-2671
ATTN: Dr. Doug Lewis, Douglas.Lewis.13@us.af.mil, (937) 938-2671

10. SPONSOR/MONITOR'S ACRONYM(S)

711 HPW/RHBAF

11. SPONSOR/MONITOR'S REPORT NUMBER(S)

12. DISTRIBUTION/AVAILABILITY STATEMENT
DISTRUBTION STATEMENT A. APPROVED FOR PUBLIC RELEASE; DISTRIBUTION UNLIMITED.

13. SUPPLEMENTARY NOTES
This material is declared a work of the U.S. Government and is not subject to copyright protection in the United States.

14. ABSTRACT

(The abstract can be 200 words maximum.)

This work describes a literature review which was conducted on publicly available literature on chemical, biological, radiological, and nuclear (CBRN) decontamination to understand the body of knowledge and gaps in this body of knowledge, including the assumption that disrobing after a CBRN incident will remove 90% of contamination. Also included is a description of the design and characterization of an aerosol test chamber which was constructed for use in this research. Finally, the bulk of this work describes the development of a semi-quantitative methodology for visualizing contamination. This method uses an ultraviolet fluorescent aerosol (to simulate contamination by a chemical warfare agent) and leverages image analysis to determine the difference in contamination from one step to another. This method was shown to be highly repeatable, with deposition area variability being less than 40 in^2 (total area 230 in^2). The claim of 90% contamination removal by disrobing was evaluated using this method. Several experiments were conducted which concluded that disrobing can remove up to 95% (mean 93.9%, with 95% confidence intervals of 91.0-96.8%) of contamination in situations such as when Tyvek suits are well-sealed. In situations when Tyvek suits have open cuffs, it was shown that disrobing may only remove 70% of contamination (mean 69.2% (64.9-73.6%)). While disrobing may not always remove 90% of contamination, at least 65% removal was demonstrated.

15. SUBJECT TERMS
CBRN, decontamination, aerosol, fluorescent, disrobing, image analysis, method development

16. SECURITY CLASSIFICATION OF:			17. LIMITATION OF ABSTRACT	18. NUMBER OF PAGES	19a. NAME OF RESPONSIBLE PERSON
a. REPORT	b. ABSTRACT	c. THIS PAGE			Dr. Jeremy Slagley, AFIT/ENV
U	U	U	UU	182	19b. TELEPHONE NUMBER *(Include area code)* (937) 255-3636, ext 4632 (NOT DSN) (Jeremy.slagley@afit.edu)

Standard Form 298 (Rev. 8-98)
Prescribed by ANSI Std. Z39-18